

Delft University of Technology
Department of Chemical Technology and Materials Science
Section Fracture Phenomena and Sustained Behaviour of Materials

FORMATION OF BEACH MARKS ON ALCLAD 2024-T3 SHEET

K. M. Mussert

Supervisors: NLR: Dr R. J. H. Wanhill
TU Delft: Dr ir J. Zuidema

Delft, December 1995

Final report of the graduation project which forms a part of the requirements to obtain a
Master's degree in Materials Science

SUMMARY

In the present investigation aluminium Alclad 2024-T3 sheet material was tested. The aim of this investigation was to achieve a method by which fracture surfaces of short cracks (crack growth under the rivet heads of lapjoint specimens) can be marked by the use of periodic changes in the environment in the low crack growth rate region, and at very low cycle frequencies. These so-called "beach marks" could then be traced back after the test and enable measurement of crack growth and calculation of crack growth rates.

To obtain fracture surface markings through periodic changes in the environment, centre cracked tension specimens with a thickness of 1 mm were tested, using a climate chamber clamped on the specimen. It turned out that testing at frequencies ranging from 0.1 Hz to 10 Hz did not result in beach marks on the fracture surfaces when testing in the crack growth range from 10^{-8} m/cycle to 10^{-7} m/cycle. During investigation in the SEM it turned out that it was very difficult to find any flat facets on which beach marks could be found. Furthermore, when changing from fatigue testing in wet air to fatigue testing in dry air, the crack tip most probably works like a "pump", so that it takes several cycles before the crack is really dry with a relative humidity $< 5\%$.

On the whole, it is not yet possible to use the method of exposing a growing crack alternately to environments of high and low humidity in order to obtain fracture surface marking of short cracks.

The same type of specimen was used to investigate basic da/dN versus ΔK constant amplitude fatigue crack growth data in laboratory air (R.H. $\sim 45\%$), dry air (R.H. $< 5\%$), and wet air (R.H. $> 95\%$). For these tests it turned out that the tests did not reproduce well, and that the formation of shear lips cannot be systematically correlated with transitions in the fatigue crack growth curves.

For further investigation into fracture surface marking of Alclad 2024-T3 it is proposed to apply marker loads during testing, i.e. applying a marker load at the beginning of a beach mark and a marker load at the end of a beach mark. Furthermore it is proposed to examine other environments for testing, like distilled water and 0.1% aqueous NaCl.

TABLE OF CONTENTS

SUMMARY	3
TABLE OF CONTENTS	5
NOMENCLATURE	7
1 INTRODUCTION	9
2 THEORETICAL BACKGROUND	11
2.1 Fatigue Crack Propagation at Low Crack Growth Rates	11
2.1.1 Transitions in Crack Growth Curves According to Mackay [3]	11
2.1.2 Transitions in Crack Growth Curves According to Wanhill [4]	11
2.2 Frequency Effects in Fatigue	12
2.2.1 Frequency Effects in Dry and Wet Air	12
2.2.2 Frequency Effects in Aqueous Environments	13
2.3 Environmental Effects on Fatigue Crack Propagation	13
2.3.1 Influence of Atmosphere	13
2.3.1.1 Effect of Air and Vacuum	13
2.3.1.2 Effect of Oxygen	13
2.3.2 Influence of Aqueous Environments	14
2.3.2.1 Effect of Water Vapour	14
2.3.2.2 Effect of a Sodium Chloride Solution	15
2.4 Beach Marks	15
2.4.1 Beach Mark Formation	15
2.4.2 Mechanism for Formation of Beach Marks	16
2.4.3 Beach Marks for Calculation of Crack Growth Rates	16
3 TEST PROGRAMME	19
3.1 Material and Specimen Type	19
3.2 Fatigue Loading and Crack Growth Regime	19
3.3 Cycle Frequencies and Waveforms	20
3.4 Types of Tests	21
3.4.1 Environmental Effect Tests	21
3.4.2 Basic da/dN Versus ΔK Tests	22
4 EXPERIMENTAL DETAILS	23
4.1 Test Set-up	23
4.2 Crack Length Measurement	23
4.3 Experimental Procedures	24
4.3.1 Environmental Effect Tests	25
4.3.2 Basic da/dN Versus ΔK Tests	26
5 RESULTS	27
5.1 Environmental Effect Tests	27
5.1.1 Influence of Climate Chamber	27
5.1.2 Microfractography	27
5.2 Basic da/dN Versus ΔK Tests	30

5.2.1	Calculation of Crack Growth Rates	30
5.2.2	Fatigue Crack Growth Curves in Laboratory Air, Dry Air, and Wet Air	31
5.2.3	Macrofractography	31
6	DISCUSSION	33
6.1	Environmental Effect Tests	33
6.1.1	Influence of Climate Chamber	33
6.1.2	Microfractography	33
6.2	Basic da/dN Versus ΔK Tests	36
6.2.1	Calculation of Crack Growth Rates	36
6.2.2	Fatigue Crack Growth Curves in Laboratory Air, Dry Air, and Wet Air	36
6.2.3	Macrofractography	37
7	CONCLUSIONS	39
7.1	Environmental Effect Tests	39
7.2	Basic da/dN Versus ΔK Tests	40
8	RECOMMENDATIONS FOR FURTHER INVESTIGATION	41
	ACKNOWLEDGEMENTS	43
	REFERENCES	45
	APPENDIX 1: TABLES	49
	APPENDIX 2: FIGURES	55

NOMENCLATURE

Symbols:

a	: crack length
a_i	: initial crack length
a_f	: final crack length
C	: Paris constant
da/dN	: fatigue crack growth rate per cycle
f	: frequency
ΔK	: stress intensity factor range = $K_{max} - K_{min}$
ΔK_i	: initial stress intensity factor range
ΔK_f	: final stress intensity factor range
ΔK_I	: cyclic stress intensity amplitude
ΔK_{th}	: threshold stress intensity factor range
K_{max}, K_{min}	: maximum and minimum stress intensity factors
m	: Paris exponent
n	: reduction number
N	: total number of cycles
ΔP	: load range = $P_{max} - P_{min}$
P_0, P_1, P_2, P_3	: coefficients used for potential drop measurement/Howden coefficients
P_{max}, P_{min}	: maximum and minimum load
R	: stress ratio = S_{min}/S_{max}
ΔS	: stress range = $S_{max} - S_{min}$
S_a	: stress amplitude
S_m	: mean stress
S_{max}, S_{min}	: maximum and minimum cyclic stress levels
T_1, T_2, T_3	: transitions in fatigue crack growth curves
W	: specimen width

Abbreviations:

BM	: beach mark
CCT	: Centre Cracked Tension
max	: maximum
MSD	: Multiple Site Damage
min	: minimum
NLR	: Nationaal Lucht- en Ruimtevaartlaboratorium/National Aerospace Laboratory
pct	: percentage
ppm	: parts per million
R.H.	: Relative Humidity (%)
SEM	: Scanning Electron Microscope
S-N	: Stress (S) versus total number of cycles (N) constant amplitude fatigue data

1 INTRODUCTION

Fatigue cracks in aircraft structures generally originate in areas of local stress concentrations, such as cutouts, bolt or rivet holes or other structural holes. Because crack initiation takes time, they tend to occur more frequently in ageing aircraft structures. A dangerous situation can occur when cracks initiate in a structural part with a more or less uniform stress field, e.g. in the longitudinal lap splices of a pressurized fuselage. Cracks can initiate simultaneously from several rivet holes, grow in a similar manner and can suddenly coalesce to form a single critical crack which can lead to a catastrophic failure of the structure. This so-called multiple site damage (MSD) was one of the main reasons for the Aloha Airlines Boeing 737 accident in 1988, when a large section of the fuselage was lost during flight.

When MSD occurs the fatigue crack growth of medium-to-long cracks and the fracture characteristics are significantly different from those of the isolated cracks on which current damage tolerance requirements are based.

The main purpose of this report is to investigate a method for marking fracture surfaces of 2024-T3 Alclad sheet. The method should give markings on the fracture surface that can be traced back after a test and enable measurement of crack growth and calculation of crack growth rates under the rivet heads in lap splices. In contrast to medium-to-long cracks, for which crack growth can be followed directly on the specimen surface, the crack growth rate under the rivet head has to be established in an indirect way, because the cracks initiate at the faying surfaces and will not be externally detectable before their leading dimensions exceed the sheet thickness.

Darvish and Johansson [1] showed that a periodic change in environment (high and low humidity) will cause the formation of markings ("beach marks") on the fracture surface in the very low crack growth rate region. Furthermore, Jansen and Wanhill [2] examined fatigue cracks in longitudinal lap splices from the pressure cabins of two F28 aircraft. Fracture surface corrosion was found and so-called "beach marks" that may represent a periodic change in environment.

This report describes the experimental work done to obtain fracture surface markings by periodic changes in the environment in the low crack growth rate region and at a very low cycle frequency.

In chapter 2 a theoretical background is provided which includes a description of fatigue crack propagation at low crack growth rates, frequency effects in fatigue, some environmental effects on fatigue crack propagation, and a definition of beach marks. In chapter 3 the test programme is described, including the material and specimen type used for the experiments. After discussing the experimental details in chapter 4, the results are presented in chapter 5 and discussed in chapter 6. Finally conclusions (chapter 7) and recommendations for further investigation (chapter 8) are given.

2 THEORETICAL BACKGROUND

To investigate a method for marking fracture surfaces of 2024-T3 Alclad sheet, several aspects have to be considered. Darvish and Johansson [1] found markings on fracture surfaces in the very low crack growth rate region. Crack growth data in the low-to-medium ΔK range are of importance, because this is the region comprising most of the fatigue lifetime of transport aircraft (the aircraft of interest in this investigation). Sub-section 2.1 presents a general description of fatigue crack propagation in this region of crack growth rates. Frequency effects in fatigue are described in sub-section 2.2: a frequency of 0.003 Hz is representative of the cabin pressurization rate during a real flight. Because a periodic change in environment caused the formation of markings in the investigation done by Darvish and Johansson, some environmental effects on fatigue crack propagation are described in sub-section 2.3. In fractography many terms can have differing meanings. Therefore the last sub-section, 2.4, gives a definition of beach marks as used in this investigation.

2.1 Fatigue Crack Propagation at Low Crack Growth Rates

2.1.1 Transitions in Crack Growth Curves According to Mackay [3]

Mackay [3] investigated the fatigue crack propagation rate at low ΔK of 2024-T3 sheet material. The fatigue crack growth rates at low stress intensity were determined at several stress ratios R (0.05, 0.2, 0.4 and 0.6), and in laboratory air. The results are shown in figure 1. There is a region between approximately 10^{-7} and 2×10^{-7} in/cycle (in figure 1 da/dN is defined in inches/cycle!) where the shape of the da/dN curve changed markedly for all stress ratios.

After examination by scanning electron microscopy, fractographic features were correlated with crack propagation rates (see figure 2). At the lowest stresses and crack propagation rates, "brittle cleavage" regions were observed on flat plane strain fracture surfaces. In the intermediate stress region plane strain is the controlling mode of fracture, and at the highest stresses plane stress becomes the controlling mode of fracture.

2.1.2 Transitions in Crack Growth Curves According to Wanhill [4]

In research done by Wanhill [4], constant amplitude fatigue crack growth properties of five batches of aluminium alloy 2024 in the naturally aged T3 and T351 conditions were compared. It appears that low stress intensity constant amplitude fatigue crack growth curves for aluminium alloys show several "knees" or transitions. On a double logarithmic scale, da/dN versus ΔK crack growth curves can be approximated by multilinear plots like the one illustrated schematically in figure 3. Crack growth tests were carried out in laboratory air at cycle frequencies of 13-15 Hz and several values of stress ratio were used. In figure 4 an example is given of crack growth curves for 2.3 mm thick 2024-T3 sheet. Different materials tested with the same R -value were also compared. Figure 5 gives an example of constant amplitude fatigue crack growth rates for $R = 0$. From the results Wanhill [4] concludes the following:

- Transitions in crack growth curves corresponding to T_1 , T_2 , and T_3 in figure 3 exist.
- There is a strong effect of R on the positions of crack growth curves.
- At a given R the crack growth curves for different materials are similar.

The fracture surfaces of the specimens investigated by Wanhill [4] were also examined by scanning electron microscopy, and examination took place over the crack growth curve range from ΔK_{th} to just above T_3 . The fracture appearances were as follows:

- Between ΔK_{th} and T_1 : faceted fracture with a mixture of large, nearly planar facets and "feathery" corrugated facets.
- Between T_1 and T_2 : faceted fracture with isolated large, nearly planar facets and predominantly corrugated facets.
- Between T_2 and T_3 : gradual change from faceted fracture to continuum-mode fracture characterized by striations.
- Just above T_3 : continuum-mode fracture, with a close correspondence between striation spacing and the macroscopically measured crack growth rates.

2.2 Frequency Effects in Fatigue

Fatigue testing of full-scale structures is usually performed at frequencies of the order of 0.2 Hz [5]. Apparently, dynamic loads in the very low frequency range, as well as in the very high frequency range, are poorly represented by conventional testing procedures. Since fatigue is generally thought to be essentially cycle-dependent, a logical way to accelerate a test would be to raise the number of cycles per unit time, i.e. the frequency. However, it is often found that an increase in frequency affects test results significantly, especially in aggressive environments.

2.2.1 Frequency Effects in Dry and Wet Air

Hartman, Jacobs, Nederveen, and De Rijk [6] examined the combined effects of the humidity of the air and the load frequency. For 2024-T3 Alclad, crack propagation tests with different load frequencies were done for two environmental conditions, dry air (< 0.05% R.H.) and wet air (100% R.H.).

Figure 6 shows that a lower frequency of loading can be coupled to a shorter fatigue crack growth life. Furthermore, it turns out that the frequency effect is larger in dry air than in wet air: an increase of the frequency of loading with a factor of 100 leads to an increase in fatigue life $N_{25-1.5}$ (number of cycles for crack growth from 1.5 to 25 mm) by a factor of approximately 3.5, which is about twice the factor for wet air.

Figures 7 and 8 show the effect of the load frequency on the crack growth rate curves for 2024-T3 Alclad. Figure 7, for tests in wet air, indicates a regular increase of crack growth rate with a decrease of load frequency at short crack lengths. The differences between the crack growth rates become smaller at larger crack lengths and probably are unimportant at crack lengths > 10 mm.

The crack growth rate curves in figure 8 for the tests in dry air show similar trends. The mean crack growth rates in figure 8 at crack lengths of 2, 3, 5, and 10 mm are plotted versus the load frequency in figure 9. This figure shows that for 2024-T3 specimens in dry air and frequencies in the range of 30-3000 c/min a straight line on a double logarithmic plot represents the relation between crack growth rate and load frequency to a fair approximation. The smaller effect of load frequency on the crack growth rate at larger crack lengths and higher crack growth rates is reflected in figure 9 by the steeper slopes of these lines for shorter crack lengths.

Wanhill [7] reviewed the effects of load frequency and humidity of the air. He concluded that the effects of frequency and humidity are interrelated and the overall behaviour is such that there should be relatively little variation in crack growth rates at low frequencies and/or in natural air ($\geq 5\%$ R.H.).

Figure 10 shows that for high frequencies the crack growth rates in nominally dry air at low ΔK may be an order of magnitude slower than in wet air. The differences become small at ΔK values of 20-30 $\text{MPa}\sqrt{\text{m}}$, depending on the stress ratio R . However, the behaviour is frequency dependent. Figure 11 shows that reducing the frequency increases crack growth rates more in dry air than in wet air at low ΔK , but the opposite occurs at high ΔK .

2.2.2 Frequency Effects in Aqueous Environments

Most tests with aqueous environments have used salt water. In this environment average crack growth rates are 2-4 times higher than in air for ΔK values between 4 and 30 $\text{MPa}\sqrt{\text{m}}$, see figure 12, except at very low and very high ΔK there is no difference [7].

According to Wanhill [7] frequency effects are usually small in aqueous environments, especially if an alloy is immune to stress corrosion (e.g. 2219-T87 in figure 13). However, the same figure shows that an alloy highly susceptible to stress corrosion (7079-T651) exhibits an extreme frequency dependence at frequencies low enough to allow stress corrosion.

2.3 Environmental Effects on Fatigue Crack Propagation

2.3.1 Influence of Atmosphere

2.3.1.1 Effect of Air and Vacuum

Traditionally, measurements of fatigue crack propagation have been made by testing in air. Meyn [8] shows results of tests on a number of alloys which indicate that the crack propagation phase is at least as affected by the test atmosphere as the crack initiation phase. In 2024 aluminium alloy, testing in vacuum in comparison to testing in air causes both a reduction in crack growth rate and a change in the mechanism of crack propagation.

Figure 14 shows the crack growth rate, da/dN , versus ΔK_I for 2024-T3 tested in air and vacuum [8]. Except for data at the highest amplitudes, it is noticed that crack propagation rates in air are about 3 times those in vacuum for the same ΔK_I . At low amplitudes the data obtained from tests in vacuum have the same overall trend as the test data in air. However, at the highest amplitudes, they curve upward towards the data obtained from tests in air. This indicates that when da/dN approaches $0.5 \mu\text{m}/\text{cycle}$ or more, the propagation mechanisms in air and in vacuum may not be very different.

2.3.1.2 Effect of Oxygen

Normal fatigue tests are defined as fatigue tests in the laboratory, with air as environment, and corrosion fatigue tests as tests with a corrosive environment like an aqueous salt solution. This division into normal and corrosion fatigue tests suggests that during fatigue tests in air corrosion of the metal does not occur or is so slight that it has a negligible effect on the result. However, normal air consists for approximately 20% of the reactive gas oxygen and always contains amounts of water vapour depending on the temperature and the

relative humidity. Corrosive effects during fatigue tests in air can therefore not be ruled out [9].

In their investigation, Hartman and Jacobs [9], studied the propagation of fatigue cracks in 2024-T3 Alclad sheet under fluctuating tension in different atmospheres. Tests were done in dry and wet argon, and in dry and wet oxygen. Results of the tests in dry argon were used as a basis for comparison, to determine the effect of oxygen on the crack growth.

Figure 15 gives the S-N curves for crack growth from 2 to 25 mm in the four environments. This figure shows that both wet environments yielded the same endurance. For the two dry gases the increase in endurance was not similar, but depended on the stress amplitude. The S-N curves for dry oxygen and dry argon intersect at a stress amplitude of 4.5 kg/mm^2 , this is about 45 MPa (figure 15 defines the stress amplitude S_a in kg/mm^2 !); at higher stress amplitudes dry argon gives the shorter endurance and at lower stress amplitudes dry oxygen. If it is assumed that dry argon does not have any effect on the endurance, this suggests an ambiguous effect of oxygen on the crack growth, accelerating at low stress amplitudes and decelerating at high stress amplitudes.

2.3.2 Influence of Aqueous Environments

2.3.2.1 Effect of Water Vapour

Wei, Pao, Hart, Weir, and Simmons [10] investigated the influence of water vapour on fatigue crack growth in aluminium alloys. The results suggest that enhancement of fatigue crack growth by water vapour in aluminium alloys occurs through a "hydrogen embrittlement" mechanism. The results also confirm the earlier suggestion by Bradshaw and Wheeler [11], that the enhancement of crack growth is a function of water vapour pressure and time available for reaction, that is, of exposure (pressure \times time).

A schematic illustration of various sequential processes involved in embrittlement by external gaseous environments is given in figure 16 [12]. Besides a sequential process that could cause hydrogen embrittlement, the same process is considered to describe environmentally assisted fatigue crack propagation in the Paris regime (in this regime a linear dependence between da/dN and ΔK is found on a double logarithmic scale). It is assumed, that hydrogen production results from the dissociative chemical adsorption of molecules after physical adsorption on freshly created surfaces at the crack tip. Hydrogen is then dragged by mobile dislocations into the process zone, where the embrittling reaction takes place at some specific, but ill-identified sites.

On the other hand it is also believed that the physical adsorption step can by itself alter the fatigue resistance of the material [13]. According to Lynch [14-16], active species adsorption or chemisorption on a few atomic layers would be sufficient to enhance fatigue crack propagation by facilitating dislocation nucleation. This approach, based on a surface phenomenon, is therefore radically different from the theory proposed by Wei [12], which considers embrittling reactions in bulk material.

On the basis of experimental data obtained on aluminium alloys in purified nitrogen containing traces of water vapour, and in high vacuum, Henaff, Marchal, and Petit [13] have distinguished two different mechanisms for environmentally assisted fatigue crack propagation:

- At crack growth rates lower than a critical crack growth rate $(da/dN)_{cr}$ (which depends upon several factors such as surrounding partial pressure of water vapour, load ratio, test frequency, chemical composition, and microstructure), a hydrogen assisted crack growth mechanism takes place, resulting in highly accelerated crack growth rates and very low effective threshold values as compared to what happens in vacuum.

- At crack growth rates higher than $(da/dN)_{cr}$ the crack growth mechanism is controlled by plasticity as in vacuum, but can still be assisted by gas adsorption.

Summarising, three main concepts are proposed [13] to account for the influence of environment on fatigue crack propagation:

- the surface adsorption concept,
- the hydrogen-embrittlement concept, and
- superimposition of the two processes.

2.3.2.2 Effect of a Sodium Chloride Solution

Since there are two mechanisms affecting crack growth in corrosion fatigue (a mechanical and a corrosive mechanism), the total crack growth data can be split up into a mechanical component and a corrosion component.

Selines and Pelloux [17] performed tests on 7075-T6 alloys in a 3.5 pct sodium chloride solution at low ΔK values, using frequencies of 0.1, 1, and 10 Hz. They used dry argon as a reference environment. If it is assumed that the crack propagation rate in dry argon at 10 Hz represents the mechanical component of corrosion fatigue, than figure 17 shows that in the total crack growth rate, the corrosion component is an extremely significant factor. At low stress intensity ranges, the corrosion component is as much as ten times the mechanical component. However, at high stress intensity levels, it can be seen that although the absolute corrosion component increases with rising values of ΔK , its relative importance compared to the mechanical component decreases significantly. In other words, at high stress values, the mechanical component of corrosion fatigue will overshadow the corrosion component and the crack growth rate is a much more sensitive function of ΔK only.

Since fatigue crack extension in an inert environment takes place only during the opening part of the load cycle [18], one has to distinguish the opening time, the time at peak load and the closing time. Following Barsom [19], Selines and Pelloux [17] take the approach that the accelerated crack growth in corrosion fatigue is caused by the interaction between the environment and the loading part of the transient tensile load in each cycle rather than by the time spent at peak load. Furthermore, the most important test variable should be the time available for the reaction to take place, since the environmental effect which appears is due to the reaction between the corrosive medium and the freshly exposed metal surfaces at the crack tip.

2.4 Beach Marks

2.4.1 Beach Mark Formation

The different behaviour of short cracks compared with long ones, typically a higher crack growth rate at the same stress intensity factor, is a good reason for increasing attention to this region. Studies of short cracks and near-threshold fatigue crack growth may be easier to perform if one could create markings on the fracture surface, especially if they can be directly related to the macroscopic crack growth. In the low crack growth region, periodic patterns like striations have not been observed and therefore the macroscopic crack growth rate cannot easily be related to the microscopic one. With the use of external factors such as variations in environment or loading conditions one can produce periodic markings on the fracture surface.

In a previous investigation [20], the author has shown that for Alclad 2024-T3 sheet material, satisfactory crack front markers cannot be obtained by periodic variations in cyclic loading; tests were done by variation of the R-value, by using tensile overloads (up

to 40% of S_{max}) and using programme loading. Especially during the early stages of crack growth, for which fatigue fracture is faceted and without resolvable load cycle striations, no markers were found.

However, Darvish and Johansson [1] proposed a new method for studying fatigue crack growth at near-threshold crack growth rates. This method (called *cyclic condensation*) is based on exposing the growing crack alternately to environments of high and low humidity. As a result of these variations, markings (beach marks) will form on the fracture surface. Each beach mark is an indication of crack extension during one environmental cycle, and consists of two parts: one caused by growth in the dry environment and the other by growth in the wet environment. The markings form only when the crack growth rate is low and disappear as the crack growth rate increases. Furthermore, they form at the initiation zone and in the threshold region.

Darvish and Johansson found that the microscopic crack growth rate obtained from beach mark spacings corresponded with the macroscopic rate obtained from crack length measurements.

2.4.2 Mechanism for Formation of Beach Marks

The exact mechanism for the formation of beach marks is unclear, but in both aluminium alloys investigated by Darvish and Johansson (7075 Al-alloy and 8090 Al-Li-alloy) the same mechanism seemed to be involved. It turned out that it is not only the mechanism of appearance of beach marks which is difficult to explain, but also the absence of beach marks for high crack growth rates.

Beach marks stopped forming when their spacing had increased enough due to the increase in crack growth rate. The size of beach marks which are formed in the middle of the fracture surface increases significantly before they disappear completely on this part of the fracture surface. Furthermore, beach marks will still form at the edge surfaces of a specimen when they have already stopped forming in the middle. It was suggested [1], that this may be due to the fact that a condition of plane strain prevails in the middle and as a consequence the crack growth rate in the middle is higher than that at the edges.

The study of fracture surfaces at low crack growth rates near the threshold stress intensities [21] showed that beach marks form in specimens which are exposed to cyclic condensation environments, and the formation of beach marks is supposed to depend on both material and stress ratio. Both for short and long cracks, the disappearance of beach marks occurs at the beginning of the Paris regime, which corresponds to crack growth rates from about 2×10^{-9} m/cycle to 10^{-6} m/cycle, see also sub-section 3.2. The markings cannot be observed when their spacing becomes too large and very small, and they can be most clearly seen when their spacing is between 2-4 μm .

2.4.3 Beach Marks for Calculation of Crack Growth Rates

Most studies of fatigue crack growth have been concentrated in the Paris regime, and at crack growth rates larger than 2×10^{-8} m/cycle. In this region, fatigue striations exist, and each striation represents an increment in crack growth during one loading cycle. The relation between striation spacing and crack growth rate disappears as the stress intensity factor approaches the threshold value (ΔK_{th}). At the threshold level no clear striations have been observed. Either they do not form in this region, or their small size makes observation impossible [1].

In order to get beach mark formation, the environmental cycle time should be related to the crack growth rate [1]:

$$\text{BM spacing} = \frac{da}{dN} \times f \times t_{\text{tot}} < 10\mu\text{m} \quad (1)$$

where: f = frequency
 t_{tot} = time for an environmental cycle

Equation 1 indicates that when the crack growth rate is very low, the environmental cycle time should be longer and should be adjusted as the crack growth rate increases in order to get beach mark formation.

In order to compare the crack growth rate obtained by measuring the crack length with the crack growth rate calculated by using beach mark spacings, the spacing of each marking must be measured. The spacing of beach marks is directly related to the crack growth rate according to equation 1. To calculate the crack growth rate this relation can be rewritten:

$$\frac{da}{dN} = \frac{\text{BM spacing}}{f \times t_{\text{tot}}} \quad (2)$$

By using this method, the successive positions of the crack front and the local crack growth rate can be obtained from the presence of beach marks. The same information can be obtained from the presence of striations.

The difference between beach marks and striations is that a striation forms by one loading cycle at relatively high crack growth rates, while a beach mark forms by one environmental cycle at low crack growth rates [22]. The topography of beach marks turns out to be similar to that for striations, but the profiles of beach marks are not as sharp as those of striations.

3 TEST PROGRAMME

The test programme to investigate a method for marking fracture surfaces of 2024-T3 Alclad sheet is given in table 1a, and table 1b gives the test programme to obtain basic fatigue data for the specimen type used in this investigation. Detailed comments about these test programmes are given in the following sub-sections.

3.1 Material and Specimen Type

For all tests 1 mm thick 2024-T3 Alclad sheet was used, because this is an appropriate gauge for the pressure cabins of small-to-medium size transport aircraft. Typical mechanical properties for this material are: $\sigma_y = 310$ MPa, $\sigma_u = 450$ MPa, $\delta = 18\%$ [23].

CCT specimens, as shown in figure 18, were used for all tests. This specimen type is appropriate as a simplification of the geometry of lap joint specimens, furthermore this configuration excludes the complications of secondary bending and multiple fastener holes. The specimens were provided with a cylindrical hole with a diameter of 3.0 mm. To start the fatigue crack at either side of the hole, a 0.5 mm long slit was made by spark erosion. All specimens were loaded in the rolling direction of the sheet material.

3.2 Fatigue Loading and Crack Growth Regime

Tests were conducted under constant amplitude fatigue loading conditions with a stress ratio $R = 0.05$. A stress ratio $R = 0$ is appropriate to major areas of pressure cabins, but to avoid the occurrence of a compressive load it was decided to apply $R = 0.05$.

From the literature [2] it appears that in lap joints fatigue crack growth rates, even for very small cracks in mild environments like normal air, will be above 10^{-8} m/cycle. On the other hand, environmental effects on fatigue crack growth in 2024-T3 become progressively much less at crack growth rates above 10^{-7} m/cycle [6, 24, 25]. It is assumed that testing over the range 10^{-8} m/cycle - 5×10^{-6} m/cycle, based on crack growth in normal air, should be more than sufficient for investigating the combined effects of environment and cycle frequency.

A summary of short and long fatigue crack growth data is given in figure 19 [26]. On average, little or no difference is to be expected in the behaviour of short and long fatigue cracks in the testing range from 10^{-8} m/cycle to 5×10^{-6} m/cycle. From this it is concluded that tests with long cracks, as in CCT specimens, are most likely sufficient to establish environmental and cycle frequency effects for short-to-long fatigue crack growth in lap joint test specimens. Another feature which can be concluded from figure 19 is that the long fatigue crack growth rates above 5×10^{-9} m/cycle can be approximated by two "Paris law" equations. The Paris equation gives a description of the crack growth rate curve and is written as follows [27]:

$$\frac{da}{dN} = C(\Delta K)^m \quad (3)$$

where: C = Paris constant
m = Paris exponent

To calculate the fatigue crack growth life for 2024-T3 CCT specimens as a function of stress range, ΔS , over the range 10^{-8} m/cycle - 10^{-7} m/cycle, the lower positioned equation has been used:

$$\frac{da}{dN} = 9.18 \times 10^{-13} (\Delta K)^{5.06} \quad (4)$$

For the da/dN range mentioned before, the initial and final stress intensity factor ranges, ΔK_i and ΔK_f are determined using equation 4. The initial and final crack lengths, a_i and a_f are calculated, using ΔK_i , ΔK_f , various values of ΔS , and the following equation [27]:

$$\Delta K = \Delta S \sqrt{\pi a} \quad (5)$$

To calculate the fatigue crack growth life (the number of cycles), equation 4 is integrated, which results in the following integration equation:

$$n = \frac{2}{(2-m)C(\Delta S\sqrt{\pi})^m} (a_f^{(2-m)/2} - a_i^{(2-m)/2}) \quad (6)$$

where: ΔS = stress range
 a_i = initial crack length
 a_f = final crack length

The calculation of the fatigue crack growth life for 2024-T3 CCT specimens is given in table 2, and the results are shown in figure 20. Figure 20 demonstrates that the number of cycles, and hence test duration, to cover a given range of crack growth rates depends strongly on the applied stress range. It turns out that the maximum feasible stress range for the CCT specimen configuration shown in figure 18 is $\Delta S = 70$ MPa. This limit is imposed by the requirement that the initial crack length, a_i , be longer than 2.0 mm, which is half the starter notch size.

3.3 Cycle Frequencies and Waveforms

For every environmental effect test, one of the following combinations of cycle frequency and waveform was chosen (see table 1a):

- 10 Hz sinewave loading is a convenient type of loading for fatigue testing. Furthermore, it has been demonstrated to result in beach marks when the environment is periodically changed from low to high humidity air [1, 21].
- 0.003 Hz positive sawtooth loading is representative of the cabin pressurization rate during a real flight. This frequency is tested since environmental effects at such low frequency have not yet been investigated for 2024-T3 over the range 10^{-8} m/cycle - 5×10^{-6} m/cycle.
 When testing at such a low frequency, a positive sawtooth waveform instead of a sinewave will save a lot of testing time. Since only uploading is important for fatigue crack growth [18], this change of waveform is allowed.
- 0.1 Hz, 0.5 Hz, and 0.9 Hz are intermediate frequencies which represent some "bridging" frequencies between 0.003 Hz and 10 Hz. These frequencies are also applied with a positive sawtooth waveform.

The basic da/dN versus ΔK tests are all performed with a cycle frequency of 10 Hz and the applied waveform is a sinewave (see table 1b).

3.4 Types of Tests

3.4.1 Environmental Effect Tests

Testing at 10 Hz, Darvish and Johansson found that beach marks were best observed when their spacing was 2 - 4 μm , and they did not find beach marks at crack growth rates above 4×10^{-9} m/cycle [1]. On the other hand, the NLR found service-induced beach marks down to less than 1 μm in width and up to about 10 μm in width, at crack growth rates up to about 6×10^{-8} m/cycle [2].

At present it is not known whether:

- the two types of beach marks stem from the same cause, namely periodic changes in environmental humidity, or
- the formation of environmentally-induced beach marks depends on load cycle frequency, such that lower frequencies enable beach mark visibility at higher crack growth rates.

Constant amplitude fatigue crack growth testing times have been calculated in normal air using the method described in sub-section 3.2 and the matching equations 4, 5, and 6. Actually, for crack lengths longer than about 10 mm the integration is no longer correct because of the finite width of the CCT specimens. However, this was ignored for the purpose of illustration. The results are shown in table 3 for cycle frequencies 0.003 Hz, 0.1 Hz, and 10 Hz. It is evident that *continuous* testing is acceptable for a frequency of 10 Hz; just acceptable for a frequency of 0.1 Hz; and unacceptable for a frequency of 0.003 Hz.

The solution is to do *discontinuous* testing, whereby a small amount of crack growth is permitted at selected ΔK values. To perform a discontinuous test, a test is divided into several blocks. The environmental effects are accomplished at the lower frequency (for example 0.003 Hz), and the intermediate blocks are done at a frequency of 10 Hz.

From table 1a it can be seen that every test was started with a block of cycles until a specific crack length a . This specific crack length was determined as follows. It was assumed that testing over the range 10^{-8} m/cycle - 5×10^{-6} m/cycle should be more than sufficient for investigating the combined effects of environment and cycle frequency (see sub-section 3.2). From this range three values of da/dN were chosen and using equation 4, the matching ΔK -values were calculated, see table 4. For all tests $R = 0.05$ was applied, see sub-section 3.2, and $\Delta S = 66.5$ MPa was applied, see sub-section 3.4.2. The remaining unknown parameter now was the crack length a , which had to be solved numerically. With the help of a calculation programme called Maple V for Windows (Release 3.0) it was possible to calculate the crack length going with the calculated ΔK -values from table 4. To determine the crack length a the following equation was used for ΔK :

$$\begin{cases} \Delta K = f\left(\frac{a}{W}\right) \cdot \Delta S \cdot \sqrt{\pi a} \\ f\left(\frac{a}{W}\right) = \left(1 + 0.256 \cdot \left(\frac{a}{W}\right) - 1.152 \cdot \left(\frac{a}{W}\right)^2 + 12.2 \cdot \left(\frac{a}{W}\right)^3\right) \end{cases} \quad (7)$$

The calculated crack lengths are shown in table 5.

3.4.2 Basic da/dN Versus ΔK Tests

Basic constant amplitude fatigue tests have to be done to investigate the behaviour of a CCT specimen with the configuration as mentioned in sub-section 3.1, and the fatigue loading and crack growth regime as mentioned in sub-section 3.2. All tests will be performed at a frequency of 10 Hz, an R-value of 0.05, and a stress range $\Delta S = 66.5$ MPa. In the first instance $R = 0$ was suggested, which means $\Delta S = S_{\max}$. When it was decided to apply an $R = 0.05$, by accident ΔS was calculated again, but now using $S_{\max} = 70$ MPa, this results in $\Delta S = 66.5$ MPa. Using a stress range $\Delta S = 66.5$ MPa means a load range $\Delta P = 3.99$ kN. The only parameter which will alter between the different experiments is the environment, so that an overview is obtained for the different environments mentioned in table 1b: laboratory air (R.H. $\sim 45\%$), dry air (R.H. $< 5\%$), and wet air (R.H. $> 95\%$).

4 EXPERIMENTAL DETAILS

In this chapter the experimental details of this investigation are given. Sub-section 4.1 describes the test set-up, sub-section 4.2 describes the method used for crack length measurement, and sub-section 4.3 explains how the experiments were carried out.

4.1 Test Set-up

An overview of the experimental test set-up is given in figure 21, and figures 22 and 23 show how the climate chamber is clamped on the specimen. Figure 22 gives a front view and figure 23 gives a rear view. The tests were carried out in a Schenck Hydropuls-Electronic S 56 PSB fatigue testing machine with 100 kN maximum load capacity. The command signal for this system was generated by a PC controlled function generator.

The material chosen for the climate chamber is polycarbonate, which, unlike perspex, does not absorb moisture. The chamber was constructed in four parts that could easily be separated and rejoined. To prevent leakage (and thus protect the hydraulic actuator of the load frame), two O-rings (GACO R 2112) were put around the specimen, 10 stainless steel M4 bolts were tightened, and an elastomeric sealant on the basis of polyurethane called Puraflex-2005 was used (silicone sealant could not be used since this gives off acetate).

The inlet of the chamber was made at the bottom of the front side, and the outlet was made at the top of the rear side, so the air stream could flush gradually through the chamber, and thus gradually through the growing crack. At the rear side of the chamber there was also an inlet for the hygrometer (type HT-732-M-00 from Rense Instruments B.V.) which measures the relative humidity and the temperature, and an inlet was made for the potential drop apparatus.

When fixing a specimen in the machine it had to be insulated from the grips to prevent undue disturbance of the electrical signal. To obtain this insulation, adhesive tape was stuck on the edges of the specimen and small plates of Pertinax were taped over the flat sides.

4.2 Crack Length Measurement

During all fatigue tests the crack length was measured continuously using pulsed direct current potential equipment (the apparatus used for this purpose was a Howden). Since crack growth increases the electrical resistance of a material, the potential drop over a crack is a measure for the crack length. Figure 18 shows the holes where the apparatus is connected to the specimen. These holes are drilled along the centre line of the specimen and they are present in pairs, equidistant from the crack starter notch. The outer pair are 4 mm holes containing a bolt on which the current leads of the apparatus are connected.

The voltage pickups are connected to 2 mm bolts, for which the holes are drilled with a diameter of 1.6 mm and then tapped till 2 mm, using only the first and second tap. From the front the bolts are threaded through the specimen and clamped on the back side with an insulating fibre ring, followed by a stainless steel ring, then the cable socket connected to the Howden, and finally the nut.

The potential drop apparatus amplifies the voltages picked up and divides the inner voltage by the outer voltage and multiplies the result by 10. The potential drop apparatus output is

fed as a 0-10 Volt signal to a 12 bit analogue/digital conversion card, which digitizes the potential drop output for the computer. The output signal is converted back to crack length by a third order polynomial.

Since CCT specimens with a thickness of 1 mm and a length as shown in figure 18 were never used before, several fatigue tests were performed to calibrate the crack length measured with the potential drop against the crack length measured with a travelling microscope. The optically determined crack length is obtained by measuring the crack lengths on the left and right side of the specimen surface and averaging the result. Figure 24 shows an example of the calibration data set obtained during a constant ΔK test; the potential drop output voltage is plotted versus a/W (W is the specimen width).

A third order polynomial as shown in equation 8 was fitted through the data points:

$$\frac{a}{W} = P_0 + P_1(V) + P_2(V)^2 + P_3(V)^3 \quad (8)$$

In this third order polynomial P_0 , P_1 , P_2 , and P_3 are called Howden coefficients and these values are used by the computer to calculate the crack length. The following values were determined:

$$\begin{aligned} P_0 &= -0.5111 \\ P_1 &= 0.4395 \\ P_2 &= -0.1118 \\ P_3 &= 0.0109 \end{aligned}$$

4.3 Experimental Procedures

To explain the experimental procedures, a schematic illustration of the experimental test set-up is given in figure 25, in this figure all connections between the different stages consist of silicone tubes. Both types of tests, the environmental effect tests, and the basic da/dN versus ΔK tests follow this test set-up.

A test starts with the air supply from the laboratory, see figure 25. Fortunately, the compressed air supply at the Laboratory of Materials Science has an initial relative humidity $< 6\%$. This simplifies matters for tests or blocks of tests which are performed in dry air (the required relative humidity in this environment is below 10%). The compressed air supply has a pressure of about $7 - 7.5$ bar. Since this is too high for the test set-up, a reduction valve is installed after the air supply outlet. The compressed air now passes through an adjustable flowmeter (Brooks [type R-2-15-A]), which ensures that the air flow through the climate chamber is the same for every test.

After the air has passed through the flowmeter, the experimenter can choose between a block of cycles in dry air, or a block of cycles in wet air. To create dry air the air should follow the by-pass line, and this means that the dashed taps in figure 25 should be closed. For testing in wet air, it is just the reverse: the other taps should be closed, and then the air is forced into the container of demineralised water. It is difficult to achieve wet air in a short time, and it is assumed that this may be due to cooling of the water in the container by the air. To obtain wet air (and keep it at a relative humidity $\geq 95\%$) the solution was to keep a constant water temperature of about 35°C (this is about the temperature of the specimen when clamped in the machine as a result of heating of the actuator), and bubble the air through the water.

To get warm water, a 25 W aquarium heater was used. This element has an adjustable temperature and has a thermocouple to keep the temperature at a constant value. To check

the temperature, a thermometer was placed in the container. Bubbling the air through the water turned out to be an important variable. The finest distribution of bubbles was obtained using a porous aquarium "stone". Furthermore, attention had to be paid to the length of the silicone tubes: the shorter the tubes the quicker the relative humidity of the air reached a value of 95%.

After the demineralised water container or the by-pass line, the air enters the climate chamber through the inlet, flushes through the chamber and leaves through the outlet which has an open end in the laboratory. The hygrometer or R.H. meter continuously measures the relative humidity and the temperature. The output of the hygrometer is a 0-10 Volt signal, which corresponds to 0-100°C in temperature and 0-100% in relative humidity, and this signal is fed into a recorder.

Finally, the crack length is measured with the potential drop apparatus and this signal is fed back to the computer as described in sub-section 4.2.

4.3.1 Environmental Effect Tests

All tests were performed according to table 1a, i.e. the environment was alternately laboratory air, dry air, or wet air. When tests, or parts of tests were performed in laboratory air, the inlet and outlet of the climate chamber were left open and no other precautions were taken.

To perform the environmental effect tests, the command signal was generated by a PC as mentioned in sub-section 4.1. The software for this purpose was written by Bart Wiersma in QuickBasic. The control programme for these tests is called "sawteeth" and its capabilities are roughly:

- Divide a test in blocks of cycles (a maximum of 5) during which a sinus type of loading is applied for a predetermined interval of crack length, and a possibility to continue every block with new blocks (also a maximum of 5) during which a positive sawtooth load is applied for a specific number of cycles.
- Apply a constant amplitude to a specimen in every block, at a given frequency, a given R-value, and a given ΔP -value.
- Measure the crack length using potential drop apparatus and transfer the measured crack length, the number of cycles applied and the actual loads measured to a data file on a floppy disk.
- Holding the machine at minimum load after every block, so that the environment can be changed.

4.3.2 Basic da/dN Versus ΔK Tests

All tests were performed according to table 1b. In contrast with the environmental effect tests, where the environment was changed periodically from high to low humidity or to laboratory air, these tests were performed using one environment during a whole test.

The software for this part of the investigation was also written by Bart Wiersma in QuickBasic, and this programme is called "fatigue". The control programme has the following capabilities:

- Apply a constant amplitude to a specimen at a given test frequency, a given R-value, and a given ΔP -value for a predetermined interval of crack length.
- Measure the load applied to the specimen and adjust it to keep R and ΔP constant.
- Measure the crack length using potential drop apparatus and transfer the measured crack length, the number of cycles applied and the actual P_{\max} and P_{\min} measured to a data file on floppy disk.

5 RESULTS

In this chapter a distinction is made between the environmental effect tests, sub-section 5.1, and the basic da/dN versus ΔK tests, sub-section 5.2.

The environmental effect tests are divided into two topics: two experiments whereby the influence of the climate chamber clamped on a specimen was examined; and eight experiments following the conditions in table 1a. These specimens have been examined using a Scanning Electron Microscope (SEM).

For the basic da/dN versus ΔK tests ten specimens were used according to table 1b, and the data were converted into da/dN - ΔK curves. Furthermore the fracture surfaces were examined by macrofractography.

5.1 Environmental Effect Tests

5.1.1 Influence of Climate Chamber

Two specimens (unlisted in tables 1a and 1b) were used to examine whether and how the climate chamber clamped on the specimen would influence the load transfer during a test. Constant amplitude fatigue tests were done at $R = 0.1$, a frequency of 10 Hz, $\Delta P = 7.0$ kN using the computer programme "fatigue"; and the environment used for both tests was laboratory air with R.H. $\sim 45\%$. Both specimens were subjected to this programme, except that one specimen was tested with climate chamber and the other specimen was tested without climate chamber. Figure 26 shows the results plotted as crack growth rate da/dN versus stress intensity factor range, ΔK .

From figure 26 it can be seen that testing without the climate chamber resulted in higher crack growth rates up to a ΔK -value of about $18 \text{ MPa}\sqrt{\text{m}}$. At higher values of ΔK the test with climate chamber turned out to have a higher crack growth rate. The differences between the two curves were considered acceptable, and thus the environmental effect tests were done using the climate chamber clamped on the specimens.

5.1.2 Microfractography

Eight specimens were subjected to a periodically changing environment and/or frequency according to table 1a. The fracture surfaces of the specimens were examined by SEM. Most examination was done at the NLR (using a Zeiss DSM 962), and part of the examination was done at the TU Delft (using a JEOL JSM-6400 F). It can be seen from table 1a that specimens 30 and 31 had the same testing conditions. While testing specimen 30, it was found that the command signal from the programme "sawteeth" was not correct. Therefore, it was decided to repeat the test with specimen 31. Specimen 30 was omitted from examination in the SEM.

Another specimen not examined in the SEM was specimen 35. It turned out that the programme "sawteeth" was unable to conduct a positive sawtooth loading at a frequency of 0.9 Hz. This specimen was considered a failed test, and thus was also omitted from examination in the SEM.

The other specimens will be discussed according to table 1a.

Specimen 29:

The first specimen tested was specimen 29. This specimen was subjected to a 10 Hz sinewave loading in dry air up to $a = 3.62$ mm, followed by three blocks of 100 cycles of 0.0024 Hz sawtooth loading in dry air, wet air, and dry air. After the last block in dry air the environment was not changed, only the type of loading and the frequency were changed back to a 10 Hz sinewave loading. This specimen was examined at the NLR.

Figure 27 shows an overview of the fracture surface of this specimen. On both the left and right sides a transition is visible from a "light" fracture surface to a "dark" fracture surface (the arrows point at the transitions). The total crack length $2a$ of the "light" fracture surface in the photo is 5.5 cm, corresponding to $a = 3.44$ mm. This value is somewhat less than the given end crack length for block 1, i.e. $a = 3.62$ mm.

Figure 28 is a magnification of 50 times of the left fracture surface in figure 27. It turned out that at higher magnifications the transition became more difficult to find. The dashed line in figure 28 indicates the probable transition from dry air to wet air. At a crack length of $a = 3.62$ mm, the crack growth rate was supposed to be 2×10^{-8} m/cycle, so performing three blocks of 100 cycles should have resulted in three beach marks 2 μm in width. However, higher magnifications did not reveal any beach marks.

Specimen 31:

For this specimen the first and last testing blocks were done with laboratory air, unlike specimen 29. This specimen was examined at the TU Delft.

As for specimen 29, specimen 31 showed a transition from a "light" fracture surface to a "dark" fracture surface. Figure 29 shows an overview of the right fracture surface of specimen 31 at a magnification of 35 times. On this fracture surface the formation of shear lips can also be seen. Figure 30 is a magnification of 100 times of the same fracture surface, and shows the sharp transition. Most probably this is the transition from dry air to wet air, so when looking at even higher magnifications three beach marks caused by changing the environment from dry air to wet air, and back to dry air should be found. These beach marks now should be 4 μm wide since blocks of 200 cycles were applied.

Figures 31 and 32 are magnifications of 450 times and 2000 times respectively. No beach marks were found at these higher magnifications. It is concluded that the "transition" in figures 31 and 32 looks more like a stretch zone due to overload, probably as result of a control failure of the machine.

Specimen 32:

In contrast to both the previous specimens, the sequence of alternating the environment was changed for specimen 32 into wet air, dry air, wet air. The reason for this change is as follows: it was assumed from specimen 31 that it was probably the transition from

laboratory air at 10 Hz sinewave loading to dry air at 0.003 Hz sawtooth loading which did not show up on the fracture surface.

Furthermore, the first block of testing was up to $a = 5.1$ mm; at this point the crack growth rate was supposed to be 5×10^{-8} m/cycle, and thus three blocks of 80 cycles should result in three beach marks of 4 μm of width each. This specimen was examined at the NLR.

Figure 33 shows an overview of the right-hand fracture surface of specimen 32; the specimen was tilted 20° in the SEM. Unlike specimens 29 and 31, there is no difference in contrast visible at this low magnification. The beach marks should be found at $a = 5.1$ mm, i.e. 3.1 mm from the crack starter notch, as indicated by the dashed line. It turned out that this was just at the point where shear lips started.

Figure 34 is a $100\times$ magnification of the location where beach marks should be found. The dashed line indicates the transition, which became clearly visible at higher magnifications. Figure 35 gives a good overview of the transition, including possible beach marks. An even higher magnification is given in figure 36. It is not quite clear which transitions are visible in this figure. To obtain some certainty, a photo was taken at very high magnification in the "central beach mark", see figure 37. It turned out that this fracture surface was heavily corroded, so most probably this was the result of a testing block in wet air. Consequently it is concluded that in figure 36 the sequence from left to right is testing in dry air, then in wet air, and finally in laboratory air.

To be certain that the preceding figures did not show artefacts, the same location was examined on the left-hand fracture surface. Figures 38 and 39 show a strong resemblance to figures 35 and 36. Figure 39 even shows so-called "mud-cracks". For this figure the assumed sequence of environmental blocks, from left to right, is laboratory air, then wet air, and finally dry air (this is in agreement with the right-hand fracture surface). Another clear example of beach marks found on this side of the fracture surface is shown in figure 40, which is slightly below the area in figure 39.

Specimen 33:

The sequence of environmental changes for specimen 33 was the same as that for specimen 32, except that two blocks were added. Furthermore, the frequency of testing in wet air was 0.003 Hz, and the frequency of testing in dry air was accelerated to 0.5 Hz positive sawtooth loading. This specimen was examined at the NLR.

Figure 41 shows an overview of the right-hand fracture surface of specimen 33; the specimen was tilted 20° in the SEM. The final crack length for the first block was the same as for specimen 32, so examination of the fracture surface was started at $a = 5.1$ mm. As for specimen 32, this is just where shear lips started. The fracture surface was examined in the same way as specimen 32. Figure 42 shows a transition at a magnification of 500 times. At higher magnification, see figure 43, the following sequence appears to be found: dry air, wet air, dry air, wet air (?). This figure also shows a narrow dark band, which may be due to a control failure of the machine (perhaps an overload had occurred).

As before (specimen 32), the left-hand fracture surface of specimen 33 was also examined. Unfortunately, the features on the right-hand fracture surface could not be found on the left-hand side. Figure 44 shows two types of transitions, but not the clear corroded band visible in figure 43. Therefore, it is concluded that this corroded band is not directly a consequence of environmental fatigue.

Specimen 34:

Examination of the previous specimens showed it to be very difficult to find beach marks in the SEM. For specimen 34 it was therefore decided to create a "beach mark" of 1 mm width in wet air. The experiment was started directly in dry air and stopped at $a = 5.1$ mm. The crack growth rate was then approximately 5×10^{-8} m/cycle, so to create a beach mark of 1 mm required 20000 cycles. This specimen was examined at the NLR.

After breaking the specimen, a "dark" band somewhat less than 1 mm was visible to the naked eye, see figure 45; the specimen was tilted 20° in the SEM. As was found before for specimens 29 and 31, at higher magnifications it became more difficult to find the transitions from one environment to the other. Figure 46 is a $100 \times$ magnification of the transition from dry air to wet air (dashed line). It appeared that going from dry air to wet air caused a difference in roughness on the fracture surface. Figure 47 shows the same transition, but now at $1000 \times$ magnification.

Figures 48 and 49 were made to compare the fracture surface features before the transition (in dry air) and after the transition (in wet air). Figure 48 is a $20000 \times$ magnification of fatigue in dry air, showing some striations which are covered by an oxide-layer. Figure 49 was also made at $20000 \times$ magnification, for fatigue in wet air, and shows rough striations covered by an oxide-layer.

Specimen 36:

For specimen 36 it was decided to apply a frequency of 10 Hz sinewave loading during 0.5 mm of crack growth in each environment. The following sequence was applied: laboratory air, wet air, dry air, wet air, laboratory air. The computer programme "fatigue" was used. This specimen was examined at the NLR.

In contrast to specimen 34, where a "dark" band of approximately 1 mm was visible to the naked eye, no differences in fracture surface topography could be seen on the fracture surface of specimen 36, see figure 50. This specimen was also tilted 20° in the SEM. Figure 51 is a $500 \times$ magnification of a possible transition from wet air to laboratory air.

As before, it turned out that indications of a transition became less evident when looking at higher magnifications, see figure 52. The sequence of environmental changes could not be traced on the fracture surface of this specimen.

5.2 Basic da/dN Versus ΔK Tests

5.2.1 Calculation of Crack Growth Rates

In a plot of crack length a versus number of cycles N , the slope da/dN represents the crack growth rate. The crack growth rates for the specimens mentioned in table 1b were calculated from half crack lengths, equal to half the distance between both crack tips, and the number of cycles by using the following incremental formula:

$$\left(\frac{da}{dN} \right)_i = \frac{(a_{i+n} - a_{i-n})}{(N_{i+n} - N_{i-n})} \quad (9)$$

For all tests $n = 10$ was used and calculation of da/dN was started from $i = 10$. The computer programme "fatigue" allows the experimenter to give the number of cycles between data storage. To be certain enough data would be stored during a test, the number of cycles between data storage was set at 100 cycles for every test. When processing the data into crack growth rate versus ΔK plots, the data were sampled using the computer programme Microsoft Excel 5.0 for Windows, in order to reduce the number of data points to 500 before calculating the crack growth rate on the basis of equation 9.

The stress intensity factor range, ΔK was calculated using equation 7 in sub-section 3.4.1.

5.2.2 Fatigue Crack Growth Curves in Laboratory Air, Dry Air, and Wet Air

Ten constant amplitude fatigue crack growth tests were done, according to table 1b. All tests were performed with $\Delta P = 3.99$ kN, $R = 0.05$ and $f = 10$ Hz. Three tests were done in laboratory air with the climate chamber clamped on the specimen. The results of these tests are shown in figure 53. The first test in laboratory air (specimen 37) shows a remarkable change of slope, unlike the other two tests. These are also not identical, but they do not differ much. In addition, two tests in laboratory air were done without the climate chamber, as before to examine the eventual influence of the climate chamber, but now at a lower value of ΔP than was applied for the two experiments described in sub-section 5.1.1. Figure 54 shows the results of these two tests, and figure 55 shows, with omission of specimen 37, a combined plot of the two tests with climate chamber and the two tests without climate chamber. It can be seen that there is some scatter between the four tests, but it is concluded that this is acceptable.

For the tests done in dry air, specimen 38 showed so much scatter that it was assumed that one or more of the Howden voltage pickups had loosened during the experiment. This specimen was omitted from further investigation. The results of the other two experiments are shown in figure 56. It turned out that this experiment did not reproduce well.

For the experiments done in wet air the results are also plotted in one figure, see figure 57. These tests also did not reproduce well, but the two curves are similar in shape. They seem to be translated with regard to each other.

It was expected that testing in dry air would result in a lower fatigue crack growth rate than testing in wet air, see figures 10 and 11, and sub-section 2.2.1. To check this, figure 58 shows a combined plot of the four experiments. Taking into account the rather large scatter bands for all the basic da/dN versus ΔK tests, figure 58 confirms this expectation.

5.2.3 Macrofractography

It was decided to examine the fracture surfaces of the specimens which were used for the basic da/dN versus ΔK tests, to investigate a possible relation between the existence of the transitions in the fatigue crack growth curves in figures 53 to 58, and the formation of shear lips on the fracture surfaces. Specimen 37 was omitted for further investigation, since the scatter and the sudden change of slope with regard to specimens 41 and 42 was assumed to be enormous.

The fracture surfaces were examined using a $10 \times$ magnifying glass. To get an overview of the macroscopic fracture surface examination, the ΔK values at transitions in the fatigue crack growth curves were determined. Then the crack lengths where formation of shear lips started on the left-hand and right-hand fracture surfaces were measured using a ruler with a

mm distribution. It turned out that the formation of shear lips was rather unpredictable, irregular, and often asymmetric even if they formed at all.

Table 6 gives an overview of the results of the macroscopic fracture surface examination. The first column of this table shows the specimen number, the second column gives the ΔK -value at which some kind of transition, or change of slope was found in the fatigue crack growth curves, the third column gives the crack length(s) at which the formation of a shear lip was found on the fracture surfaces, and the fourth column gives the matching ΔK -values calculated with equation 7.

From table 6 it is seen that the correspondence of ΔK values at transitions in the crack growth curves and ΔK values at the start of shear lip formation is by no means definite. Some good correspondences are obtained, but other results differ significantly. The results may be summarised as follows:

1. Laboratory air with climate chamber, specimens 41 and 42: the results agree well.
2. Laboratory air without climate chamber, specimens 44 and 46: no correspondence at all for specimen 44, and a possible agreement for specimen 46.
3. Dry air, specimens 40 and 43: both tests do not seem to agree with respect to the ΔK -values.
4. Wet air, specimens 39 and 51: no correspondence for specimen 39, and two good correspondences for specimen 51.

6 DISCUSSION

This chapter discusses the results of the investigation. The distinction made in chapter 5 between the environmental effect tests, and the basic da/dN versus ΔK tests will be maintained.

6.1 Environmental Effect Tests

6.1.1 Influence of Climate Chamber

The influence of the climate chamber clamped on the specimen is shown in figure 26. Up to a ΔK -value of about $18 \text{ MPa}\sqrt{\text{m}}$ it turned out that fatigue crack growth rates were higher when testing without the climate chamber.

It is assumed that part of the load which was imposed transfers through the climate chamber instead of through the specimen. This explains why testing with the climate chamber results in a lower fatigue crack growth rate. However, it does not explain why the test with the climate chamber results in a higher fatigue crack growth rate above $\Delta K = 18 \text{ MPa}\sqrt{\text{m}}$. This question cannot be answered at the present time (insufficient information).

A possible solution to exclude any influence of the climate chamber, is to build a construction in which the climate chamber is not clamped on the specimen but is attached to bellows on the specimen clamps and rests on a support.

6.1.2 Microfractography

All specimens were subjected to a variation of environment in combination with a variation in frequency. For that purpose the tests were divided into blocks. The number of cycles in these blocks could be varied also. As described in sub-section 5.1.2, six specimens were examined in the SEM.

A remarkable result for specimens 29 and 31 was a transition at low magnification, in the sense of a change of contrast for the parts of the test with dry air and the parts with wet air. However, when examining at higher magnifications the transition disappeared and the expected beach marks could not be found.

For specimen 29 it was thought that the transition from dry air at 10 Hz sinewave loading to 0.0024 Hz sawtooth loading did not show up on the fracture surface, and also that blocks of 100 cycles were not enough. Therefore the blocks were lengthened for specimen 31. Unfortunately, there were still no beach marks on the fracture surface of this specimen, and it is thought possible that a control failure of the machine had occurred.

During examination in the SEM it turned out that the presence of many facets on the fracture surfaces was more of a problem in finding beach marks than expected, especially since Darvish and Johansson [1] found beach marks in the faceted crack growth regime, i.e. the threshold regime. Therefore, when examining a fracture surface in the SEM, flat facets should be looked for first, since it was supposed that beach marks would only show up or be visible on flat facets.

The only specimen for which a good SEM result was obtained was specimen 32. According to the results from specimens 29 and 31, the sequence of testing (dry air, wet air, dry air) was changed to wet air, dry air, wet air. From figure 36 it is concluded that the sequence on this photo was dry air, wet air, laboratory air. It is not known why the first beach mark in wet air could not be found.

At a magnification of 20000 times a photo was made at a distance of 0.5 mm from the last applied environmental change, so this part was certainly tested in laboratory air, see figure 59. In the first testing block at a = 4.5 mm, which was in laboratory air, a photo was made also, but now at a magnification of 50000 times, see figure 60. When compared to figure 59, it can be seen that the fracture surface in figure 60 was heavily corroded.

Testing 80 cycles at a frequency of 0.003 Hz takes 7.4 hours. The first block of testing in wet air results in the earlier formed fracture surface, in laboratory air, also becoming wet. This means that after the second block of testing in wet air, the first block of testing became wet again. As a result, this fracture surface was wet for approximately 15 hours. Most probably, cumulative corrosion is the reason that the first block of testing in wet air, and thus the first transition from laboratory air to wet air, cannot be observed anymore. It was not expected that saturated wet air as a result of bubbling through demineralised water, could result in so much corrosion.

For specimen 33 the testing blocks of 80 cycles in wet air were also performed at a frequency of 0.003 Hz, thus one block takes 7.4 hours. As a result, the first testing block in laboratory air was wet for approximately 25 hours after the third testing block in wet air. Most probably, this time span was sufficient to totally corrode the first-formed fracture surface. Furthermore, the testing blocks in dry air were performed at a frequency of 0.5 Hz. Since no beach marks were found, it is concluded that this frequency was too high for obtaining a fatigue environmental effect.

It was decided to perform some testing blocks at a higher frequency, since Darvish and Johansson [1] found beach marks at a frequency of 10 Hz, but it turned out that an important difference was that their tests were performed in the threshold regime at lower crack growth rates. That way the environment still has time to corrode the fracture surface.

For specimen 34 the 20000 cycles in wet air were performed at a frequency of 0.1 Hz. This means that the first formed fracture surface in dry air was wet for 55 hours. Since this fracture surface was not as much corroded as specimen 32, compare figure 49 with figure 60, it is concluded that a frequency of 0.1 Hz was still too high for the formation of beach marks on the fracture surface, but it was low enough to prevent cumulative corrosion on the fracture surface.

The same conclusion is made for specimen 36: as a result of testing at a frequency of 10 Hz the environment did not have enough time to influence the fracture surface.

For specimen 32 beach marks were found. These beach marks did not show up on the fracture surface as sharp transitions. It is concluded that the transition when going from fatigue crack growth in wet air to fatigue crack growth in dry air, was too gradual. It may be that entrapped water vapour at the crack tip continued to react with the metal for a few cycles. This means that it takes several cycles before the crack is really dry with a relative humidity < 5%. Also, when going from wet air to dry air, the climate chamber was being dried using a hot-air blower. It is possible that drying the climate chamber, and thus the crack, with a hot-air blower is not reproducible for every test. It might be thought feasible to use a vacuum-pump to obtain a dry climate chamber, but according to Wanhill [28], the

transition from air to vacuum also needs some time before the crack advances by genuine vacuum fatigue.

During this investigation, the fatigue testing machine was stopped and halted at S_{\min} between two blocks, to alter the environment. For further investigation it is suggested to stop the machine at a higher value, so that the crack is more open and easier to blow dry. To avoid the occurrence of crack closure, a value of $0.7S_{\max}$ is proposed.

Owing to the 2024-T3 sheet being uneven, some specimens were slightly bent. At first it was thought that this was also one of the reasons that no beach marks were to be found on the fracture surfaces, since the beach marks then would not be formed at the supposed crack lengths. However, after some consideration, this option was rejected, because the specimens have a thickness of just 1 mm, and the fatigue testing machine will easily "stretch" the specimen when it is clamped into the grips of the machine. Furthermore, it is concluded that as a result of testing with the potential drop method, which strikes an average between the formed crack at the left-hand side and the right-hand side, fatigue testing will be done to the correct total crack length.

Not unimportant is the influence of the fatigue testing machine itself. Since stretch zones were sometimes found on the fracture surfaces it is thought that a 100 kN load cell was too heavy for this investigation. As a result tests with $\Delta P = 3.99$ kN were most probably stretching the limit of accuracy of the load cell.

Summarizing all the results, formation of environmentally-induced beach marks on Alclad 2024-T3 sheet turned out to be difficult.

Testing at frequencies in the range from 0.1 Hz to 10 Hz did not result in beach marks on the fracture surfaces. Fatigue testing in alternating environments should be done at a frequency of approximately 0.003 Hz, although a frequency between 0.003 Hz and 0.1 Hz has not been investigated yet. Another option is to perform tests in the threshold region like Darvish and Johansson [1].

Finally, it is suggested to study the formation of environmental beach marks by using marker loads during testing, with which an environmental transition can be defined precisely. A possible method for using marker loads during testing is given by Schulte, Trautmann, and Nowack [29].

They examined the crack growth rate after application of a low-high sequence. It turned out that under this sequence an initial crack acceleration was measured for the high loading cycles, see figure 61. Figure 62 shows SEM-micrographs of the fracture surface. In figure 62a it can be seen that during the increase in load level a step was formed, which is present over the entire width of the specimen. A higher magnification of the shape of the step is given in figure 62b. In this figure the striations formed during the last cycles before the inverse in load level are clearly visible. During the first increase to the maximum load at the high loading level a stretch zone is formed, whereby two ranges of the stretch zone can be distinguished. At first the crack advance occurred perpendicular to the loading direction followed by formation of a "ramp". Figure 62c shows this behaviour schematically. It was thought that the increase of load up to the maximum load at the high loading level increases the stress intensity factor considerably, and with that the size of the plastic zone in front of the crack tip. Along with the formation of the large plastic zone during the first increase in the load, the crack first advances deeply into material regions which were intensively cyclically hardened during the loading period at the low loading level. After penetration through the cyclically hardened region the crack enters material regions which are less cyclically deformed. This may be the reason for the tilt in the crack propagation direction

within the stretched zone in figure 62c. Perhaps these "steps" can be used to better define an environmental transition on the fracture surface.

6.2 Basic da/dN Versus ΔK Tests

6.2.1 Calculation of Crack Growth Rates

It is possible to obtain a large number of $a(N)$ results when using potential drop measurements. Especially during the first part of the test, where crack initiation takes place, a large amount of data is stored. Owing to the discrete measurement levels of the potential drop apparatus, and the fact that no pre-fatigue loading was applied to get a fatigue crack growth increment of several mm, there are many measurement points with the same measured crack length in this regime. Due to this scatter in the potential drop measurements, it is even possible to obtain negative crack growth rate values when calculating the crack growth rate da/dN with equation 9.

Reducing the obtained data to approximately 500 data points eliminates much of the scatter, and a fairly smooth fatigue crack growth curve can be obtained, see figures 53 to 58.

According to equation 9, a constant reduction number n is defined. In the beginning of crack growth where a large number of measurement points are recorded at about the same crack length, a high reduction number n would be needed for smoothing the da/dN . However, in the area of higher da/dN values, the same reduction number covers a far greater crack length increment than in the beginning of crack growth. Since in this area a lower reduction number would be sufficient, a compromise was found in applying $n = 10$. The choice of the reduction number is arbitrary. The best n is that number that gives low scatter without destroying the characteristics of the fatigue crack growth curve [30].

6.2.2 Fatigue Crack Growth Curves in Laboratory Air, Dry Air, and Wet Air

A change of slope similar to that for specimen 37 has been reported in literature [31]. However, several tests agreed, and a sudden change of slope was found in this "master curve", see figure 63. In the case of specimen 37 it is concluded that this curve differs too much from the other two specimens, and that something must have gone wrong during testing.

The two specimens tested in laboratory air without the climate chamber turned out to have the least scatter of all tests. From this it can be concluded that the climate chamber must have had some influence during fatigue testing of the other six specimens. However, the scatter may also be due to the low ΔP -value of 3.99 kN, which is a very low value for the 100 kN load cell of the fatigue testing machine.

From figure 58 it can be seen that the upper curve for testing in dry air practically coincides with the lower curve for testing in wet air. It is not known whether scatter in the fatigue crack growth curves for different environments has its influence on the formation of environmental beach marks, i.e. it is not known whether the fracture surface appearances in wet air and dry air are the same if the fatigue crack growth curves coincide.

6.2.3 Macrofractography

From the macroscopic fracture surface examination it is concluded that there is no obvious relation between the transitions in the fatigue crack growth curves and the formation of shear lips on the fracture surfaces. The results sometimes fit; however, when looking at two nominally identical tests the results can differ completely.

At this moment there is no explanation for the scatter which occurred for the constant amplitude fatigue tests. Furthermore, it is presently not known whether there is any physical relation between the transitions and the formation of shear lips on the fracture surfaces.

7 CONCLUSIONS

To investigate a method for marking the fracture surface of Alclad 2024-T3 sheet material, tests were done for which the environment was changed periodically between dry air and wet air. The following conclusions are drawn from the present investigation:

7.1 Environmental Effect Tests

1. Testing at frequencies ranging from 0.1 Hz to 10 Hz did not result in beach marks on the fracture surfaces when testing in the crack growth range from 10^{-8} m/cycle to 10^{-7} m/cycle.
2. A transition in the same environment to another frequency was not visible on the fracture surfaces.
3. During investigation in the SEM it turned out that it was very difficult to find any flat facets on which beach marks could be found.
4. Water vapour as a result of bubbling through demineralised water resulted in a lot of cumulative corrosion on fracture surfaces which were formed before.
5. When changing from fatigue testing in wet air to fatigue testing in dry air, the crack tip most probably works like a "pump", so that it takes a number of cycles before the crack is really dry with a relative humidity $< 5\%$.
6. It is thought that the tests (all with $\Delta P = 3.99$ kN) were performed with limited accuracy because the fatigue testing machine had a load cell of 100 kN.
7. At the low values of ΔP applied in this investigation some influence of the climate chamber was observed, but whether this had its consequences for the formation of beach marks on the fracture surfaces is still doubtful.
8. The tests performed in this investigation have not resulted in a method for marking the fracture surfaces of Alclad 2024-T3. Further investigation is necessary to improve the method so that markings on the fracture surface can be traced back after a test and enable measurement of crack growth and calculation of crack growth rates.

7.2 Basic da/dN Versus ΔK Tests

1. It turned out that most tests did not reproduce well.
2. The tests performed in dry air had lower crack growth rates than the tests performed in wet air.
3. The fatigue crack growth curves of the tests in laboratory air performed without climate chamber lie within the curves for the tests performed with the climate chamber. From this it may be concluded that the influence of the climate chamber was not large.
4. The formation of shear lips could not be systematically correlated with the transitions found in the fatigue crack growth curves.

8 RECOMMENDATIONS FOR FURTHER INVESTIGATION

A possible test which can be done in line with the recent experiments is a test which starts with testing in laboratory air at 10 Hz sinewave loading up to a crack length $a = 5.1$ mm, followed by testing in wet air at 0.003 Hz sawtooth loading during blocks of 100 or 200 cycles (this should result in a beach mark 5 μm or 10 μm in width). To be certain the crack tip does not contain water vapour anymore before changing the environment to dry air, it is suggested to blow dry air through the climate chamber for approximately 12 hours. The last testing block should be done in dry air at 0.003 Hz sawtooth loading also during 100 or 200 cycles. After this last block of cycles the specimen should be broken directly. This way the wet air can only corrode the first formed fracture surface in laboratory air, which is of minor importance in comparison with the transition from wet air to dry air.

When the specimen is broken directly, it might be easier to determine the location from wet air to dry air in the SEM. However, it is not known whether breaking the specimen directly after 100 or 200 cycles in dry air could damage the beach marks.

Another method suggested for studying the formation of environmental beach marks is the application of marker loads during testing, i.e. applying a marker load at the beginning of an environmental beach mark and a marker load at the end of a block of cycles in a specified environment. The application of marker loads could be done in the way described by Schulte, Trautmann, and Nowack [29], see sub-section 6.1.2. This way it might be possible to determine the exact conditions for formation of beach marks.

At the beginning of this investigation it was also the intention to perform tests with other environments than dry air and wet air, i.e. the following tests were also suggested:

- periodic changes from low humidity air to distilled water or to 0.1% aqueous NaCl
- periodic changes from high humidity air to distilled water or to 0.1% aqueous NaCl
- periodic changes from distilled water to 0.1% aqueous NaCl.

Since wet air created by bubbling through demineralised water already resulted in mud-cracks on the fracture surfaces, it is most probable that this will also occur when testing in distilled water or 0.1% aqueous NaCl. However, this has not been investigated yet.

ACKNOWLEDGEMENTS

First I would like to thank both my supervisors Russell Wanhill and Jan Zuidema for their guidance and stimulating discussions.

I wish to thank all my friends of the section TMC-II for the many pleasant coffee-breaks and lunches which usually consisted of a lot of laughter and discussions.

In particular I wish to thank Bart Wiersma for his help in solving various problems related to computer software, and for the experimental work he did for me during my short stay in the hospital.

I also want to thank Theo van Soest for his technical assistance with the experiments, and Koos Roessen of the laboratory workshop for his suggestions, and helping me with the experimental test set-up.

At the NLR, my special thanks go to Jean-Paul Steyaert for the many long, but pleasant hours we spent working in the SEM.

Finally, I thank my friend Erik for his patience and unfailing support, and his belief in a successful ending of my study at the TU Delft.

REFERENCES

- [1] Darvish, M., and Johansson, S.J., 'The Cyclic Change in the Humidity of the Environment During Fatigue Crack Propagation and its Effect on Fracture Surface Appearance', *Scandinavian Journal of Metallurgy*, **21** (1992), pp. 68-77.
- [2] Jansen, E. F. M., and Wanhill, R. J. H., *The Role of Corrosion in MSD - a Case Study*, NLR Contract Report CR 94335 C, Amsterdam: National Aerospace Laboratory, 1994.
- [3] Mackay, T. L., 'Fatigue Crack Propagation at Low ΔK of Two Aluminium Sheet Alloys, 2024-T3 and 7075-T6', *Engineering Fracture Mechanics*, **11** (1979), pp. 753-761.
- [4] Wanhill, R. J. H., 'Low Stress Intensity Fatigue Crack Growth in 2024-T3 and T351', *Engineering Fracture Mechanics*, **30** (1988), pp. 233-260.
- [5] Van Leeuwen, H. P., *Predicting Material Behaviour Under Load, Time and Temperature Conditions*, AGARD Report 513, 1965.
- [6] Hartman, A., Jacobs, F. A., Nederveen, A., and De Rijk, P., *Some Tests on the Effect of the Environment on the Propagation of Fatigue Cracks in Aluminium Alloys*, NLR Report M.2182, Amsterdam: National Aerospace Laboratory, 1967.
- [7] Wanhill, R. J. H., *Environmental Effects on Fatigue of Aluminium and Titanium Alloys*, AGARD Report 659, 1977.
- [8] Meyn, D. A., 'The Nature of Fatigue Crack Propagation in Air and Vacuum for 2024 Aluminium', *Transactions of the ASM*, **61** (1968), pp. 52-61.
- [9] Hartman, A., and Jacobs, F. A., *An Investigation Into the Effect of Oxygen and Watervapour on the Propagation of Fatigue Cracks in 2024-T3 Alclad Sheet*, NLR Report M.2123, Amsterdam: National Aerospace Laboratory, 1964.
- [10] Wei, R. P., Pao, P. S., Hart, R. G., Weir, T. W., and Simmons, G. W., 'Fracture Mechanics and Surface Chemistry Studies of Fatigue Crack Growth in an Aluminum Alloy', *Metallurgical Transactions*, **11A** (1980), pp. 151-158.
- [11] Bradshaw, F. J., and Wheeler, C., 'The Influence of Gaseous Environment and Fatigue Frequency on the Growth of Fatigue Cracks in Some Aluminum Alloys', *International Journal of Fracture Mechanics*, **5** (1969), pp. 255-268.
- [12] Wei, R. P., *On Understanding Environment-Enhanced Fatigue Crack Growth - a Fundamental Approach, "Fatigue Mechanisms"*, ASTM STP 675, American Society for Testing Materials, pp. 816-840, (1979).
- [13] Henaff, G., Marchal, K., and Petit, J., 'On Fatigue Crack Propagation Enhancement by a Gaseous Atmosphere: Experimental and Theoretical Aspects', *Acta Metallurgica et Materialia*, **43** (1995), pp. 2931-2942.

- [14] Lynch, S. P., *Mechanisms of Fatigue and Environmentally Assisted Fatigue, "Fatigue Mechanisms"*, ASTM STP 675, American Society for Testing Materials, pp. 174-213, (1979).
- [15] Lynch, S. P., 'A Fractographic Study of Gaseous Hydrogen Embrittlement and Liquid-Metal Embrittlement in a Tempered-Martensitic Steel', *Acta Metallurgica*, **32** (1984), pp. 79-90.
- [16] Lynch, S. P., 'Environmentally Assisted Cracking: Overview of Evidence for an Adsorption-Induced Localised-Slip Process', *Acta Metallurgica*, **36** (1988), pp. 2639-2661.
- [17] Selines, R. J., and Pelloux, R. M., 'Effect of Cyclic Stress Wave Form on Corrosion Fatigue Crack Propagation in Al-Zn-Mg Alloys', *Metallurgical Transactions*, **3** (1972), pp. 2525-2531.
- [18] Pelloux, R. M., and McMillan, J. C., *Fatigue Crack Propagation Under Program and Random Loads, "Fatigue Crack Propagation"*, ASTM STP 415, American Society for Testing and Materials, pp. 505-532, (1967).
- [19] Barsom, J. M., 'Mechanisms of Corrosion Fatigue Below K_{ISCC} ', *International Journal of Fracture Mechanics*, **7** (1971), pp. 163-182.
- [20] Mussert, K. M., *Fracture Surface Marking of Alclad 2024-T3 Sheet*, NLR Contract Report CR 94456 C, Amsterdam: National Aerospace Laboratory, 1994.
- [21] Darvish, M., and Johansson, S. J., *Study of Near-threshold Fatigue Crack Growth by Means of Fractography in Two High Strength Al-alloys*, International Conference on Advanced Aluminum and Magnesium Alloys, ASM International, (1990), pp. 615-622.
- [22] Darvish, M., and Johansson, S. J., *The Study of Beach Marks Formation Caused by Cyclic Change in the Humidity of the Environment During Fatigue, "Aluminium Alloys: Their Physical and Mechanical Properties-Proceedings ICAA3"*, Third International Conference on Aluminium Alloys, Trondheim, Norway, (1992).
- [23] The Aluminum Association, *Aluminum Standards and Data*, Metric SI (1978), p. 29.
- [24] Feeney, J. A., McMillan, J. C., and Wei, R. P., 'Environmental Fatigue Crack Propagation of Aluminium Alloys at Low Stress Intensity Levels', *Metallurgical Transactions*, **1** (1970), pp. 1741-1757.
- [25] Wanhill, R. J. H., and Schra, L., *Corrosion Fatigue Crack Arrest in Aluminium Alloys: Basic Data*, NLR Technical Report TR 87128 U, Amsterdam: National Aerospace Laboratory, 1987.
- [26] Newman, Jr., J. C., and Edwards, P. R., *Short-Crack Growth Behaviour in an Aluminum Alloy - an AGARD Cooperative Test Programme*, AGARD Report No. 732, 1988.
- [27] Ewalds, H. L., and Wanhill, R. J. H., *Fracture Mechanics*, fourth reprint, Delft: DUM, 1989, p. 23 and p. 173.

- [28] Wanhill, R. J. H., 'Fractography of Fatigue Crack Propagation in 2024-T3 and 7075-T6 Aluminum Alloys in Air and Vacuum', *Metallurgical Transactions A*, **6A** (1975), pp. 1587-1596.
- [29] Schulte, K., Trautmann, K. H., and Nowack, H., *New Analysis Aspects of the Fatigue Crack Propagation Behaviour by SEM-in Situ Microscopy*, Fatigue Crack Topography, AGARD Conference Proceedings No. 376, 1984.
- [30] Zuidema, J., *Square and Slant Fatigue Crack Growth in Al 2024*, PhD Thesis T.U. Delft, Delft University Press, 1995, pp. 25-27.
- [31] Schra. L., *Constant Amplitude Fatigue Crack Growth Data for the Fokker 100 Lower Wing Skin Material*, NLR Memorandum SM-85-020 U, Amsterdam: National Aerospace Laboratory, 1985.

APPENDIX 1: TABLES

Table 1a Test programme to investigate a method for marking fracture surfaces of 2024-T3 Alclad sheet.

All tests are constant amplitude tests with $\Delta P = 3.99$ kN and $R = 0.05$.

Specimen		block 1	block 2	block 3	block 4	block 5	block 6	block 7
29	frequency	10.0	0.0024	0.0024	0.0024	10.0	-	-
	environment	DRY	DRY	WET	DRY	DRY	-	-
	fatigue loading	sinus	sawt. ^(*)	sawt.	sawt.	sinus	-	-
	remarks	a = 3.62 mm ^(**)	n = 100 ^(***)	n = 100	n = 100	a = 6.0 mm	-	-
30	frequency	10.0	0.003	0.003	0.003	10.0	-	-
	environment	LAB ^(****)	DRY	WET	DRY	LAB	-	-
	fatigue loading	sinus	sawt.	sawt.	sawt.	sinus	-	-
	remarks	a = 3.62 mm	n = 200	n = 200	n = 200	a = 6.0 mm	-	-
31	frequency	10.0	0.003	0.003	0.003	10.0	-	-
	environment	LAB	DRY	WET	DRY	LAB	-	-
	fatigue loading	sinus	sawt.	sawt.	sawt.	sinus	-	-
	remarks	a = 3.62 mm	n = 200	n = 200	n = 200	a = 6.0 mm	-	-
32	frequency	10.0	0.003	0.003	0.003	10.0	-	-
	environment	LAB	WET	DRY	WET	LAB	-	-
	fatigue loading	sinus	sawt.	sawt.	sawt.	sinus	-	-
	remarks	a = 5.1 mm	n = 80	n = 80	n = 80	a = 15.0 mm	-	-
33	frequency	10.0	0.003	0.5	0.003	0.5	0.003	10.0
	environment	LAB	WET	DRY	WET	DRY	WET	LAB
	fatigue loading	sinus	sawt.	sawt.	sawt.	sawt.	sawt.	sinus
	remarks	a = 5.1 mm	n = 80	n = 200	n = 80	n = 200	n = 80	a = 15.0 mm
34	frequency	10.0	0.1	10.0	-	-	-	-
	environment	DRY	WET	DRY	-	-	-	-
	fatigue loading	sinus	sawt.	sinus	-	-	-	-
	remarks	a = 5.1 mm	n = 20.000	a = 15.0 mm	-	-	-	-
35	frequency	10.0	0.9	0.9	0.9	0.9	0.9	10.0
	environment	LAB	WET	DRY	WET	DRY	WET	LAB
	fatigue loading	sinus	sawt.	sawt.	sawt.	sawt.	sawt.	sinus
	remarks	a = 5.1 mm	n = 200	n = 200	n = 200	n = 200	n = 200	a = 15.0 mm
36	frequency	10.0	10.0	10.0	10.0	10.0	-	-
	environment	LAB	WET	DRY	WET	LAB	-	-
	fatigue loading	sinus	sinus	sinus	sinus	sinus	-	-
	remarks	a = 5.1 mm	a = 5.6 mm	a = 6.1 mm	a = 6.6 mm	a = 15.0 mm	-	-

- (*) positive sawtooth loading
- (**) crack growth up to a specific crack length a in mm
- (***) n is the number of cycles
- (****) test performed in laboratory air

Table 1b Test programme to obtain basic fatigue data for the specimen type used in this investigation.

All tests are constant amplitude tests with $\Delta P = 3.99 \text{ kN}$, $R = 0.05$, and $f = 10 \text{ Hz}$.

Specimen	Testing environment	Climate chamber
37	Laboratory air (R.H. ~ 45%)	YES
41	Laboratory air (R.H. ~ 45%)	YES
42	Laboratory air (R.H. ~ 45%)	YES
44	Laboratory air (R.H. ~ 45%)	NO
46	Laboratory air (R.H. ~ 45%)	NO
38	Dry air (R.H. < 5%)	YES
40	Dry air (R.H. < 5%)	YES
43	Dry air (R.H. < 5%)	YES
39	Wet air (R.H. > 95%)	YES
51	Wet air (R.H. > 95%)	YES

Table 2 Calculation of fatigue crack growth life as a function of stress range, ΔS for 2024-T3 CCT specimens over the da/dN range 10^{-8} m/cycle - 10^{-7} m/cycle.

da/dN range: 10^{-8} m/cycle - 10^{-7} m/cycle			
$\Delta K_i = 6.28 \text{ MPa}\sqrt{\text{m}}$			
$\Delta K_f = 9.90 \text{ MPa}\sqrt{\text{m}}$			
ΔS [MPa]	a_i [mm]	a_f [mm]	N [cycles]
10	125.54	311.98	6.16E+6
20	31.38	77.99	1.54E+6
30	13.95	34.66	6.84E+5
40	7.85	19.50	3.85E+5
50	5.02	12.48	2.46E+5
60	3.49	8.67	1.71E+5
70	2.56	6.37	1.26E+5
80	1.96	4.87	9.62E+4
90	1.55	3.85	7.60E+4
100	1.26	3.12	6.16E+4

Table 3 Continuous constant amplitude fatigue crack growth testing times for 2024-T3 in normal air: centre cracked tension specimen with $\Delta S = 70$ MPa.

a _i [mm]	a _f [mm]	ΔK_i [MPa√m]	ΔK_f [MPa√m]	(da/dN) _i [m/cycle]	(da/dN) _f [m/cycle]	n [cycles]	Approximate testing time at cycle frequencies		
							0.003 Hz	0.1 Hz	10 Hz
2.56	6.37	6.28	9.90	10 ⁻⁸	10 ⁻⁷	125.936	486 days	14.6 days	3.50 hours
6.37	15.81	9.90	15.60	10 ⁻⁷	10 ⁻⁶	31.179	120 days	3.6 days	0.87 hours
2.56	15.81	6.28	15.60	10 ⁻⁸	10 ⁻⁶	157.116	606 days	18.2 days	4.36 hours

Table 4 Calculated values of ΔK at specific values of da/dN using equation 4.

da/dN [m/cycle]	ΔK [MPa \sqrt{m}]
2×10^{-8}	7.2
5×10^{-8}	8.6
1×10^{-7}	10.0

Table 5 Calculated values of the crack length a using the values of ΔK from table 4 and equation 7.

ΔK [MPa \sqrt{m}]	a [mm]
7.2	3.62
8.6	5.11
10.0	6.76

Table 6 Overview of the results of macroscopic fracture surface examination of the specimens mentioned in table 1b.

Environment	Specimen	ΔK at transition in crack growth curve [MPa \sqrt{m}]	Start of shear lips	
			Crack length [mm]	ΔK [MPa \sqrt{m}]
Lab. air in chamber	41	11.94	9.3	11.98
	42	8.57	5.5	8.94
Lab. air without chamber	44	6.91	7.0	10.19
		9.29	7.5	10.59
		11.54	11.0	13.39
	46	6.59	6.0	9.37
		10.08	6.5	9.79
Dry air	40	7.73	4.5	8.05
		9.78	5.0	8.50
		10.93	5.7	9.16
		-	6.0	9.37
	43	7.68	4.7	8.23
		8.83	5.0	8.50
Wet air	39	6.68	3.5	7.07
		10.14	4.5	8.05
		-	5.5	8.94
	51	7.13	6.0	9.37
		9.36	6.5	9.79
		9.66	7.5	10.59

APPENDIX 2: FIGURES

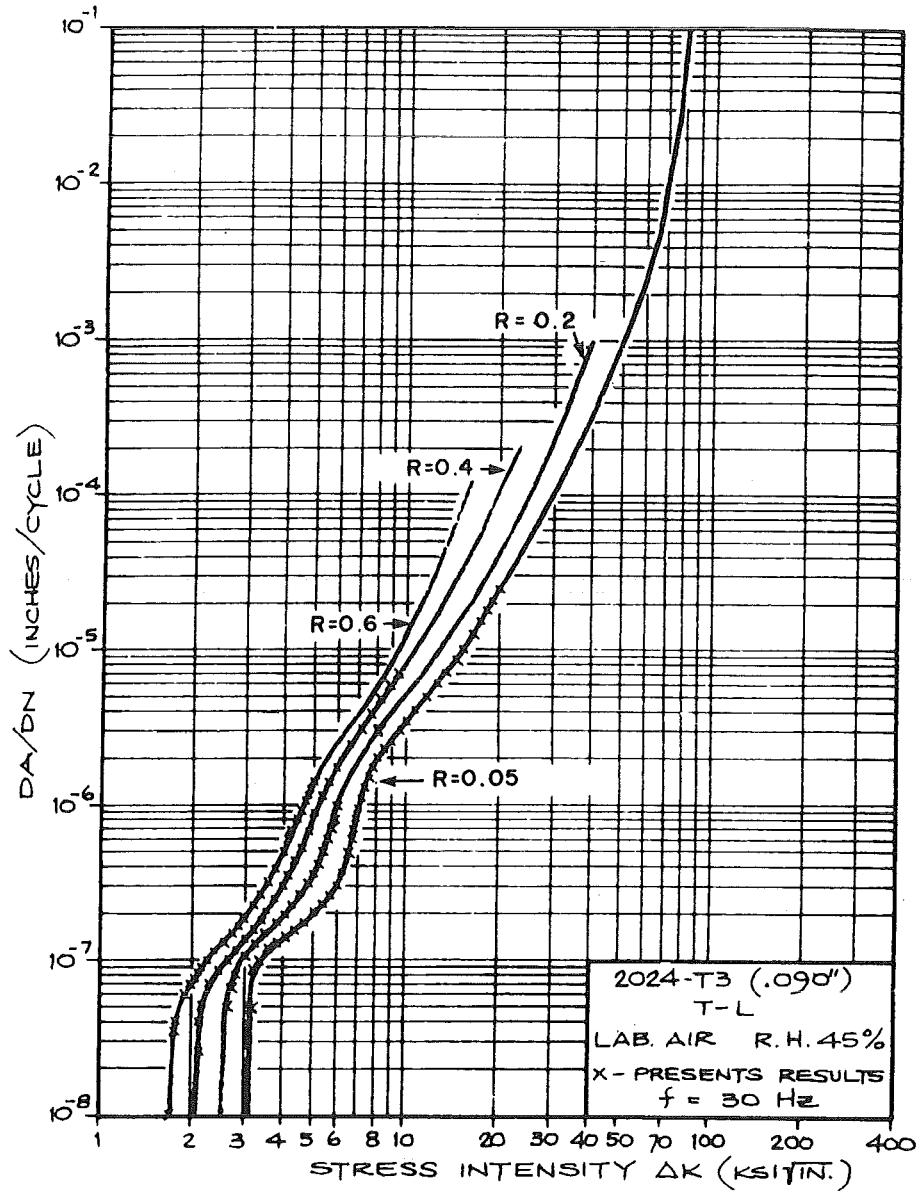


Figure 1 Fatigue crack propagation rates for 2024-T3 sheet material at several stress ratios [3].

ΔK in $\text{ksi}\sqrt{\text{in.}}$ ($1\text{ksi}\sqrt{\text{in.}} \equiv 1.081 \text{ MPa}\sqrt{\text{m}}$)

da/dN in inches/cycle ($1\mu \text{ in/cycle} \equiv 25.4 \text{ nm/cycle}$)

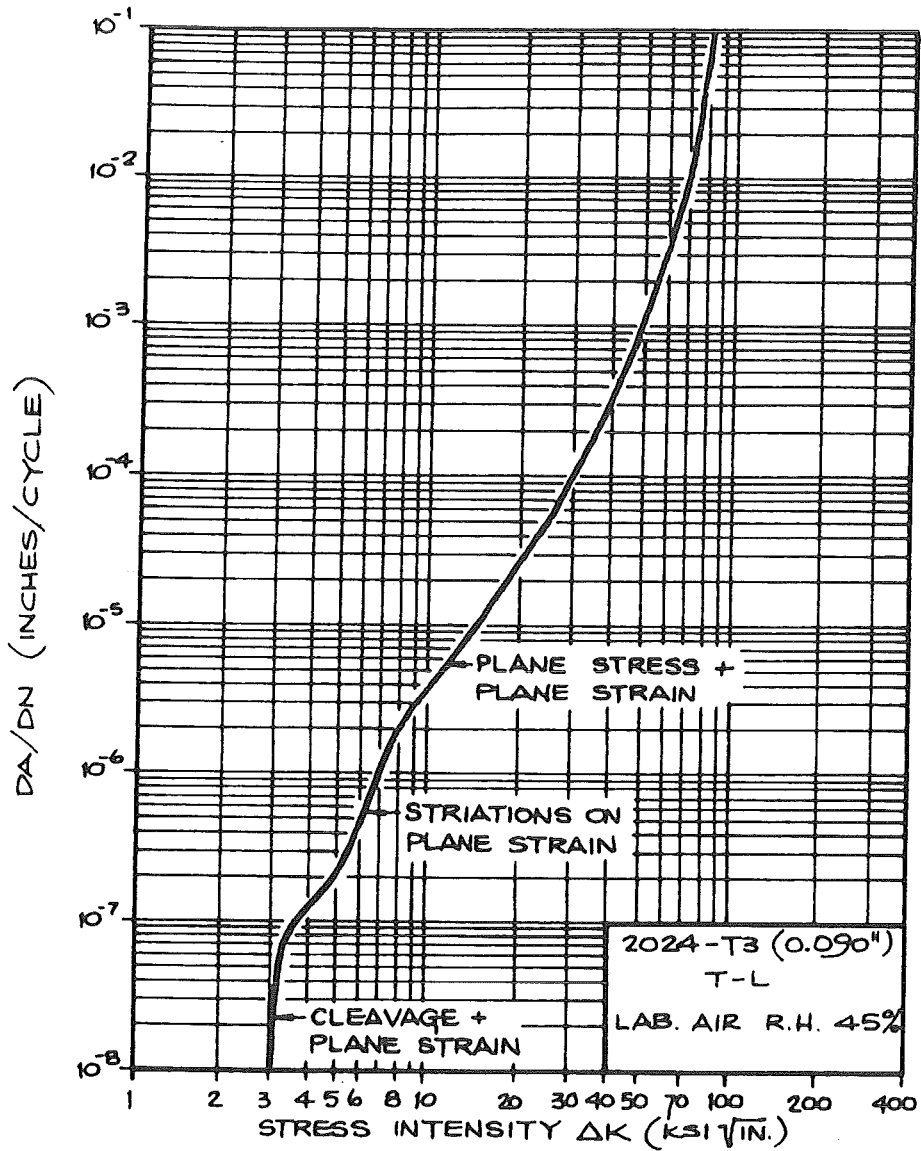


Figure 2 Fractographic features correlated with fatigue crack propagation rates for 2024-T3 sheet material [3].

ΔK in $\text{ksi}\sqrt{\text{in}}$ ($1\text{ksi}\sqrt{\text{in}} \equiv 1.081\text{MPa}\sqrt{\text{m}}$)

da/dN in inches/cycle ($1\mu\text{in}/\text{cycle} \equiv 25.4\text{nm}/\text{cycle}$)

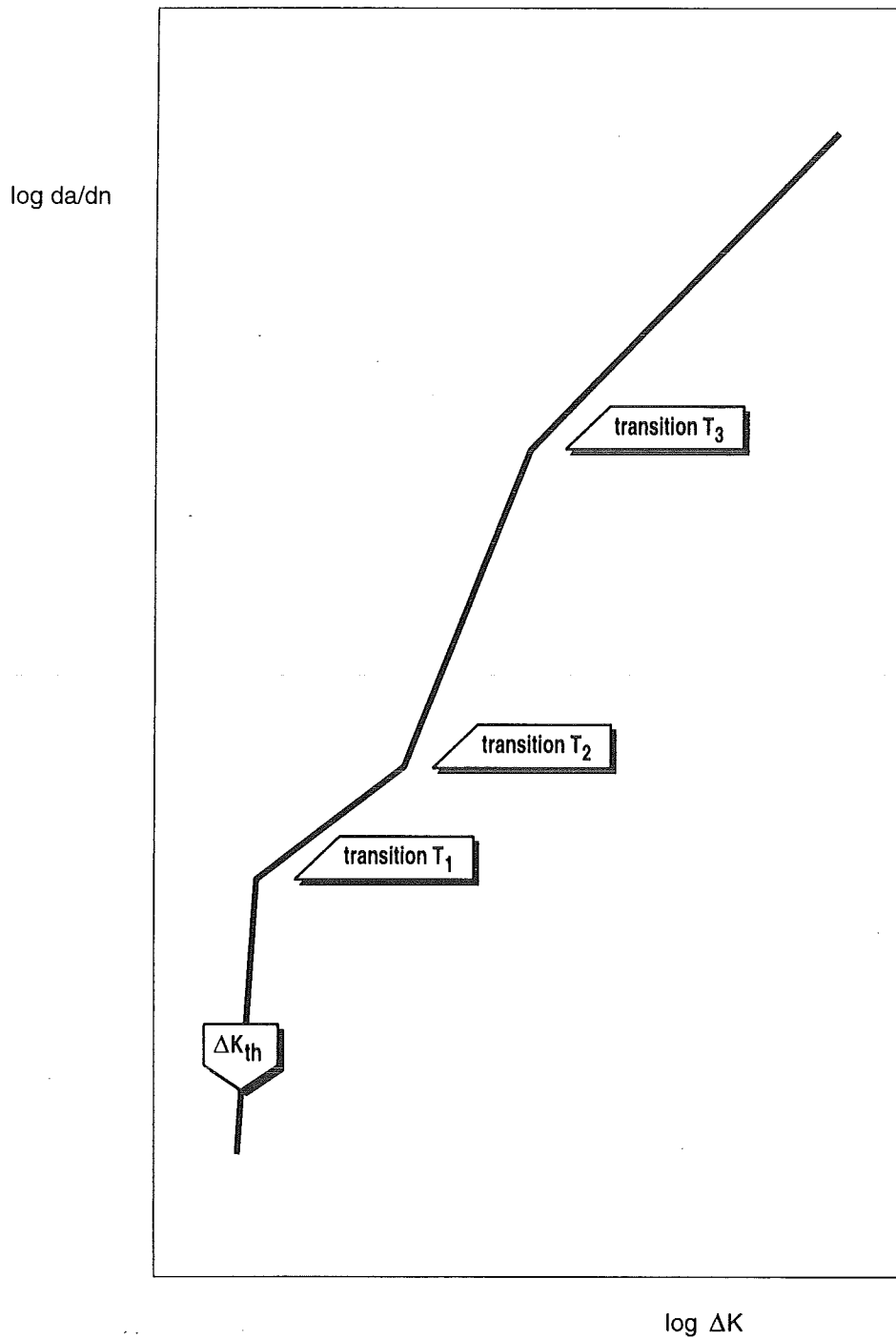


Figure 3 Schematic constant amplitude fatigue crack growth plot for aluminium alloys [4].

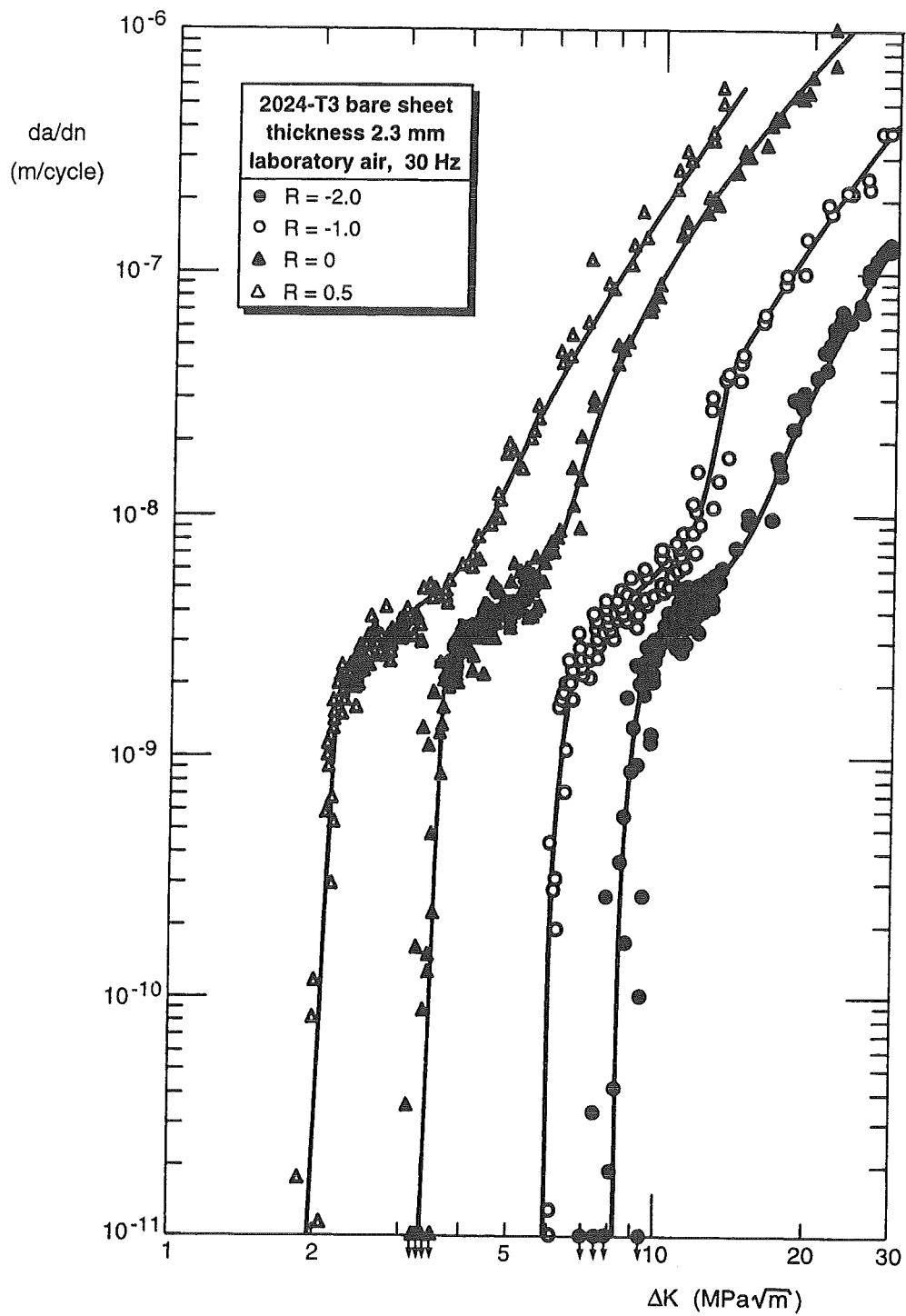


Figure 4 Constant amplitude fatigue crack growth rates for 2.3 mm thick 2024-T3 sheet [4].

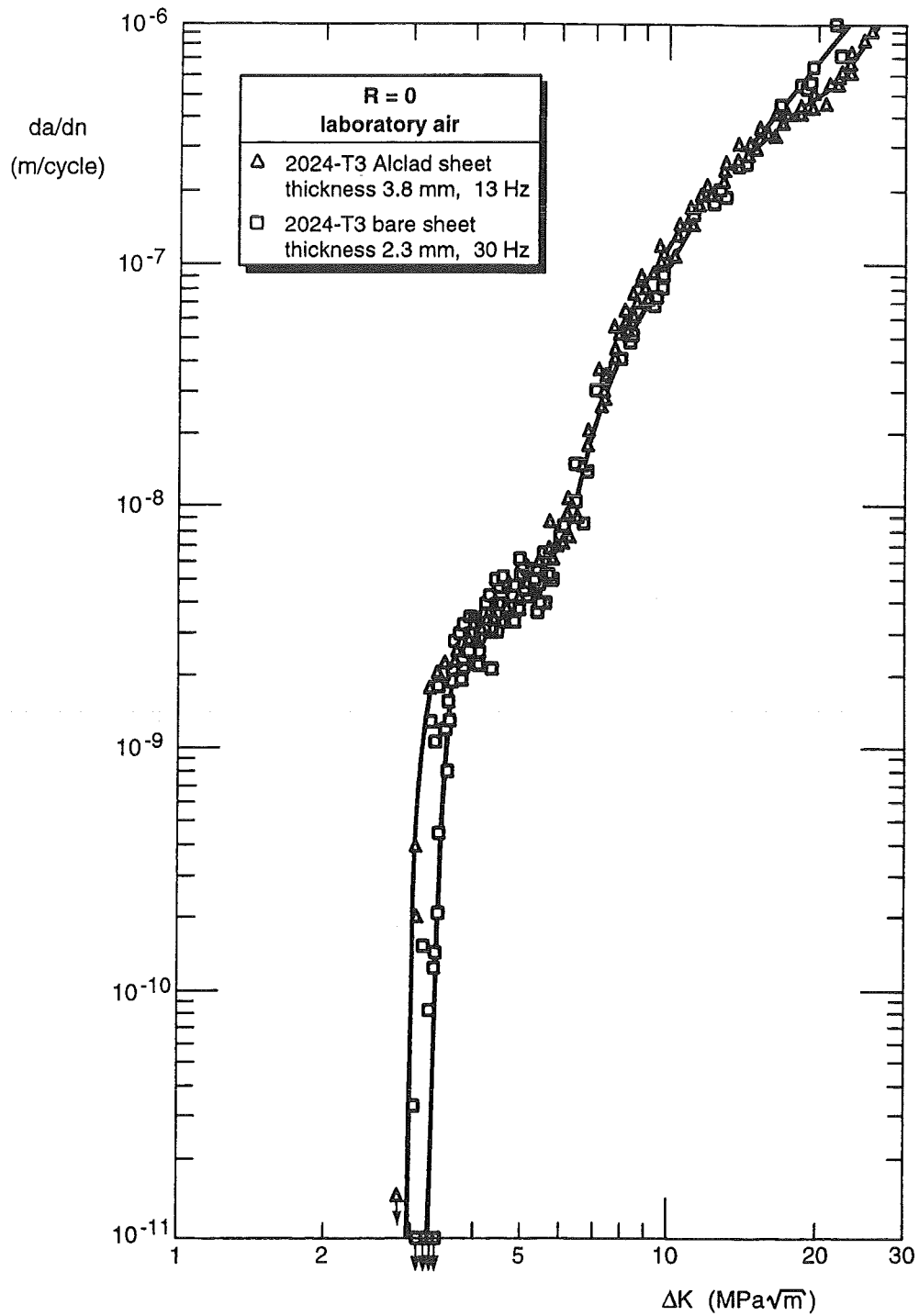


Figure 5 Comparison of constant amplitude fatigue crack growth rates for $R = 0$ [4].

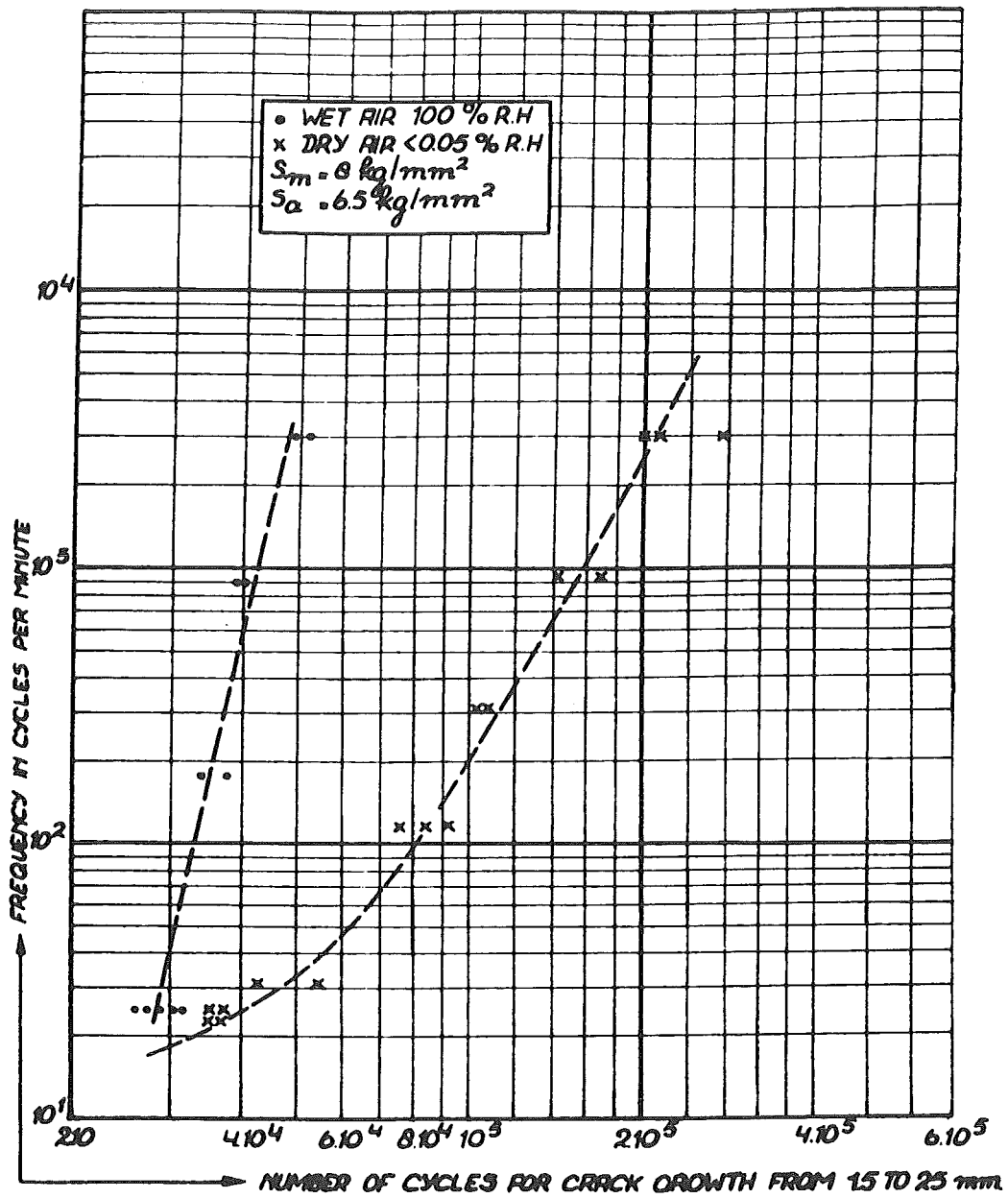


Figure 6 The effect of the load frequency on crack growth in 2024-T3 Alclad with wet or dry air as the environment [6].

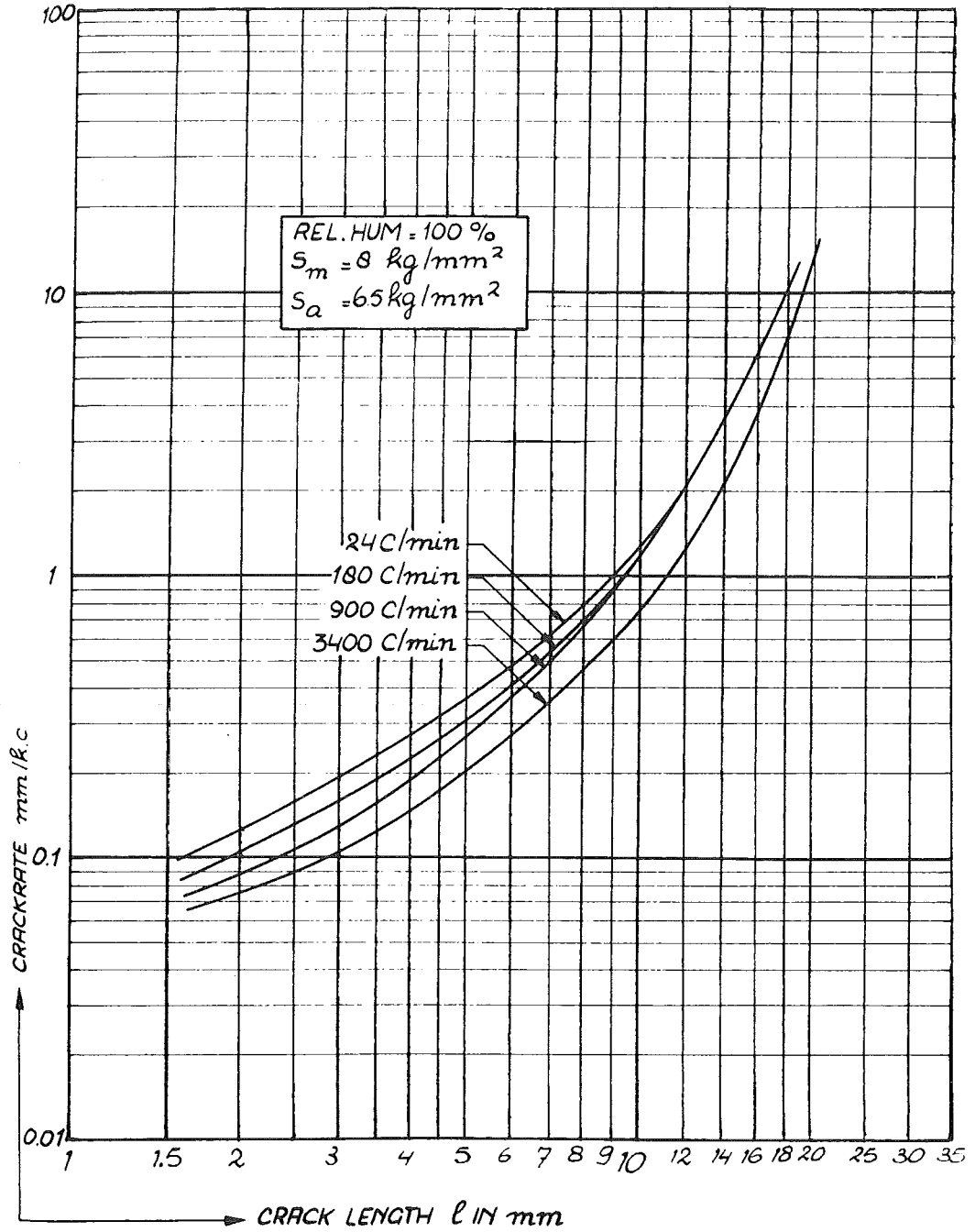


Figure 7 Crack growth rate of 2024-T3 Alclad in wet air with various frequencies of loading [6].

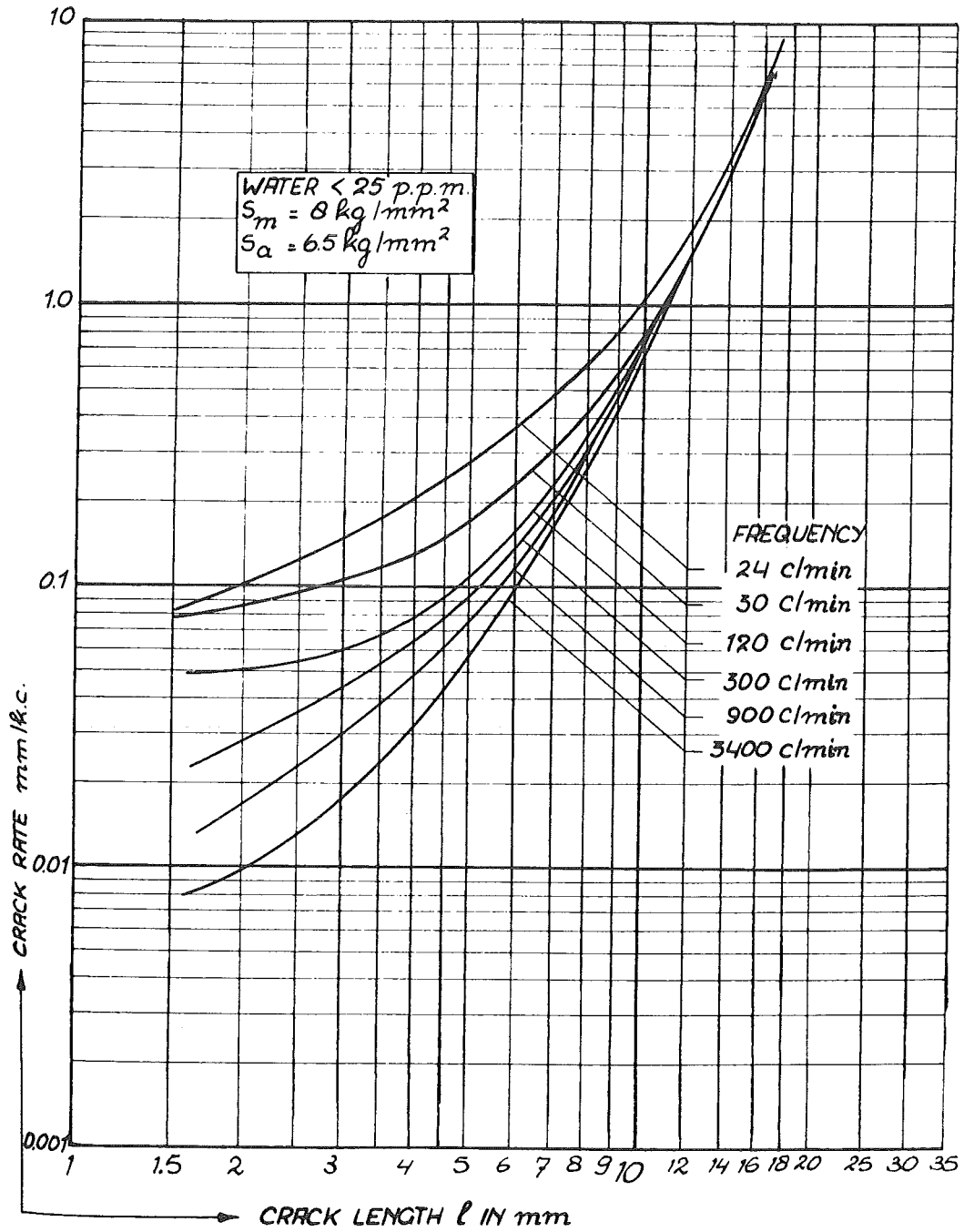


Figure 8 Crack growth rate of 2024-T3 Alclad in dry air with various frequencies of loading [6].

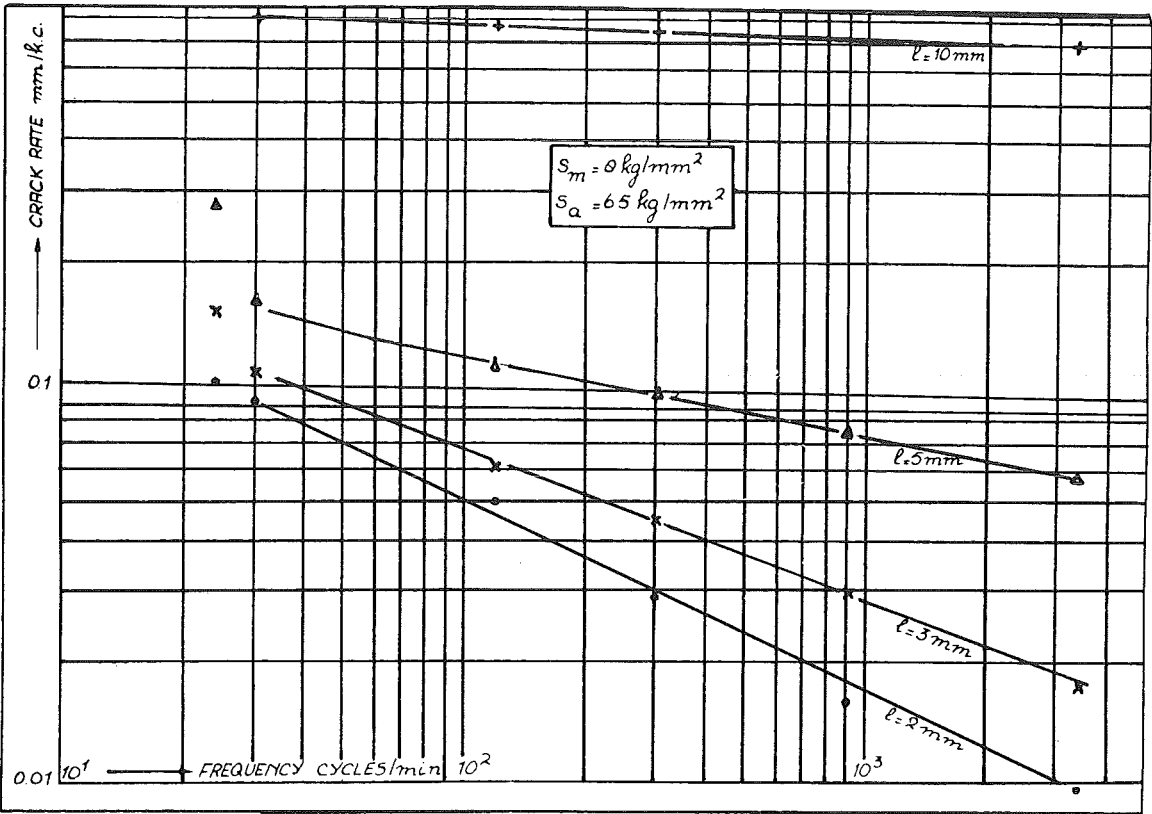


Figure 9 The mean crack growth rates in figure 8 at crack lengths of 2, 3, 5, and 10 mm versus the load frequency [6].

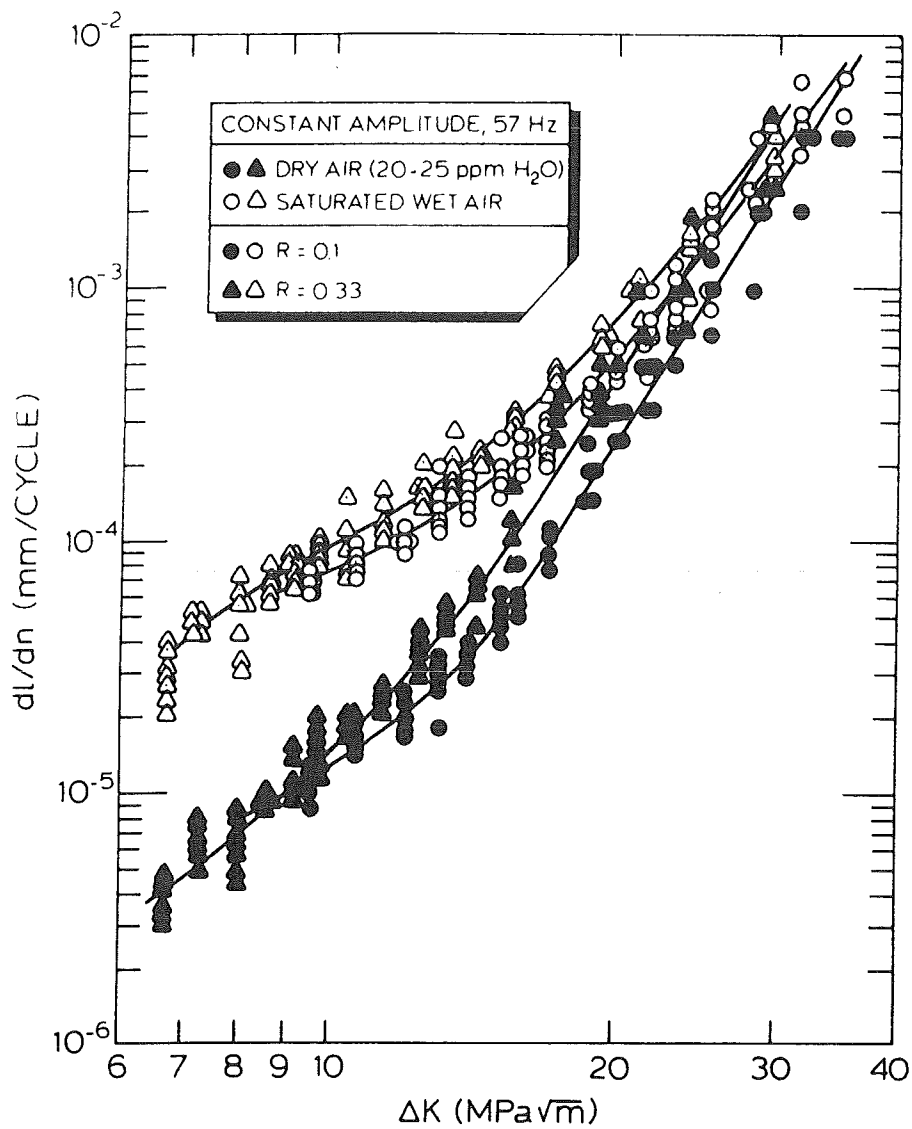


Figure 10 Fatigue crack propagation of 2024-T3 Alclad sheet in dry air and in saturated wet air at 57 Hz [7].

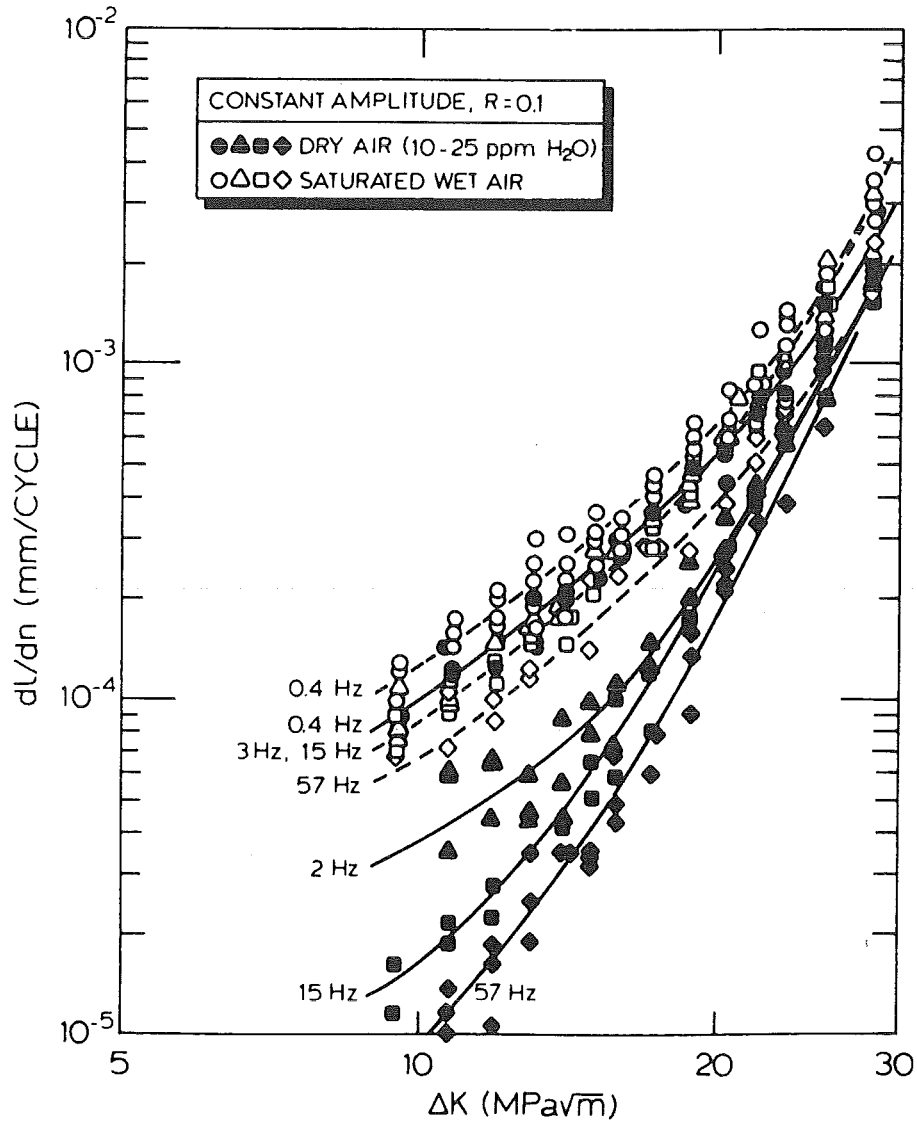


Figure 11 Frequency effects on 1 mm 2024-T3 Alclad sheet [7].

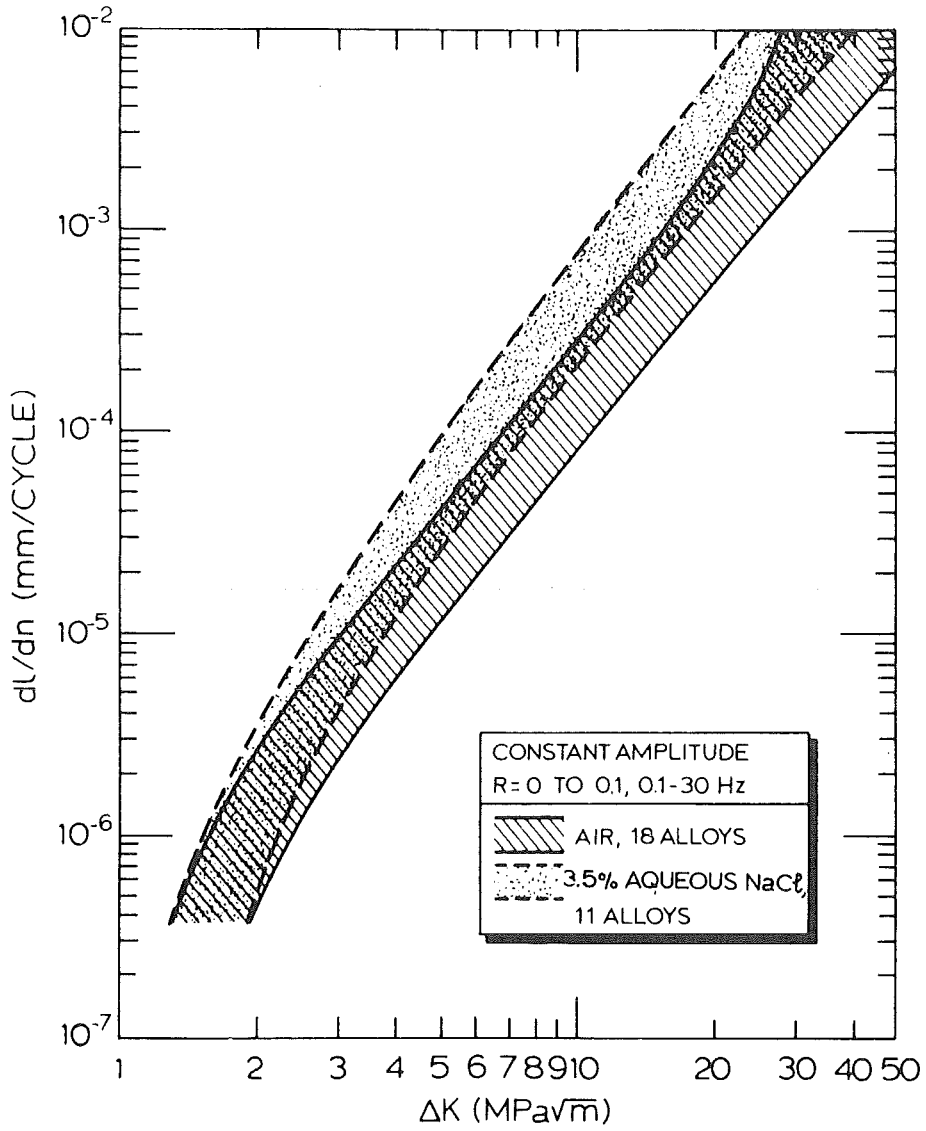


Figure 12 Crack growth rate curves in air compared with curves in aqueous NaCl [7].

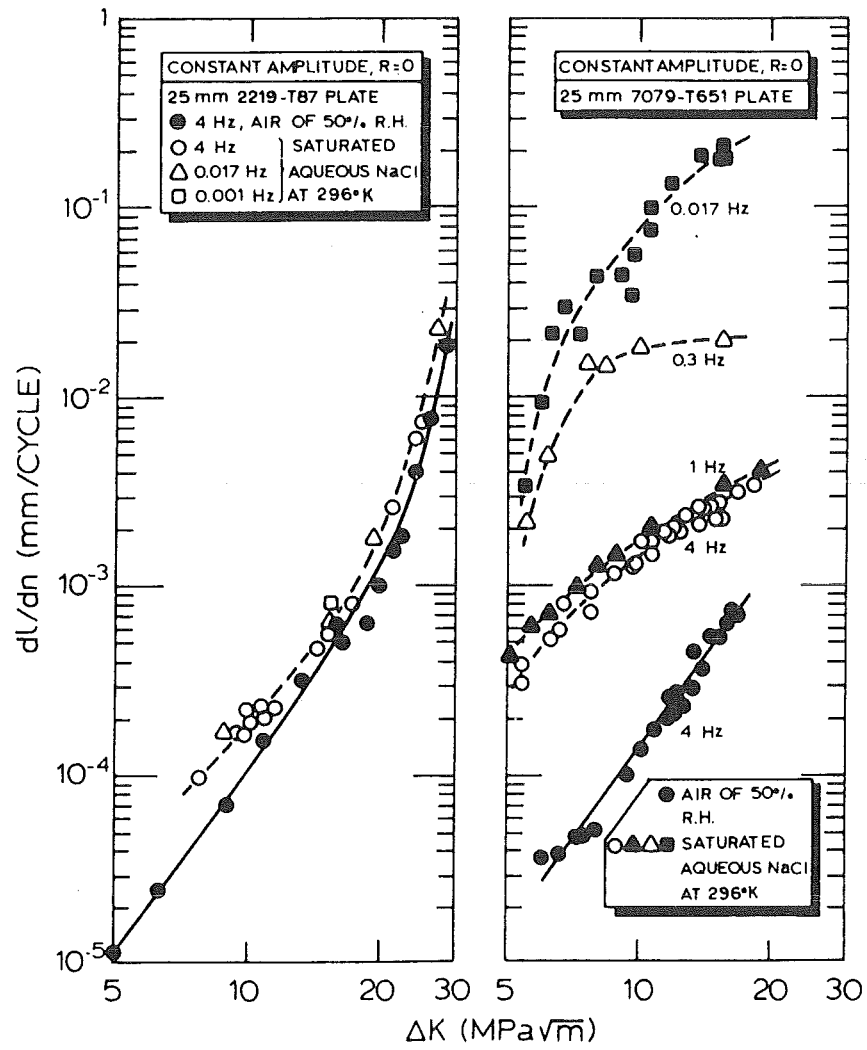


Figure 13 Frequency effects for crack growth in plate materials [7].

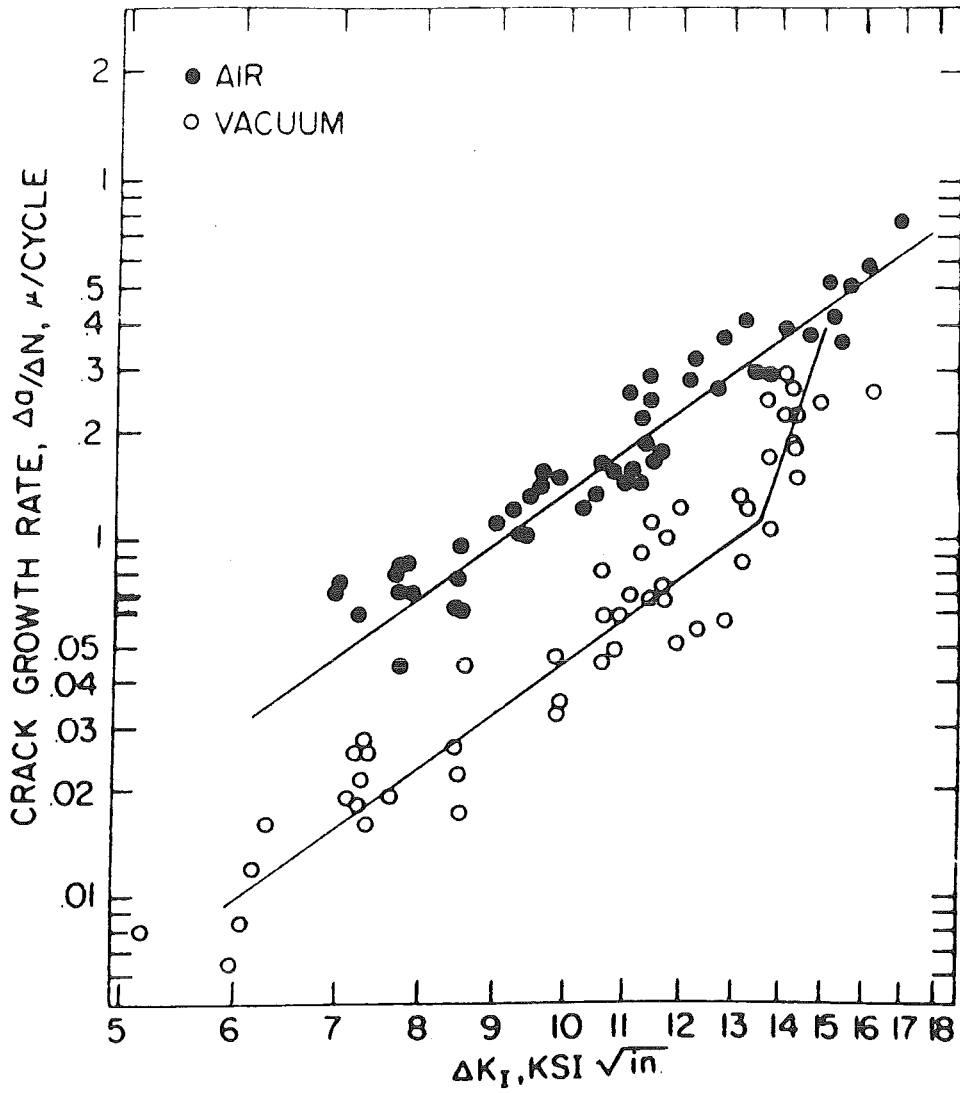


Figure 14 Crack growth rate da/dN as a function of the stress intensity amplitude, ΔK_I , for 2024-T3 aluminium in air and in vacuum [8].

ΔK in $ksi\sqrt{in}$ ($1ksi\sqrt{in} \equiv 1.081 MPa\sqrt{m}$)
 da/dN in inches/cycle ($1\mu in/cycle \equiv 25.4 nm/cycle$)

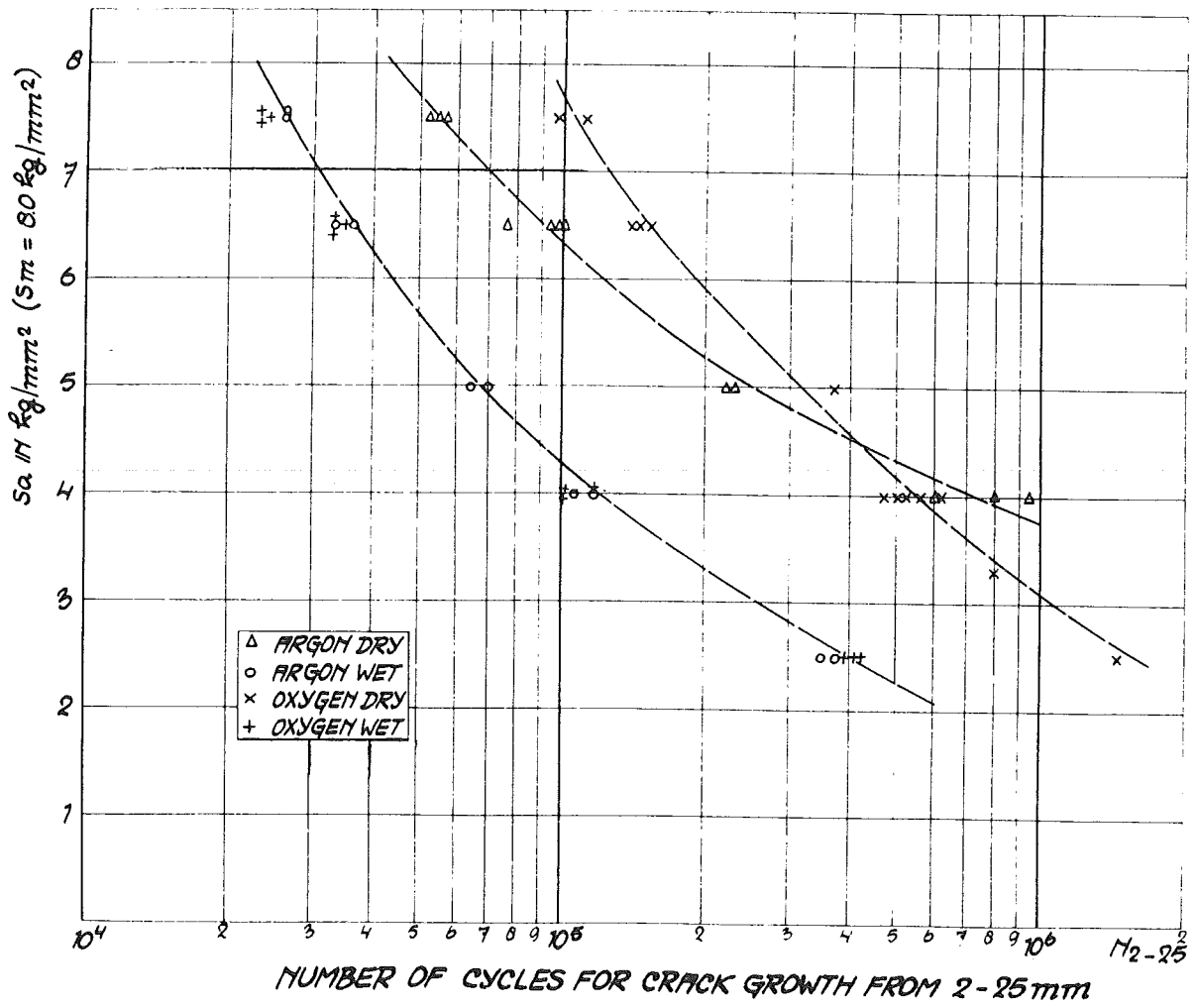


Figure 15 S-N curves for crack growth from 2 to 25 mm in dry and wet argon and in dry and wet oxygen for 2024-T3 Alclad sheet [9].

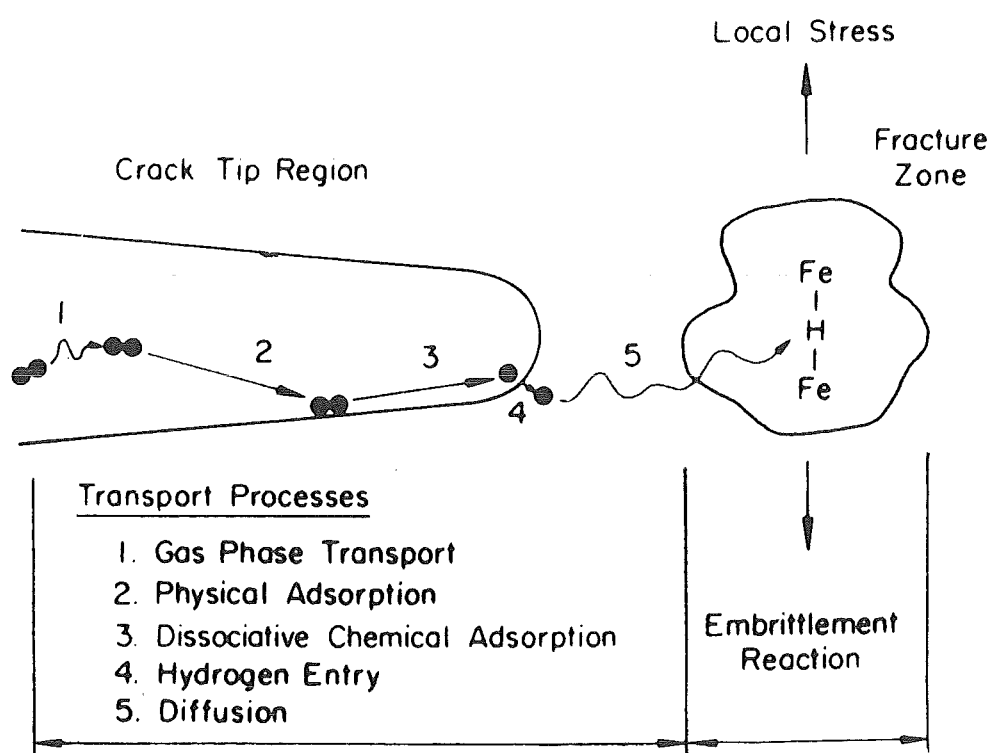


Figure 16 Schematic illustration of various sequential processes involved in embrittlement by external gaseous environments. (Embrittlement reaction is depicted schematically by the iron-hydrogen-iron bond) [12].

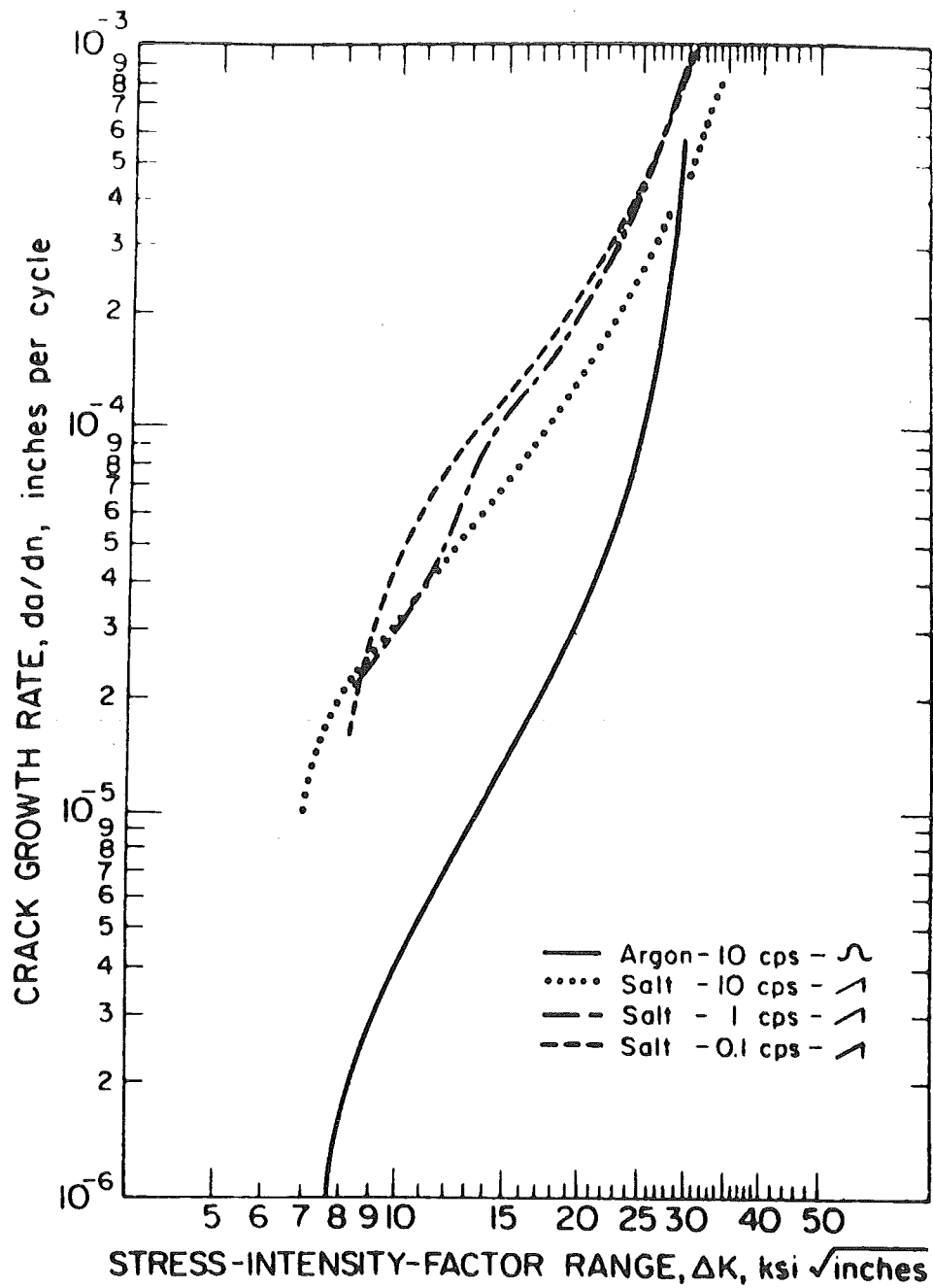


Figure 17 Crack growth rates for 7075-T6 alloys in a sodium chloride solution at 0.1, 1, and 10 Hz with dry argon used as a reference [17].

ΔK in $\text{ksi}\sqrt{\text{in}}$ ($1\text{ksi}\sqrt{\text{in}} \equiv 1.081\text{MPa}\sqrt{\text{m}}$)

da/dN in inches/cycle ($1\mu\text{in}/\text{cycle} \equiv 25.4\text{nm}/\text{cycle}$)

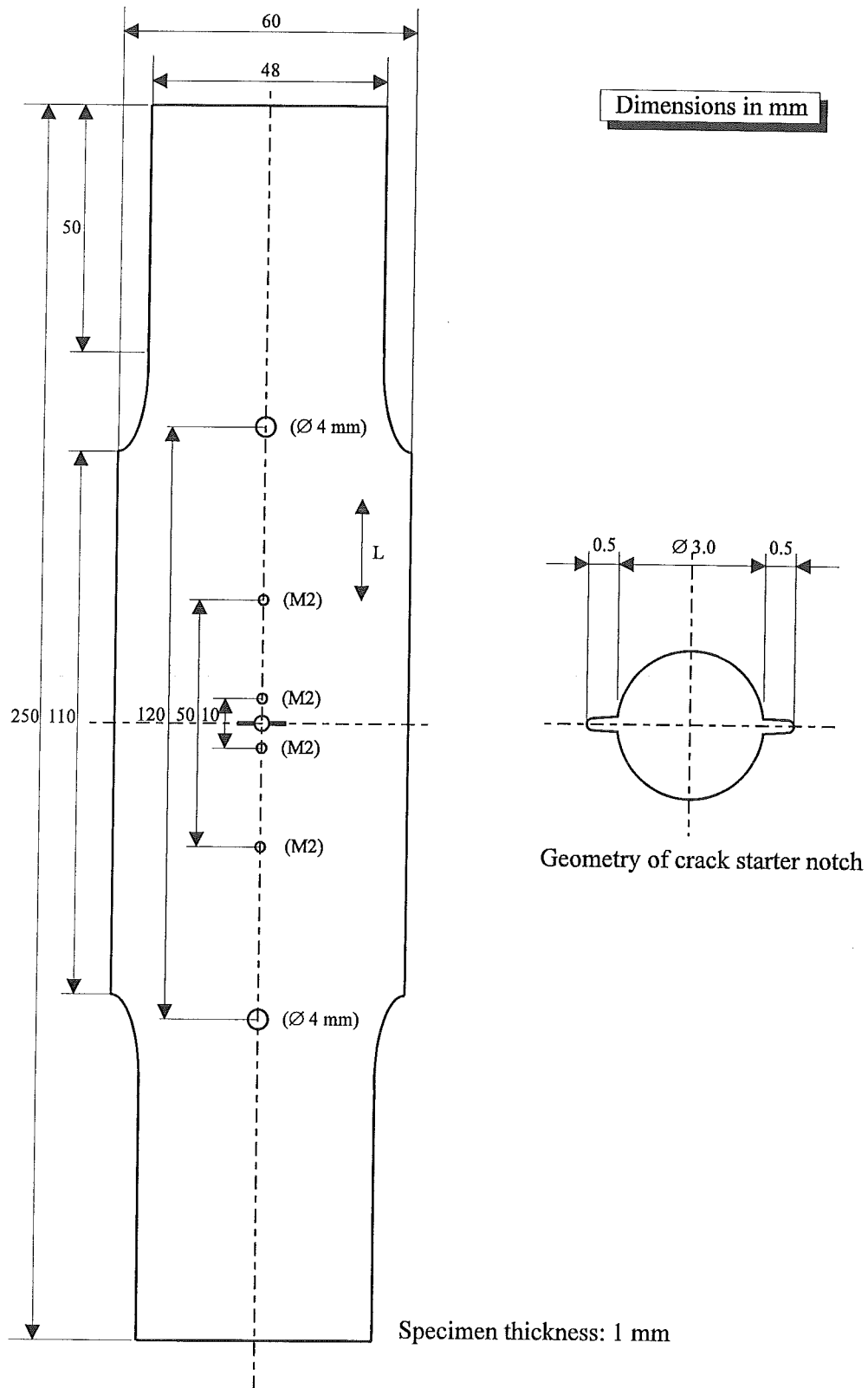


Figure 18 Centre cracked tension (CCT) specimen used for all tests: L is the longitudinal (= rolling) direction of the sheet material. Only the first and second tap were used for the cylindrical holes M2.

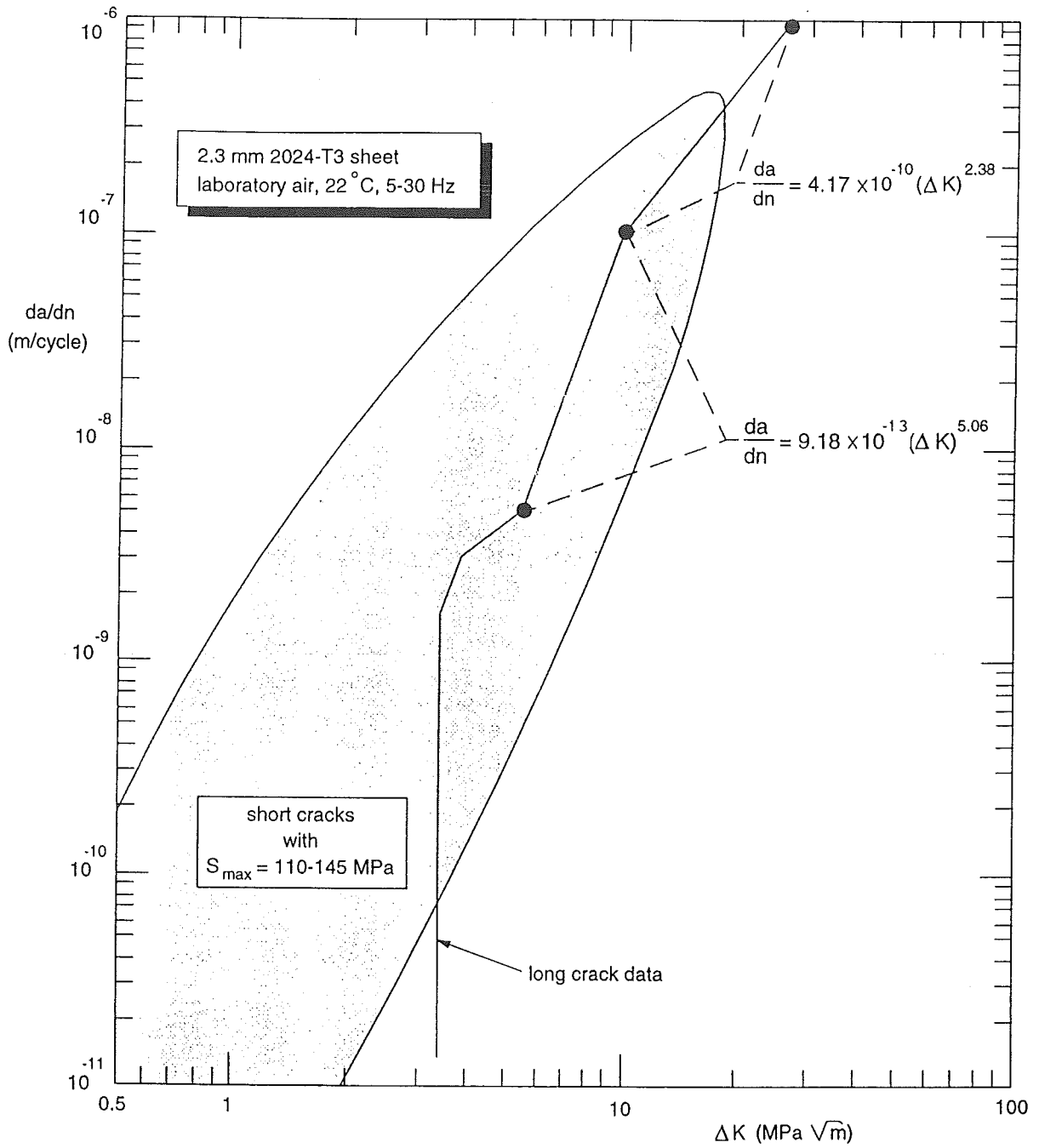


Figure 19 Summary of short and long fatigue crack growth data in 2024-T3 sheet alloy at a stress ratio $R = 0$ [26].

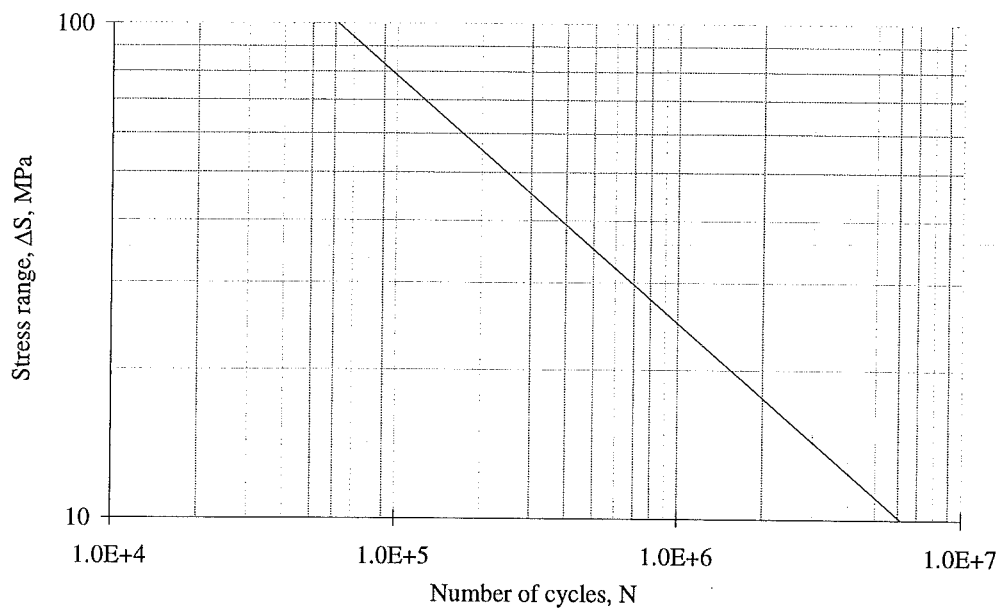


Figure 20 Fatigue crack growth life as a function of stress range, ΔS for 2024-T3 CCT specimens over the da/dN range 10^{-8} m/cycle - 10^{-7} m/cycle.

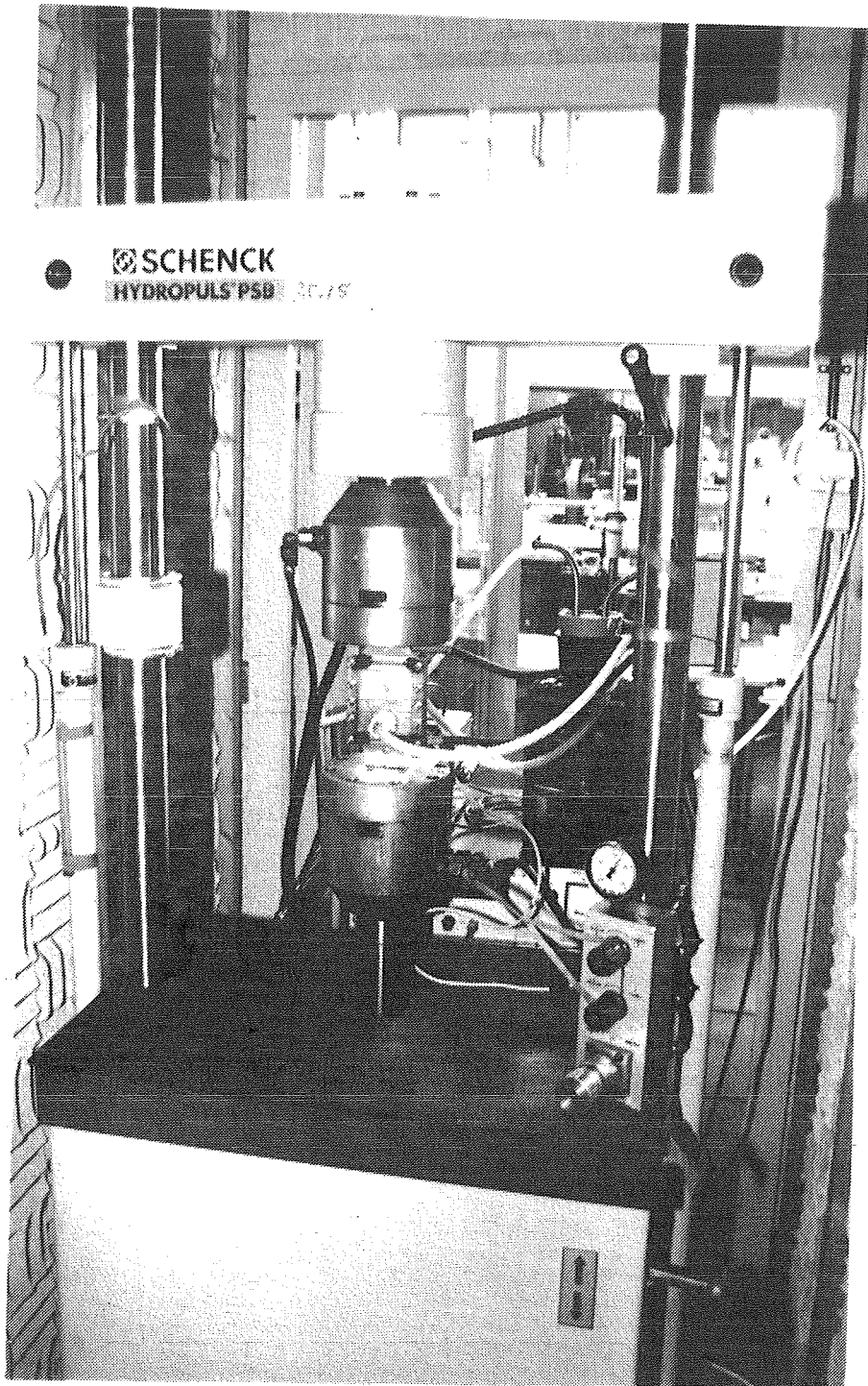


Figure 21 Overview of the experimental test set-up.

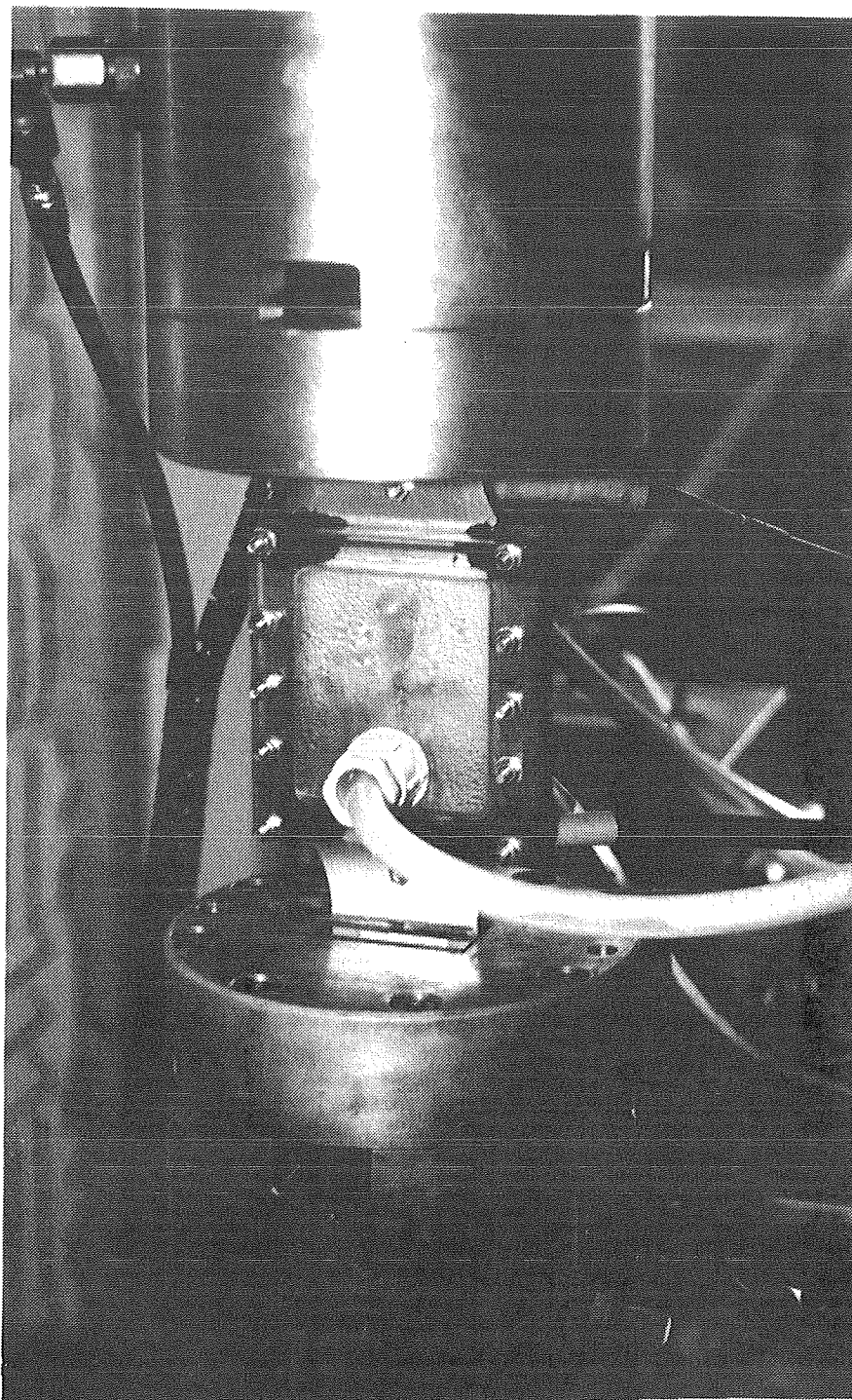


Figure 22 Front view of the climate chamber clamped on the specimen.

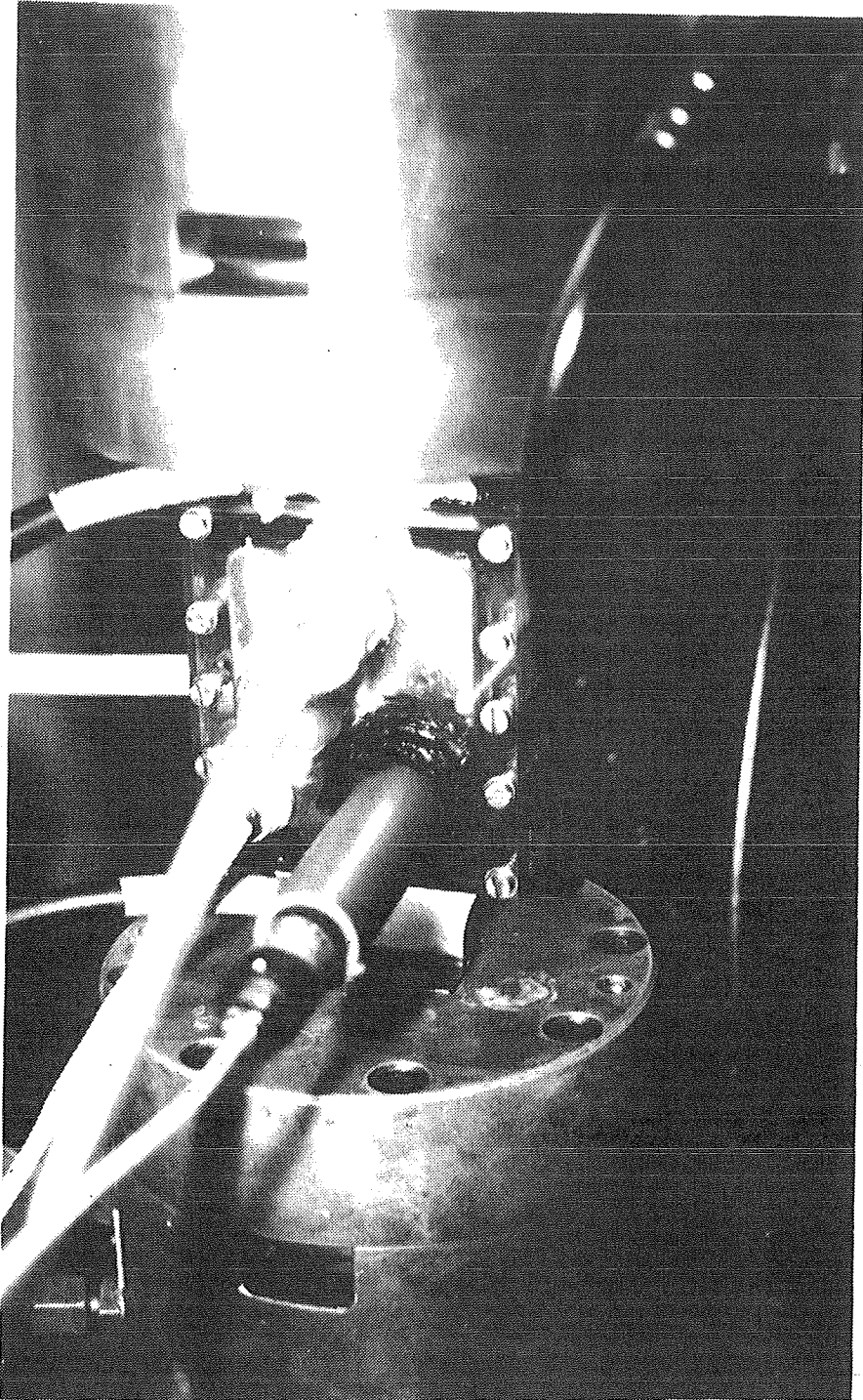


Figure 23 Rear view of the climate chamber clamped on the specimen.

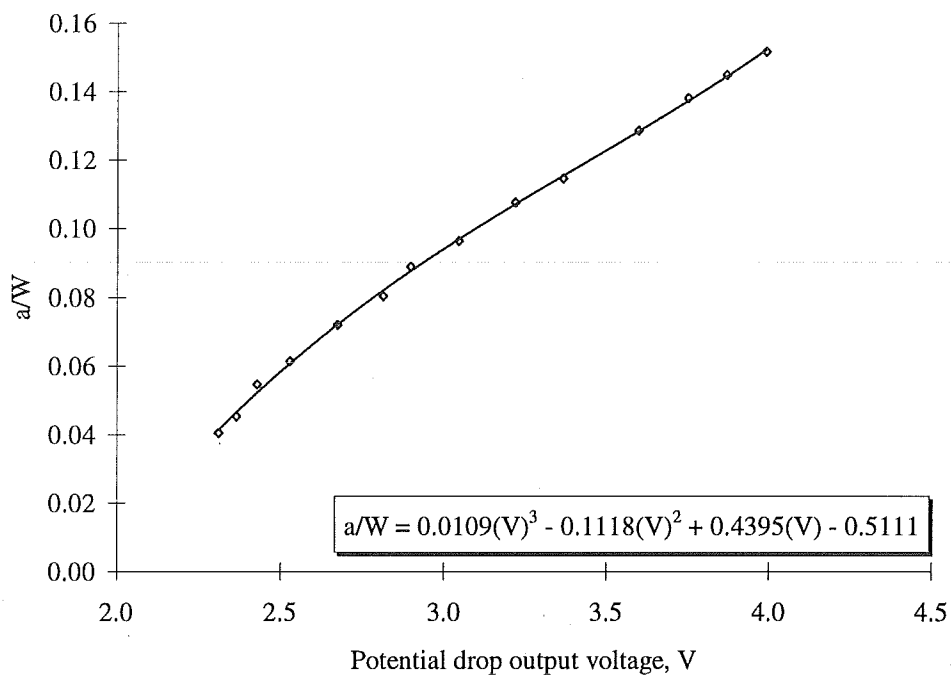


Figure 24 Potential drop calibration curve for the specimen type used during this investigation.

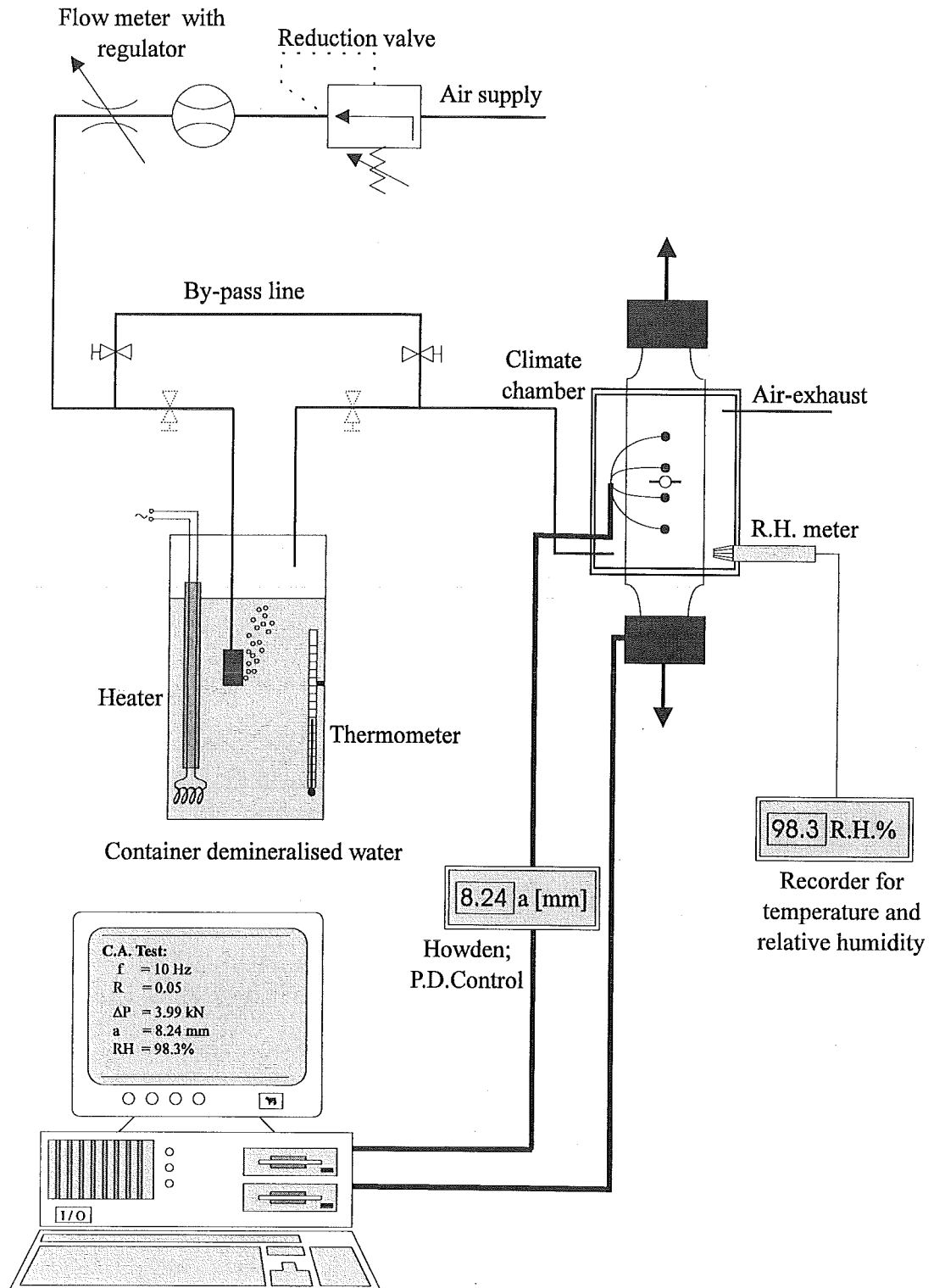


Figure 25 Schematic illustration of the experimental test set-up. The connections between the different stages consist of silicone tubes, except for the connections to the computer and the R.H. meter.

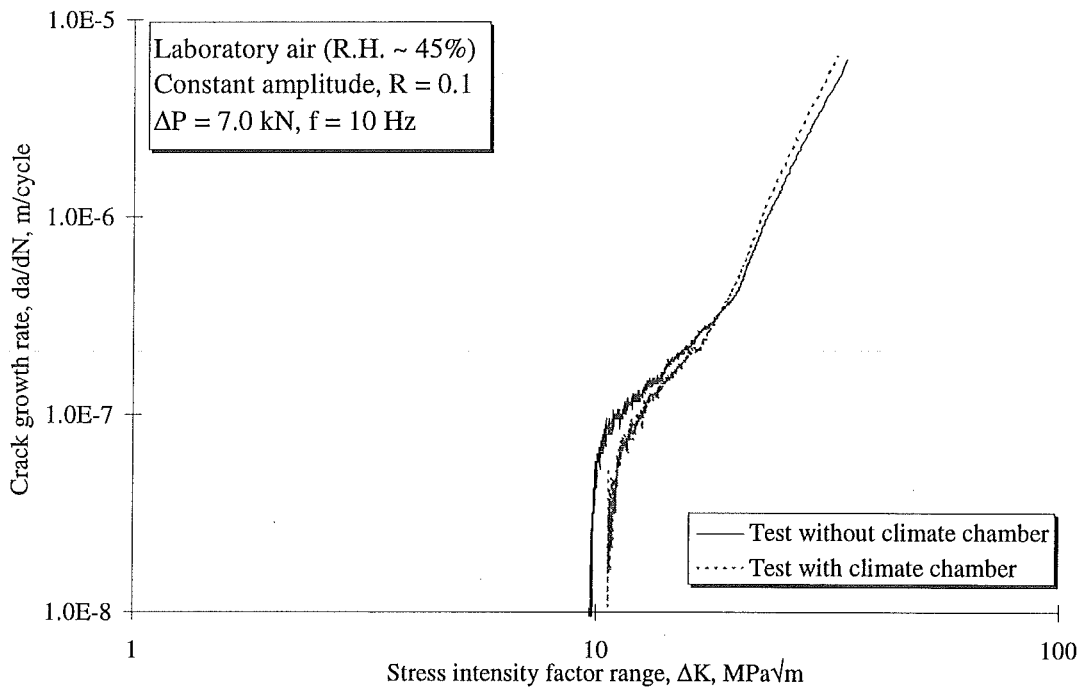


Figure 26 Crack growth rate da/dN versus stress intensity factor range ΔK for comparison of a test with climate chamber and a test without climate chamber.

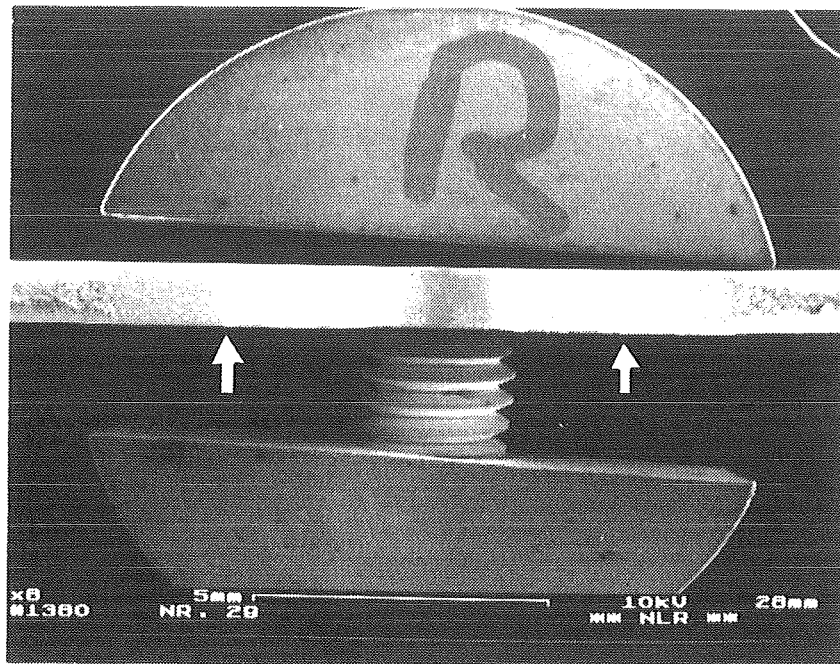


Figure 27 Overview of the fracture surface of specimen 29 at a magnification of 8 times. The arrows indicate the transition from dry air to wet air.

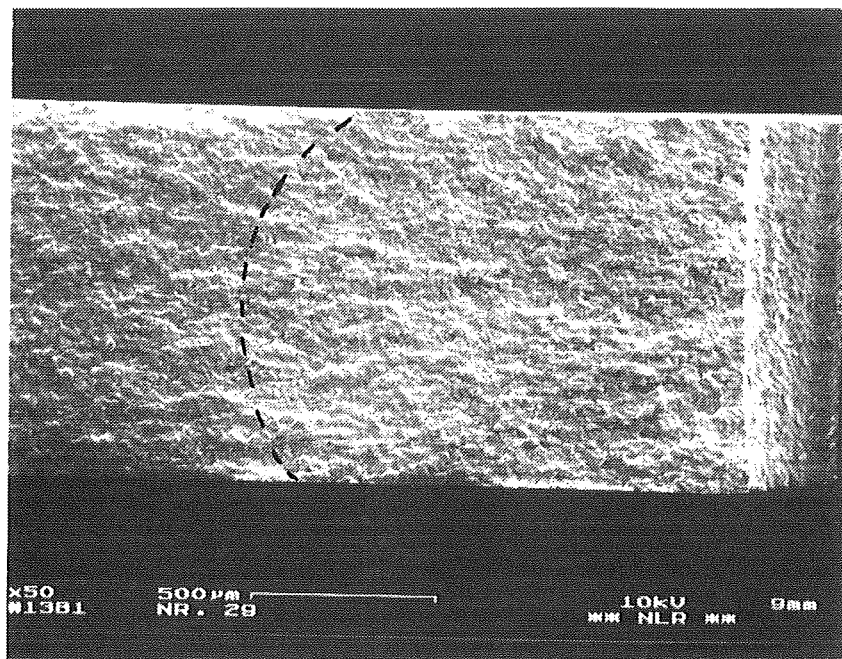


Figure 28 Probable transition on the left-hand fracture surface of specimen 29 at a magnification of 50 times: crack growth from right to left.

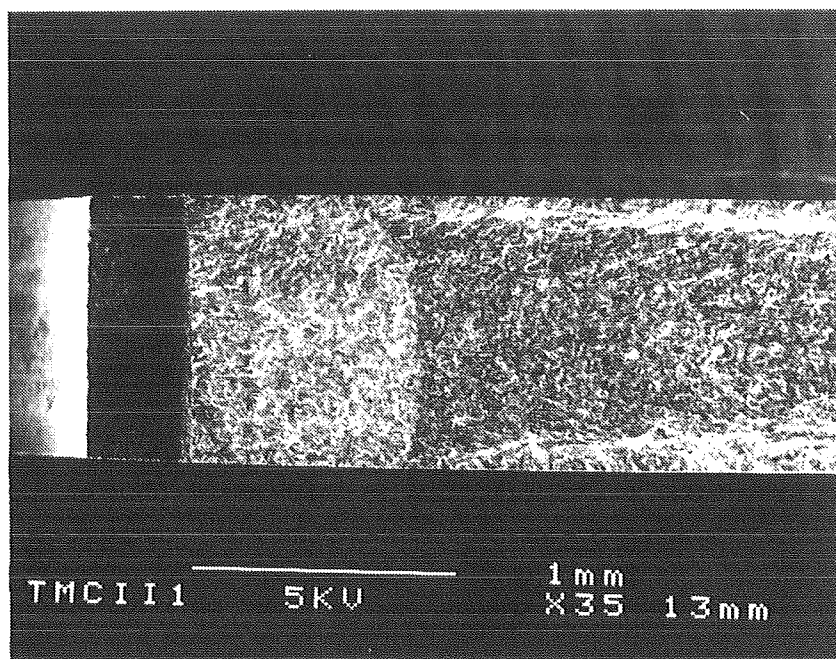


Figure 29 Transition on the right-hand fracture surface of specimen 31 at a magnification of 35 times.

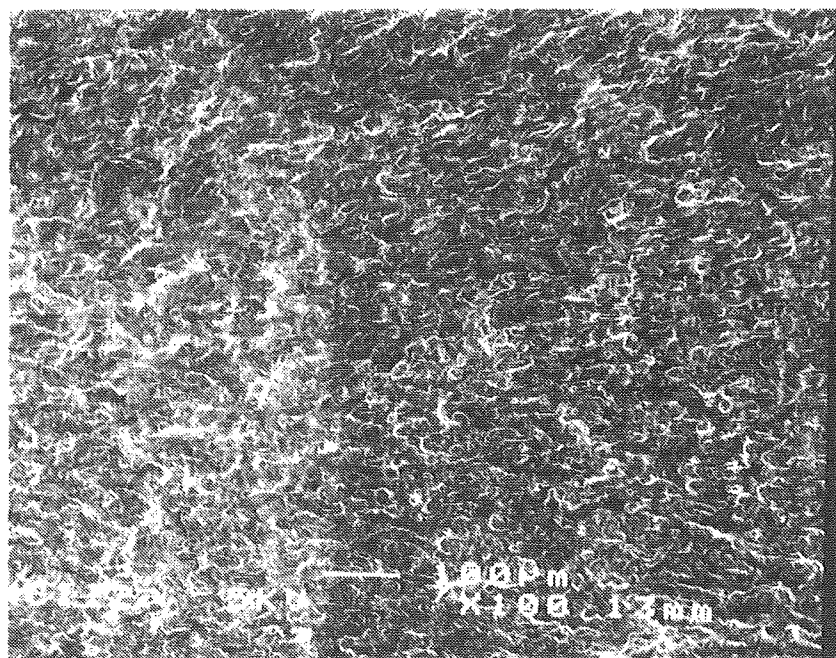


Figure 30 Transition on the right-hand fracture surface of specimen 31 at a magnification of 100 times: crack growth from left to right.

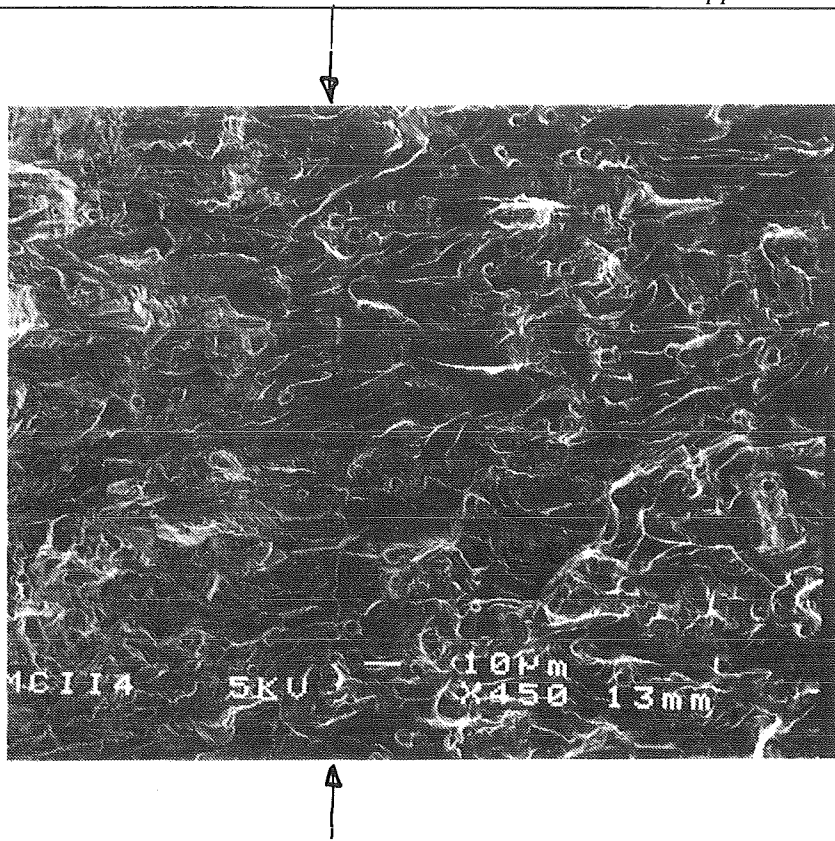


Figure 31 Transition or stretch zone on the right-hand fracture surface of specimen 31 at a magnification of 450 times: crack growth from left to right.

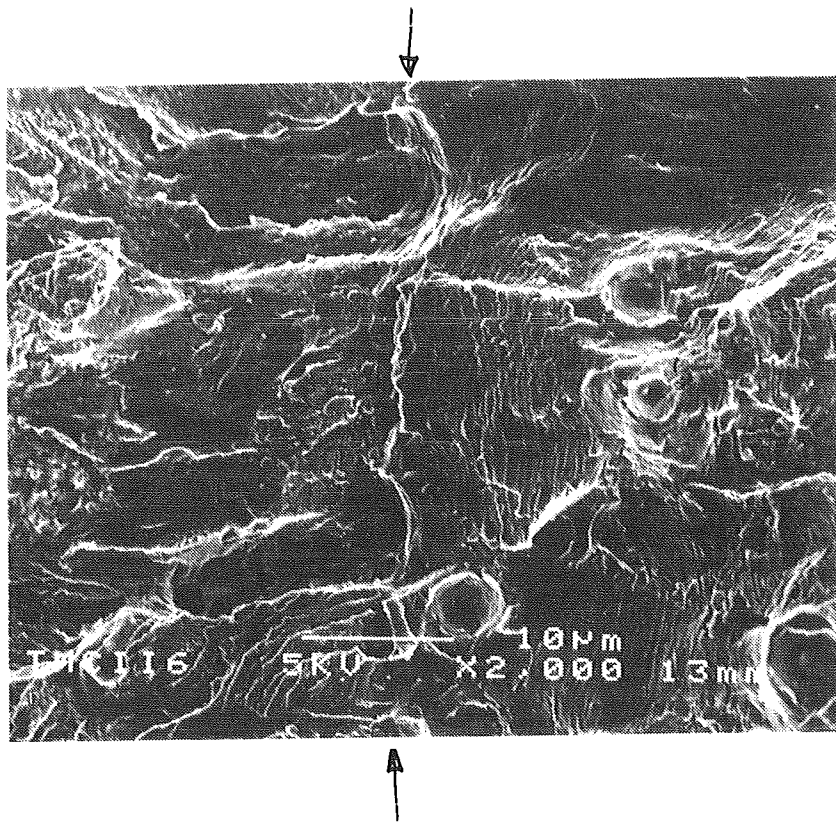


Figure 32 Detail of figure 31: crack growth from left to right.

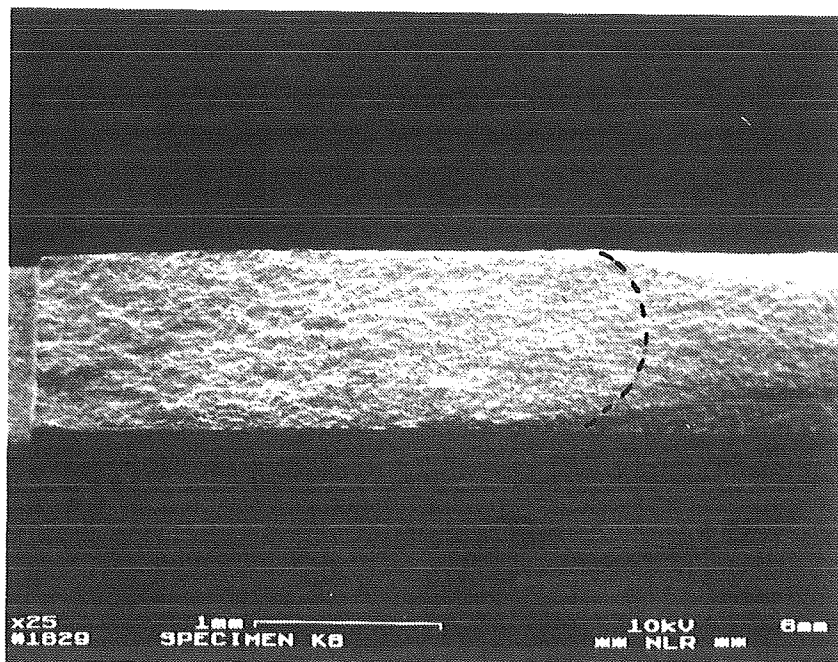


Figure 33 Overview of the right-hand fracture surface of specimen 32 at a magnification of 25 times; specimen was tilted 20°.

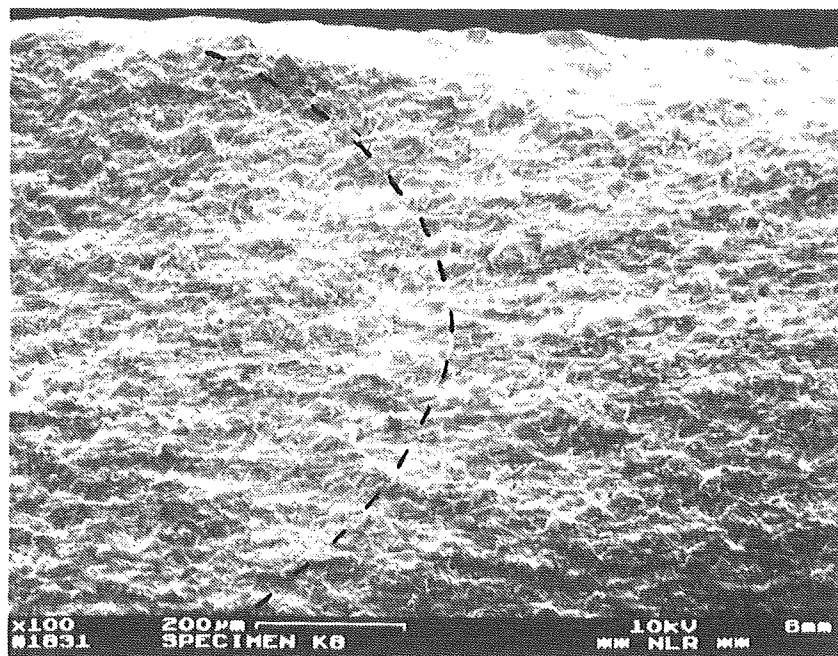


Figure 34 Transition on the right-hand fracture surface of specimen 32 at a magnification of 100 times: crack growth from left to right.

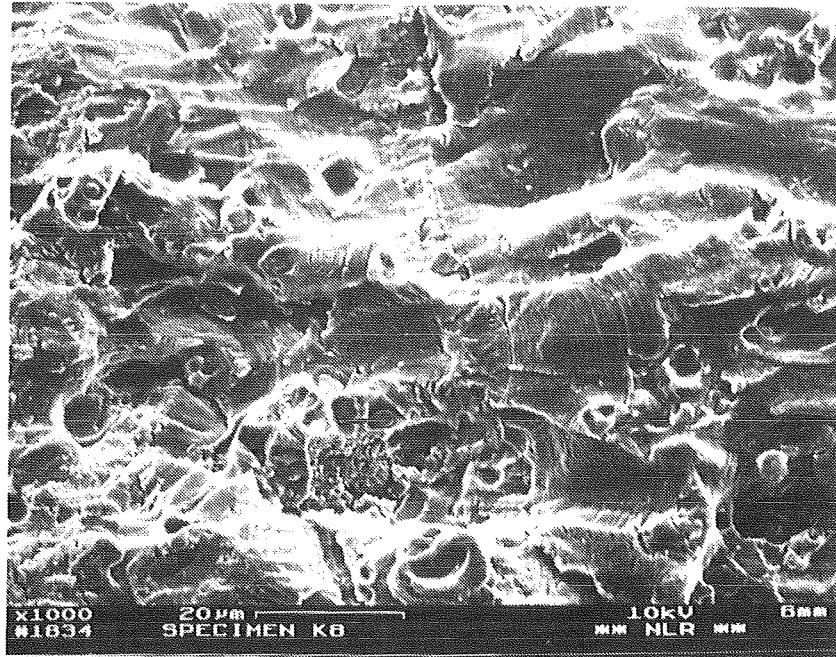


Figure 35 Transitions on the right-hand fracture surface of specimen 32 at a magnification of 1000 times: crack growth from left to right.

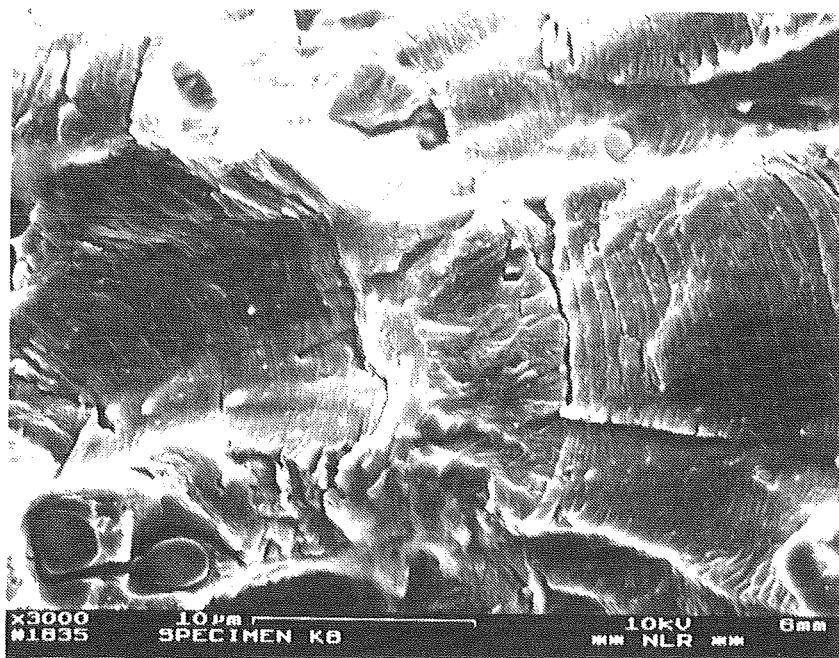


Figure 36 Magnification of figure 35 showing possible transition from dry air, to wet air, to laboratory air (from left to right): crack growth from left to right.

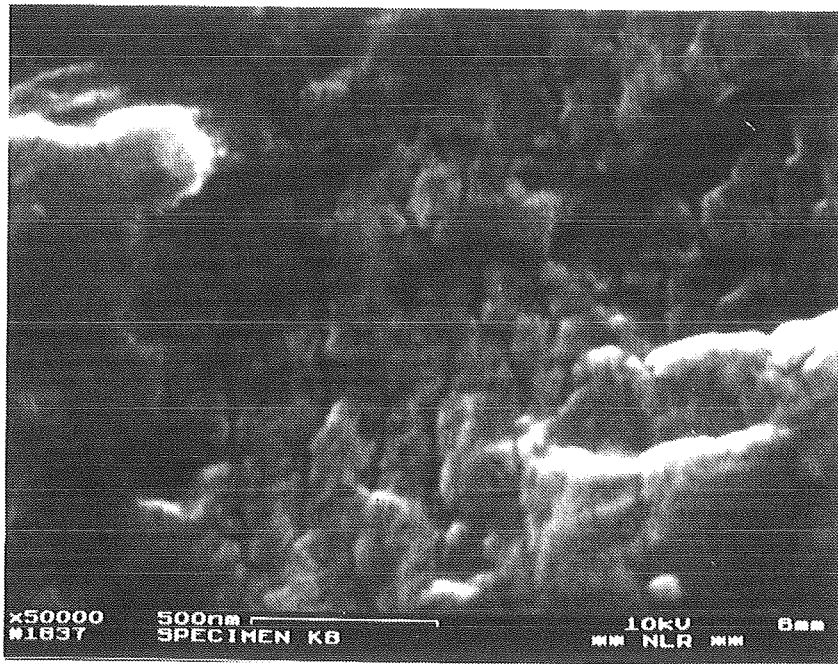


Figure 37 Magnification of 50000 times of the "central beach mark": crack growth from left to right.

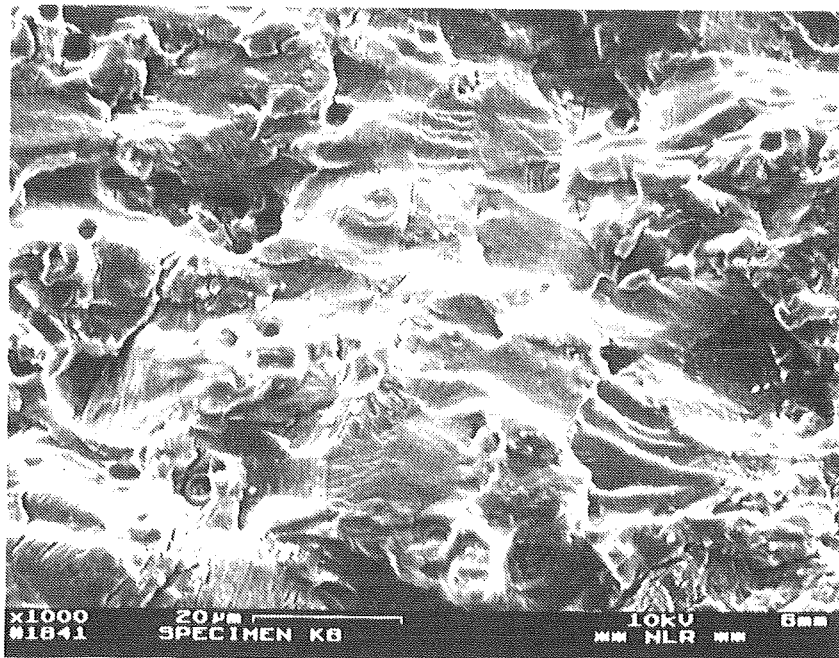


Figure 38 Transition on the left-hand fracture surface of specimen 32 at a magnification of 1000 times: crack growth from right to left.

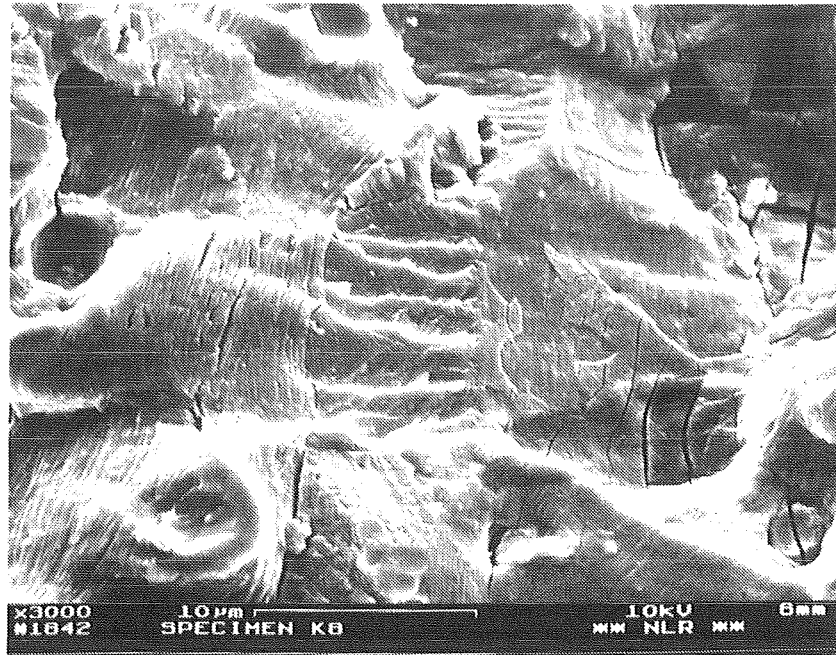


Figure 39 Magnification of figure 38 showing possible transition from laboratory air, to wet air, to dry air (from left to right) and so-called "mud-cracks": crack growth from right to left.

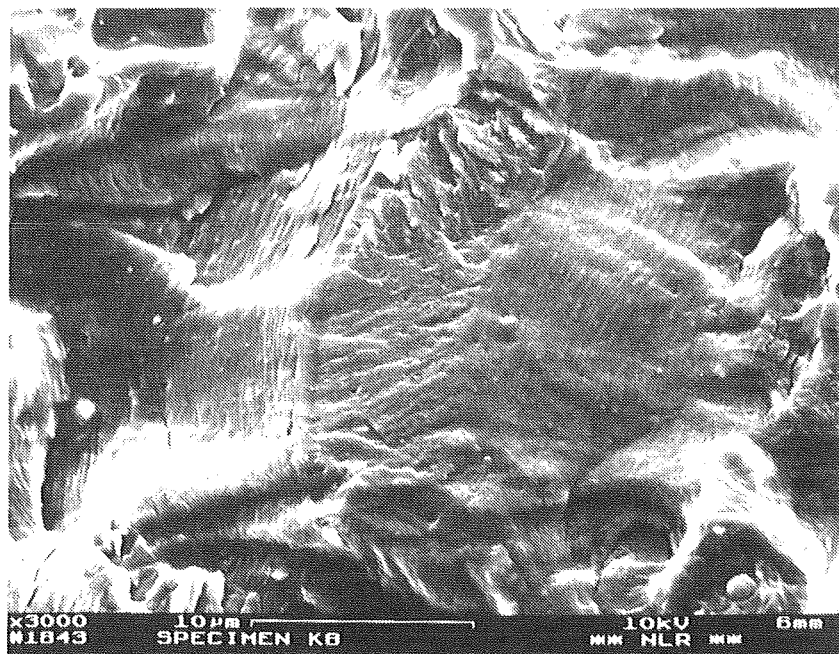


Figure 40 Another example of beach marks on a position slightly below the area in figure 39: crack growth from right to left.

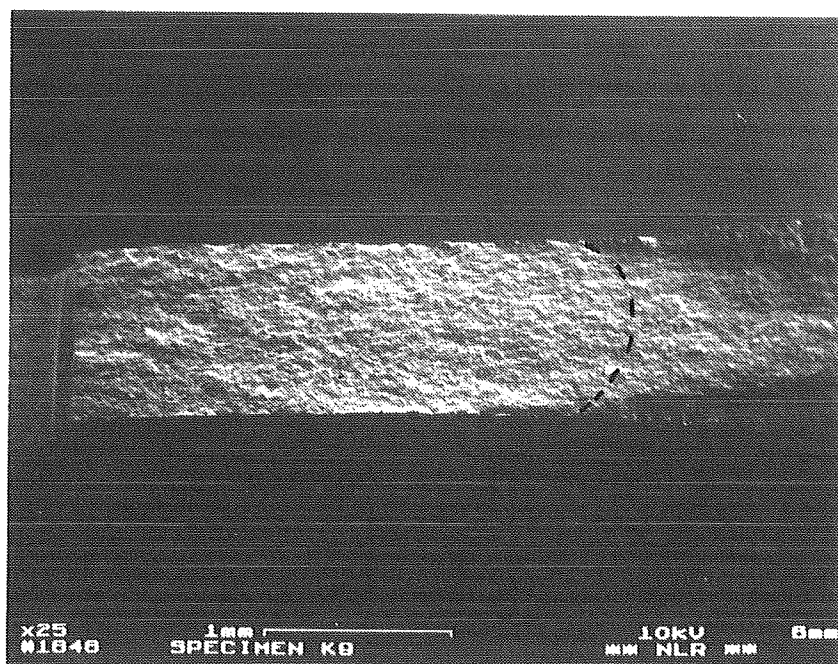


Figure 41 Overview of the right-hand fracture surface of specimen 33 at a magnification of 25 times; specimen was tilted 20°.

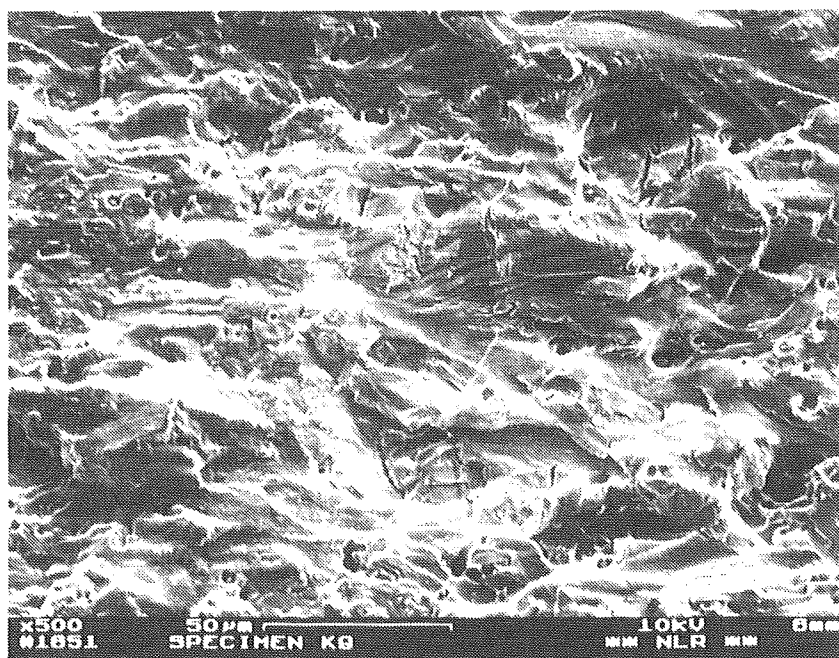


Figure 42 Transition on the right-hand fracture surface of specimen 33 at a magnification of 500 times: crack growth from left to right.

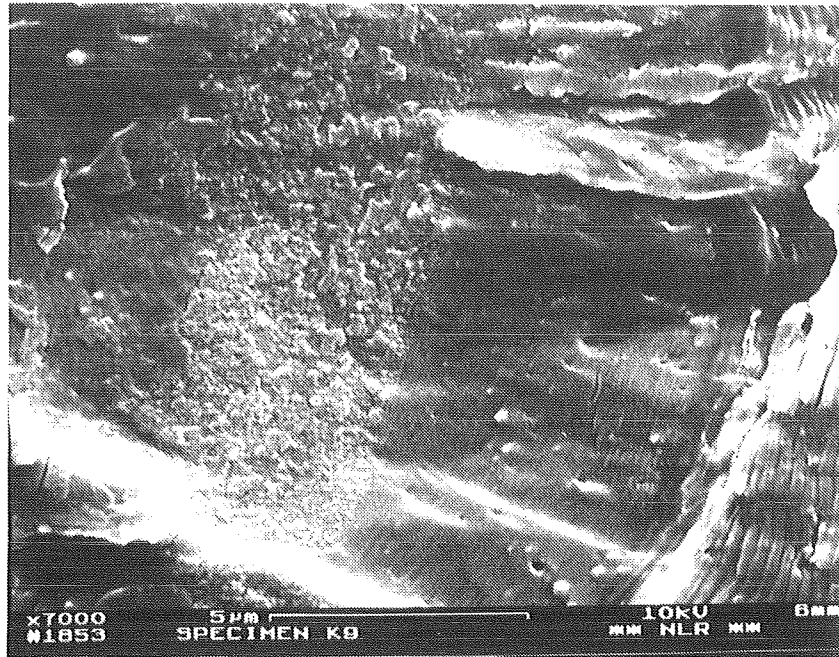


Figure 43 Magnification of figure 42 showing possible transition from dry air, to wet air, to dry air, to wet air (from left to right): crack growth from left to right.

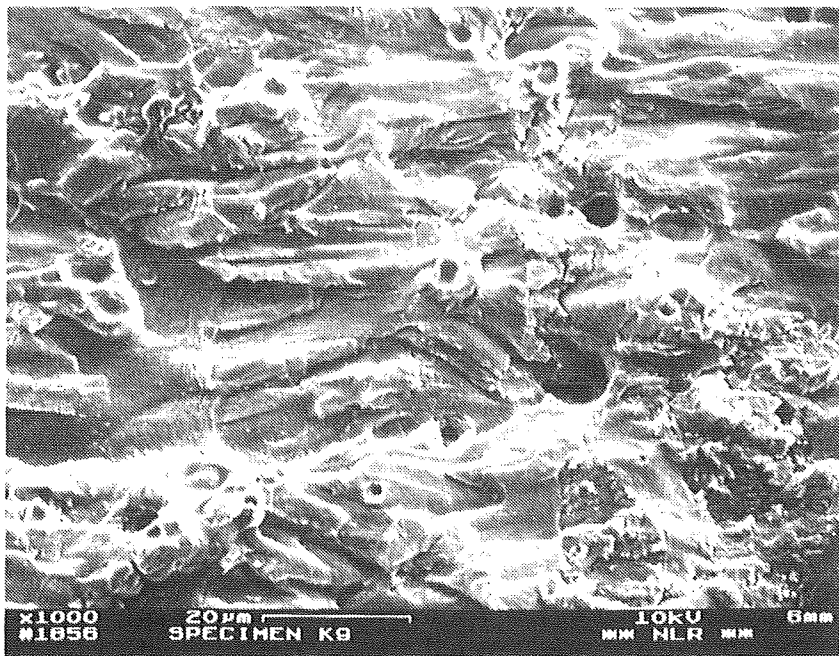


Figure 44 Transitions on the left-hand fracture surface of specimen 33 at a magnification of 1000 times: crack growth from right to left.

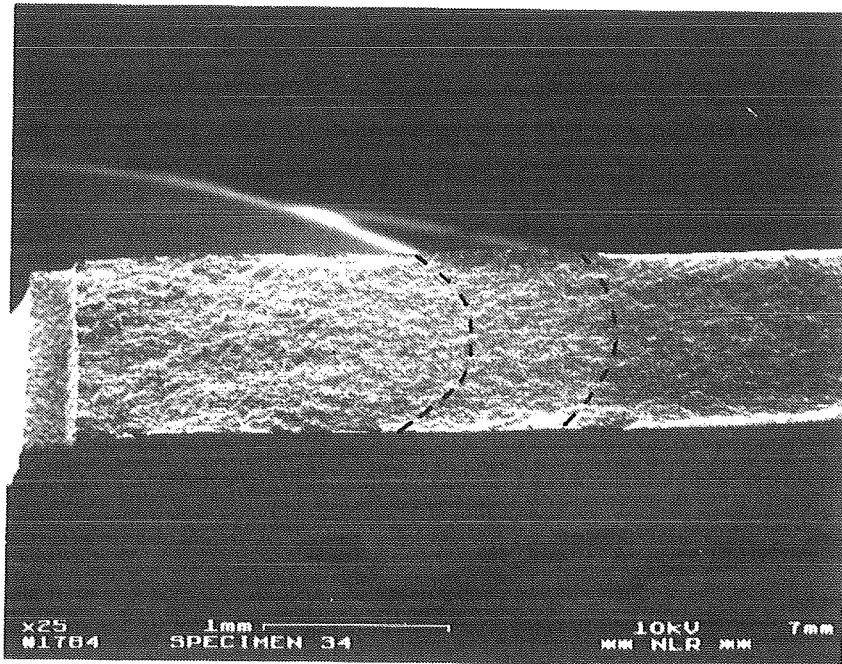


Figure 45 Overview of the right-hand fracture surface of specimen 34 at a magnification of 25 times; specimen was tilted 20°.

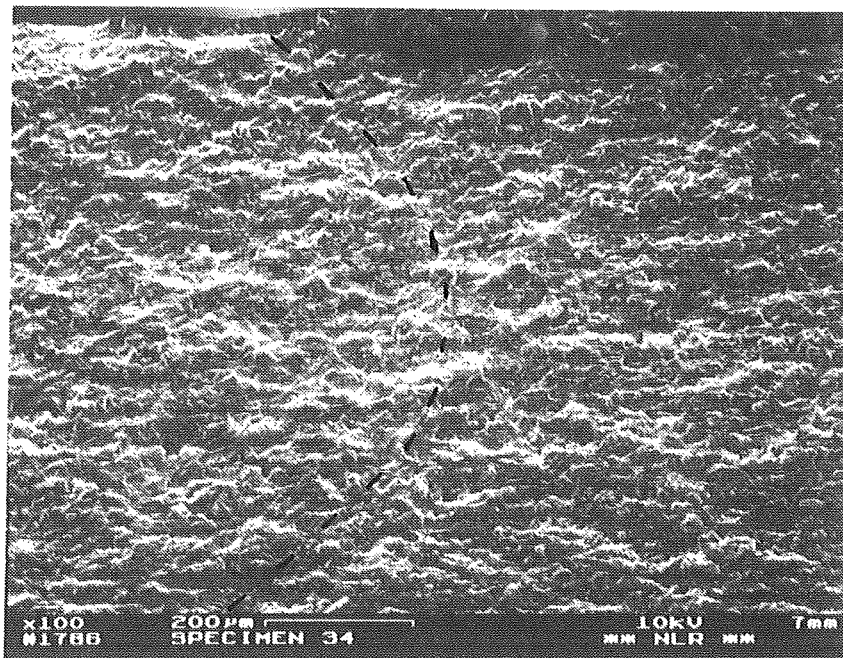


Figure 46 Transition from dry air to wet air on the right-hand fracture surface of specimen 34 at a magnification of 100 times: crack growth from left to right.

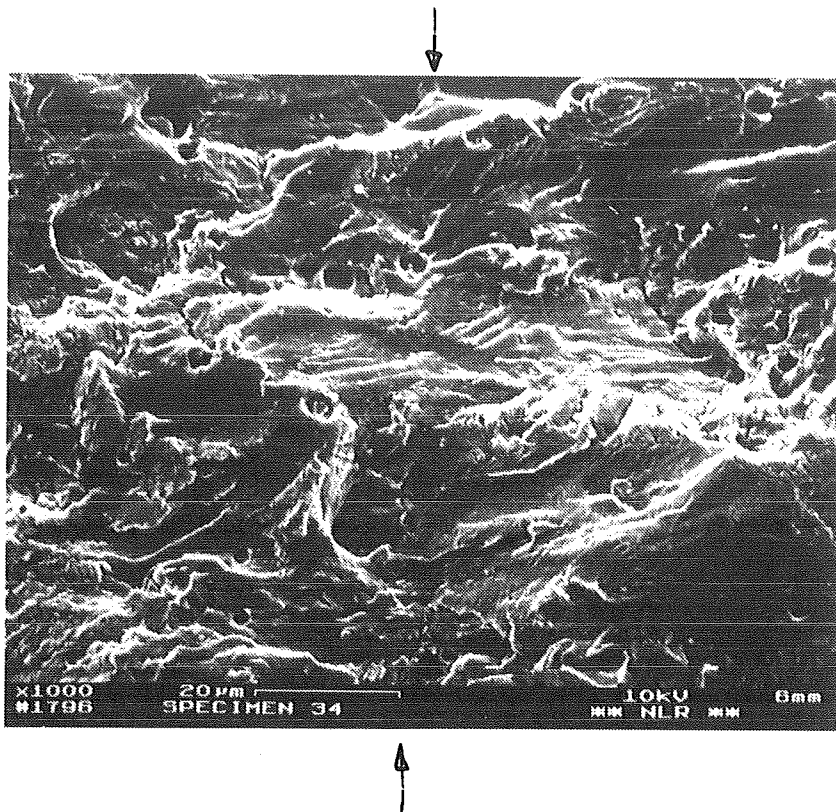


Figure 47 Magnification of figure 46 showing transition from dry air to wet air: crack growth from left to right.

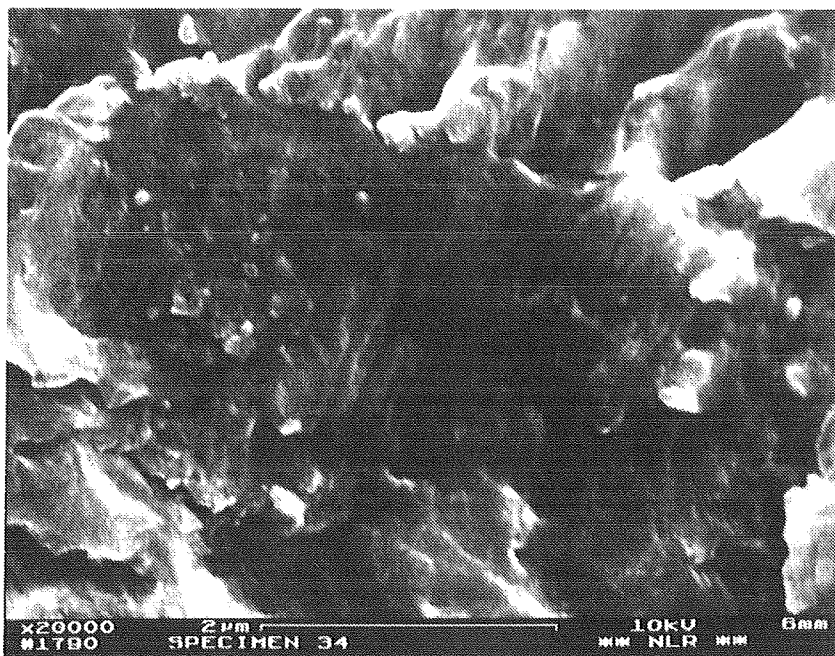


Figure 48 Magnification of 20000 times of the fracture surface before the transition (in dry air): crack growth from left to right.

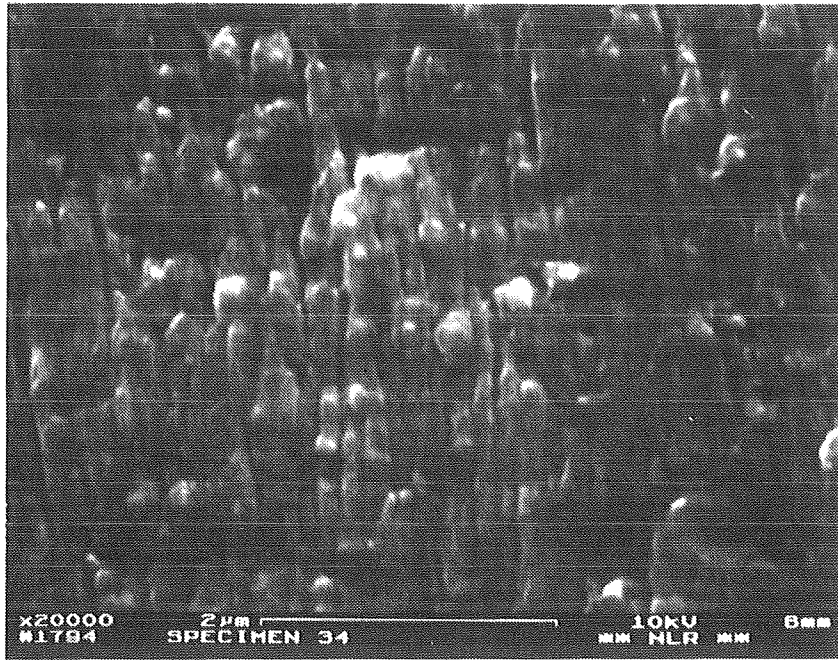


Figure 49 Magnification of 20000 times of the fracture surface after the transition (in wet air): crack growth from left to right.

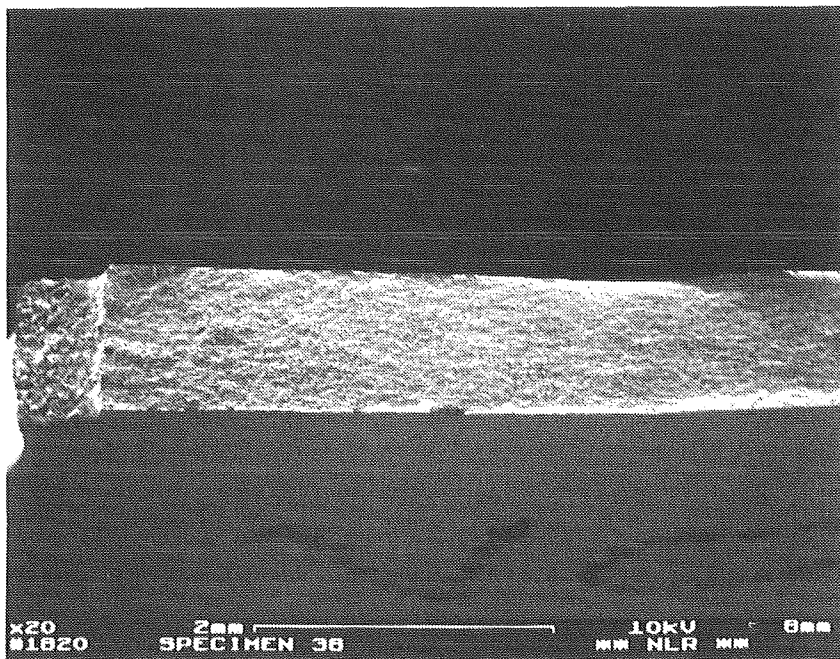


Figure 50 Overview of the right-hand fracture surface of specimen 36 at a magnification of 20 times; specimen was tilted 20°.

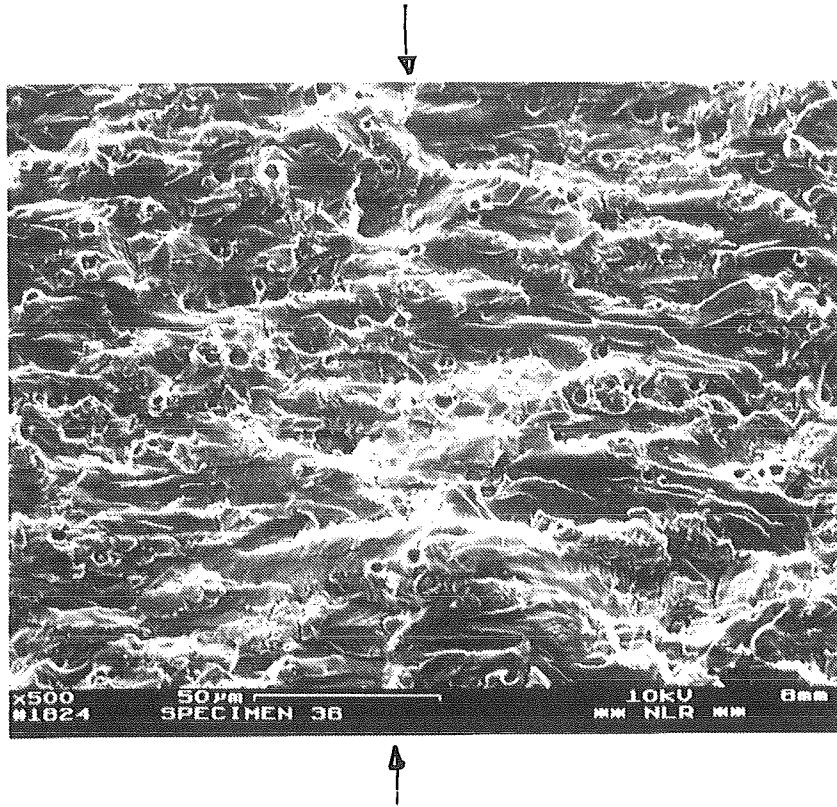


Figure 51 Magnification of 500 times of the possible transition from wet air to laboratory air: crack growth from left to right.

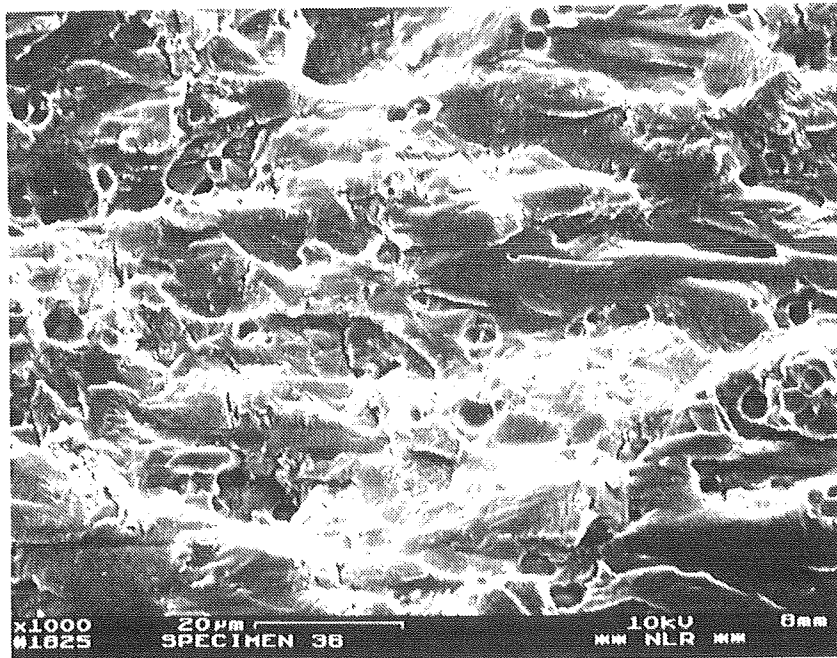


Figure 52 Magnification of figure 51 showing no more details of the transition from wet air to laboratory air: crack growth from left to right.

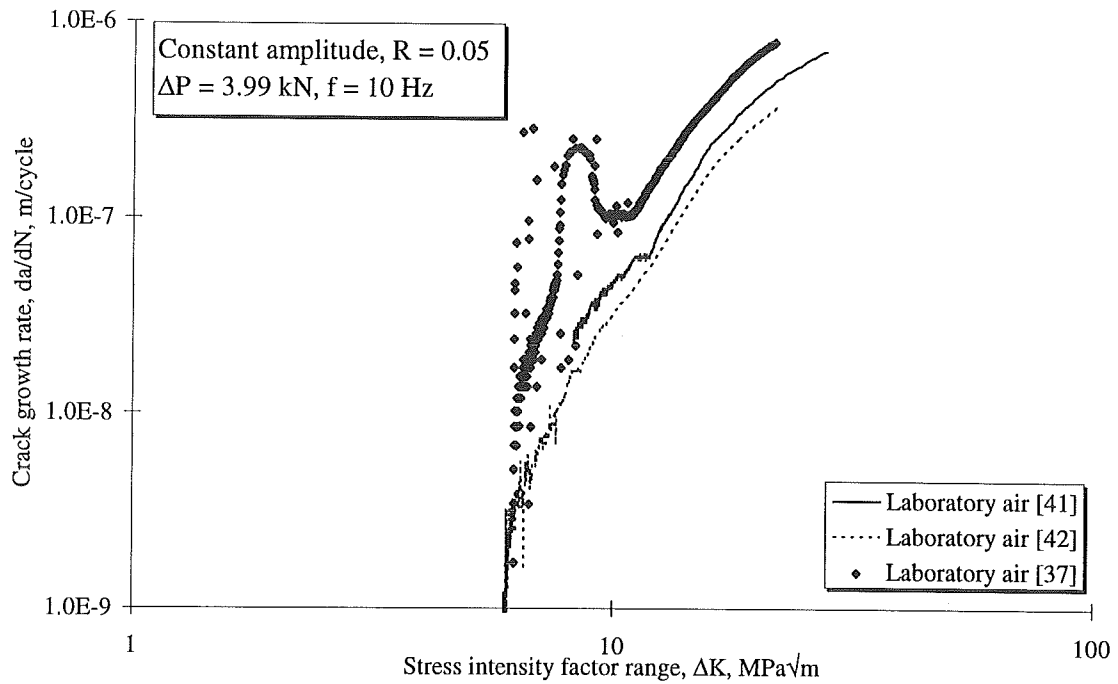


Figure 53 Fatigue crack growth rate da/dN versus stress intensity factor range ΔK for three nominally identical experiments in laboratory air.

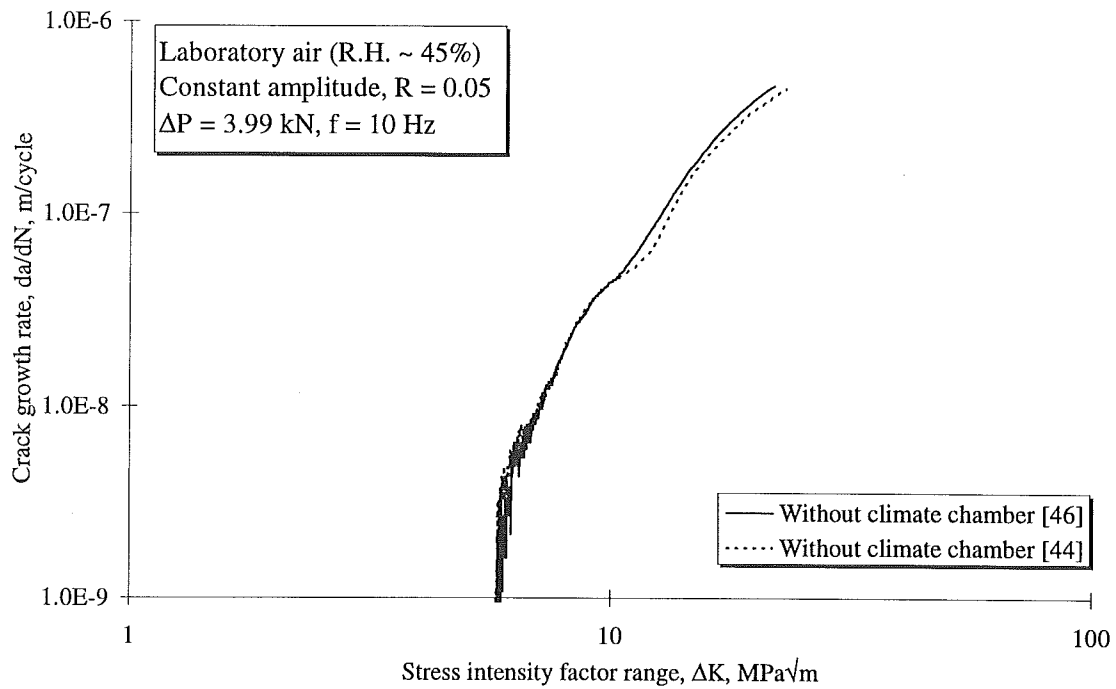


Figure 54 Fatigue crack growth rate da/dN versus stress intensity factor range ΔK for two nominally identical experiments in laboratory air, without climate chamber.

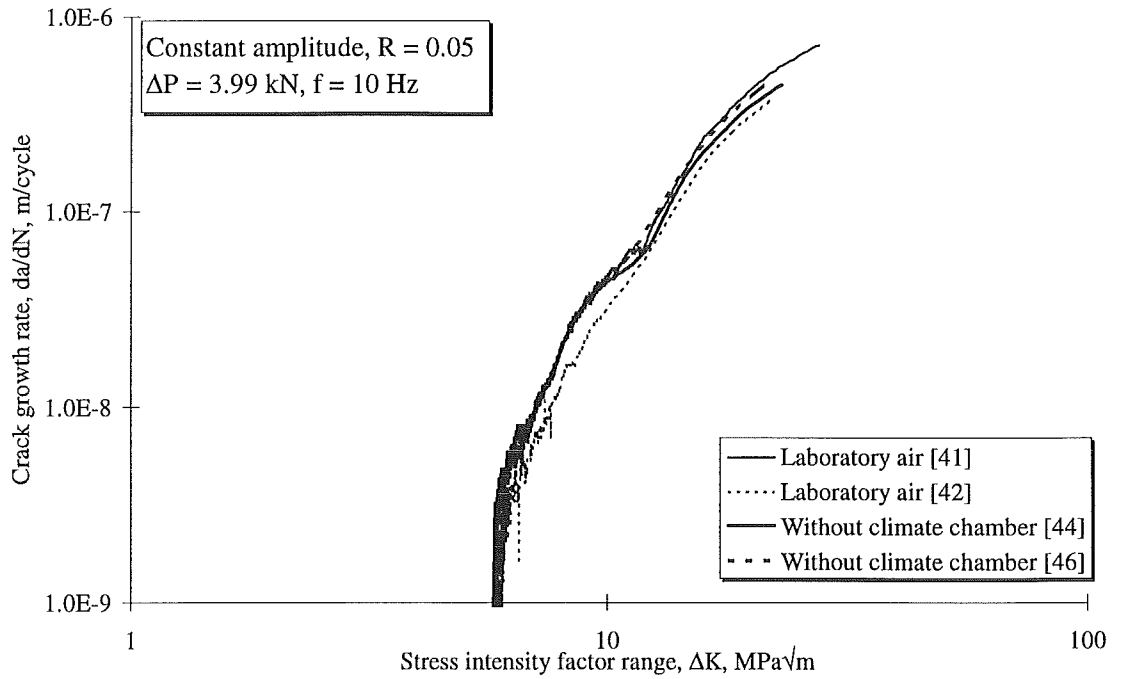


Figure 55 Fatigue crack growth rate da/dN versus stress intensity factor range ΔK for two experiments in laboratory air with climate chamber and two experiments in laboratory air without climate chamber.

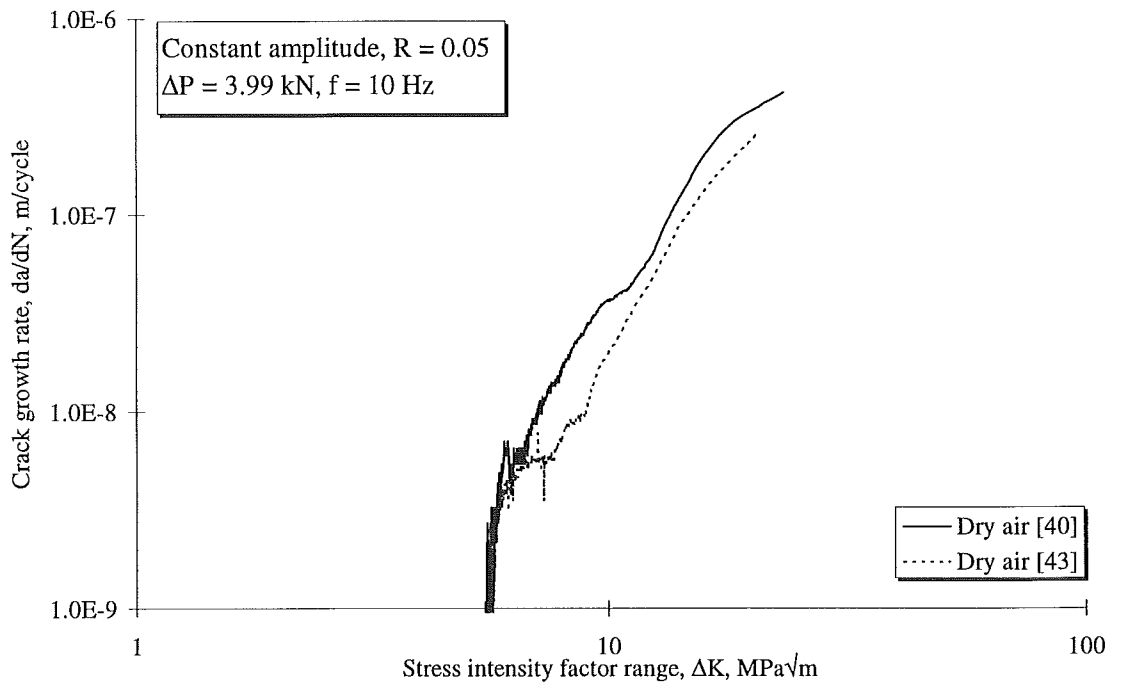


Figure 56 Fatigue crack growth rate da/dN versus stress intensity factor range ΔK for two nominally identical experiments in dry air.

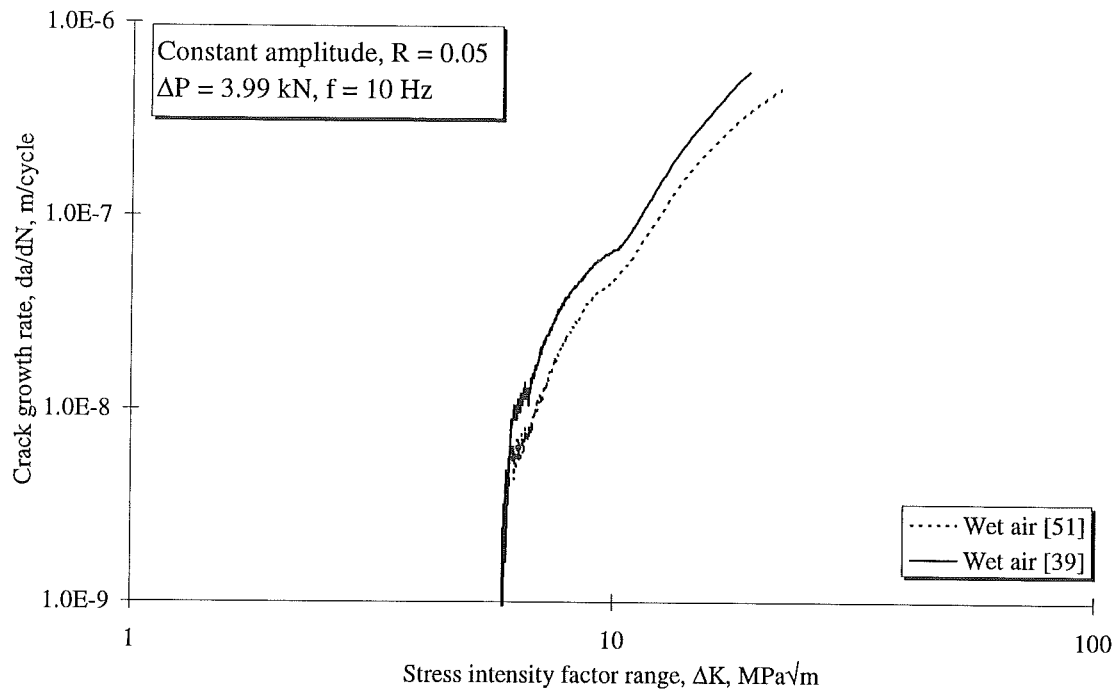


Figure 57 Fatigue crack growth rate da/dN versus stress intensity factor range ΔK for two nominally identical experiments in wet air.

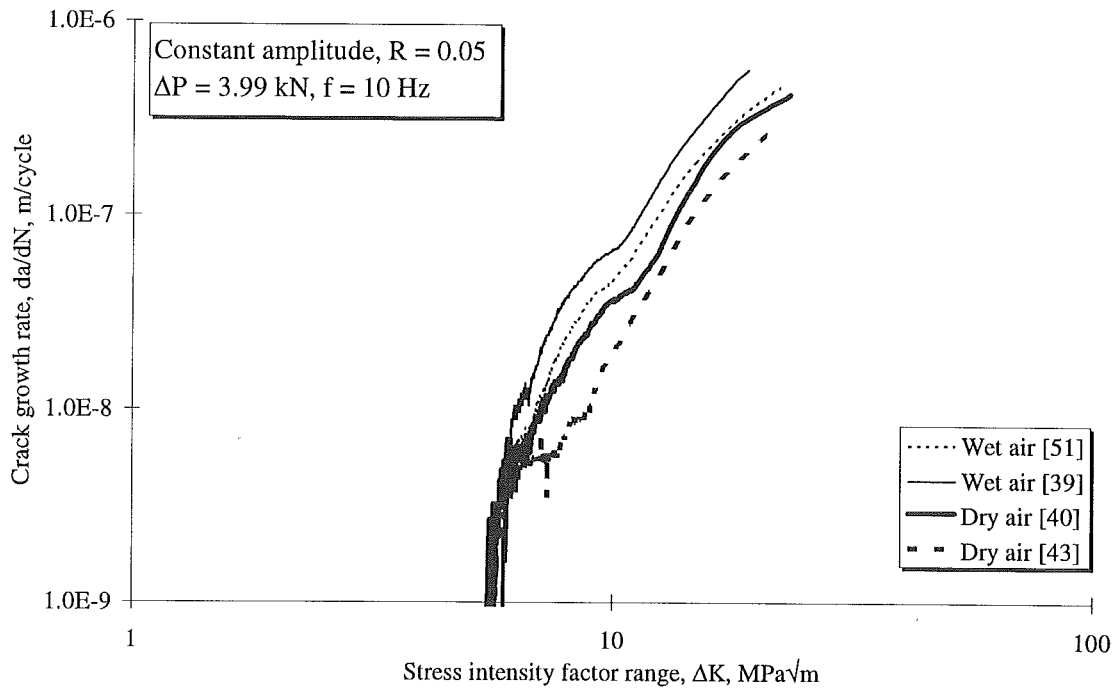


Figure 58 Fatigue crack growth rate da/dN versus stress intensity factor range ΔK for two experiments in dry air and two experiments in wet air.

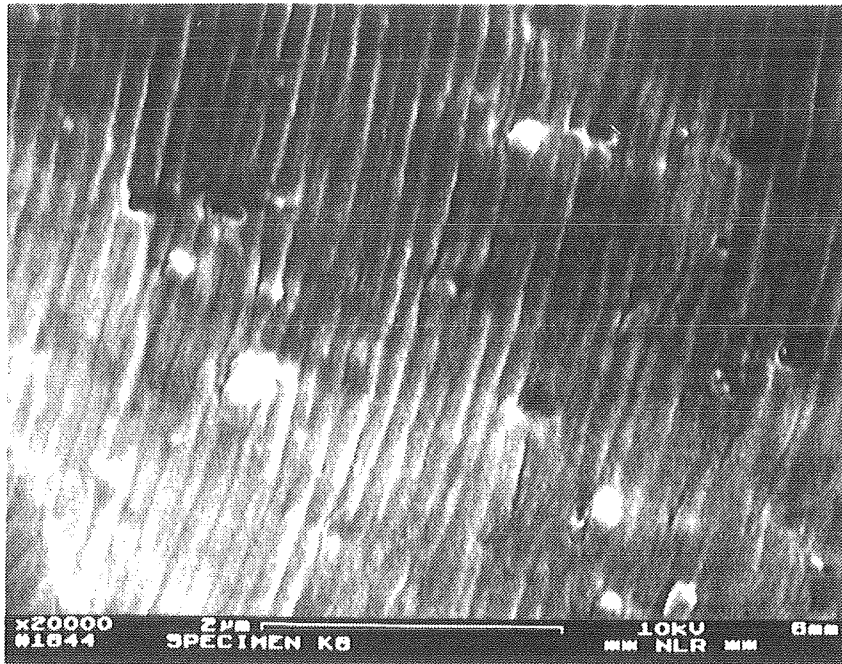


Figure 59 Magnification of 20000 times of the fracture surface of specimen 32 at a distance of 0.5 mm from the last applied environmental change.

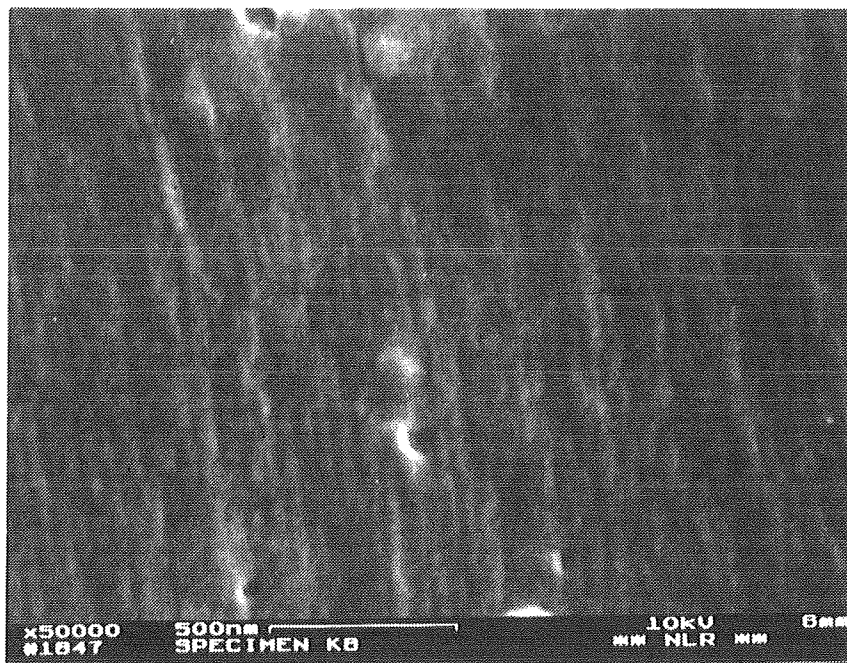


Figure 60 Magnification of 50000 times of the fracture surface of specimen 32 in the first testing block in laboratory air at $a = 4.5$ mm.

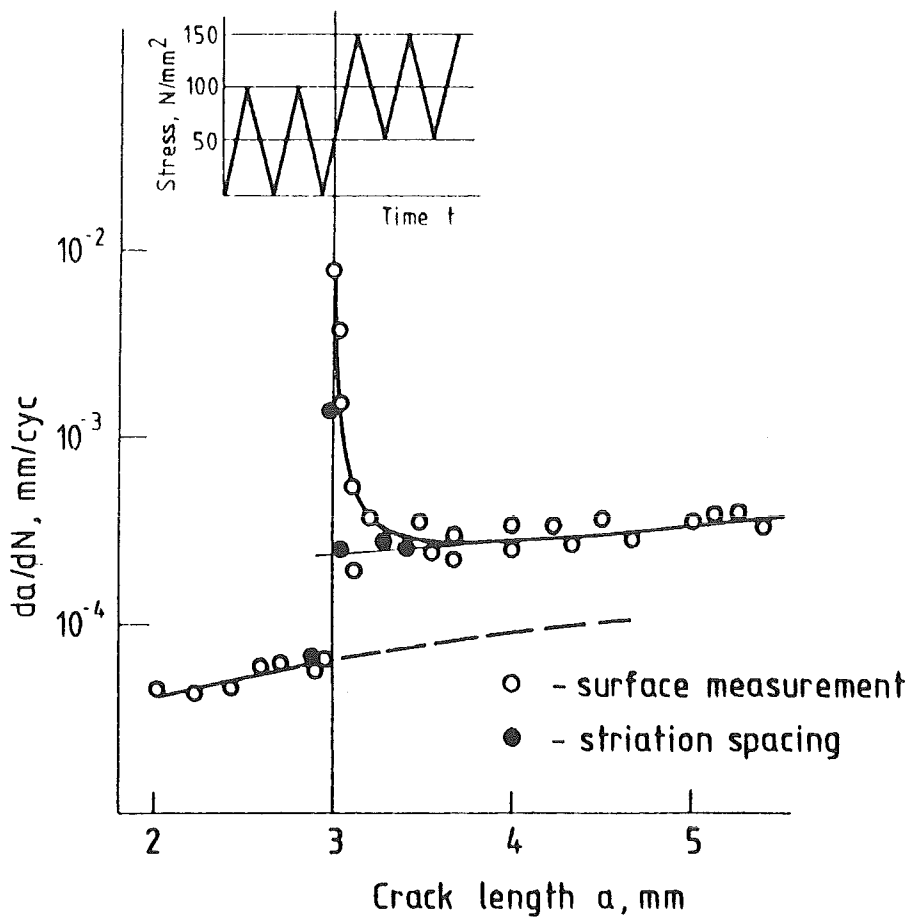


Figure 61 Fatigue crack propagation behaviour under a low-high loading sequence [29].

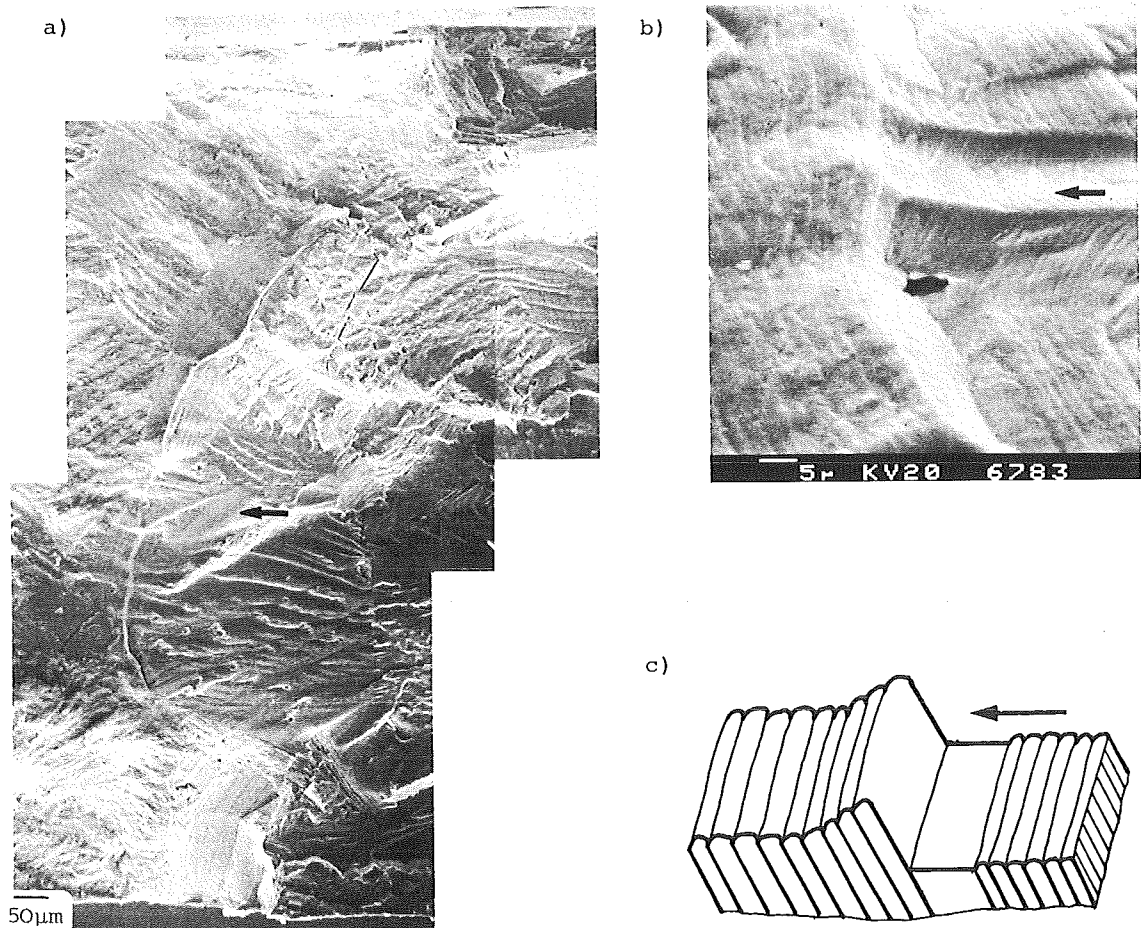


Figure 62 SEM-micrograph of the fracture surface of Al X-7075 during crack propagation under a low-high sequence: a) transition from the low to the high loading level (whole cross section of the specimen), b) formation of a step at the transition from the low to the high loading level (section of a), c) step formation shown schematically. The arrow indicates the crack growth direction [29].

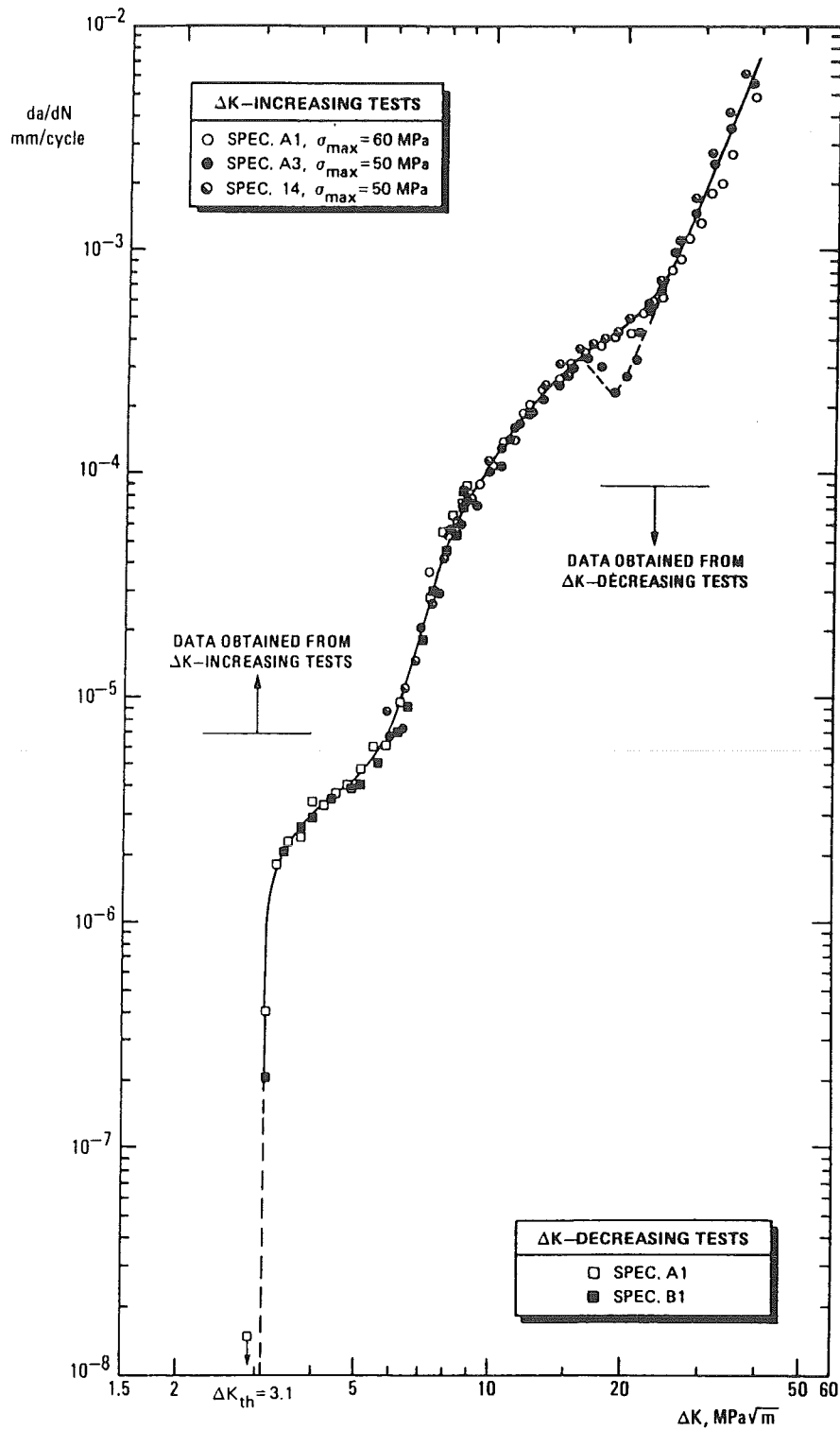


Figure 63 Constant amplitude fatigue crack growth data for a stress ratio $R = 0$, showing a sudden change of slope for one specimen [31].